FUNGAL SELF-ASSEMBLING PROTEIN LAYERS: NEW BIOTECH-TOOLS FOR BIO/NON-BIO HYBRID DEVICES

Ilaria Sorrentino

Dottorato in Biotecnologie – XXXI ciclo

Università di Napoli Federico II

FUNGAL SELF-ASSEMBLING PROTEIN LAYERS: NEW BIOTECH-TOOLS FOR BIO/NON-BIO HYBRID DEVICES

Ilaria Sorrentino

Dottorando: Ilaria Sorrentino

Relatore: Prof. Paola Giardina

Correlatore: Dr. Alassandra Piscitelli

Coordinatore: Prof. Giovanni Sannia

Alla mia famiglia
Per non dimenticare
Dove tutto ha avuto inizio ...

I have not failed
I've just found 10,000 ways
that won't work.
(Thomas A. Edison)

....

Never, never,
never give up.
(Winston Churchill)

INDEX/INDICE

RIASSUNTO

INTRODUZIONE

La progettazione e la realizzazione di bionanomateriali con proprietà e prestazioni specifiche sono caratteristiche chiave nello sviluppo di bio-dispositivi, in cui uno o più elementi biologici sono integrati con nano/micro piattaforme inorganiche. Le potenziali applicazioni dei bio-dispositivi dipendono fortemente dalla bio-funzionalizzazione delle loro superfici, che ne modifica le caratteristiche fisiche, chimiche e / o biologiche rispetto a quelle originali. I sistemi auto-assemblanti, per la stabilità chimica e meccanica delle loro strutture, sono candidati promettenti per la bio-funzionalizzazione e progettazione di nuovi biomateriali. In particolare, l'autoassemblaggio è la capacità intrinseca di numerose strutture biologiche multimeriche di assemblare dai loro componenti attraverso movimenti casuali di molecole e formazione di legami chimici deboli tra superfici con forme complementari. Eventi cellulari come la formazione di fibrille amiloidi, il riconoscimento antigene-anticorpo, l'assemblaggio della cromatina e l'autoassemblaggio della membrana fosfolipidica sono eccellenti esempi di autoassemblaggio molecolare.

Le fibrille amiloidi

Le proteine β-amiloidi sono una classe di proteine che possono subire una trasformazione strutturale dal loro stato funzionale nativo, in strutture fibrillari insolubili e altamente organizzate. Durante questa trasformazione le fibrille mature, indipendentemente dalla loro sequenza di amminoacidi o dalla loro struttura nativa, adottano una struttura più rigida rispetto ai loro precursori monomerici ed oligomerici mostrando un caratteristico pattern cross-β.

L'organizzazione molecolare unica delle fibrille amiloidi conferisce loro notevoli proprietà meccaniche e integrità strutturale persistente in presenza di alte temperature, proteasi, denaturanti e forze fisiche. Queste strutture fibrillari sono tipicamente associate a malattie neurodegenerative, come il morbo di Alzheimer e il morbo di Parkinson. Tuttavia, più recentemente è stato osservato che molti organismi, come funghi e alcuni batteri, sfruttano la capacità dei polipeptidi di formare amiloidi in una varietà di processi biologici.

Le idrofobine

Nei funghi filamentosi, le proteine amiloidi sono coinvolte in numerosi processi, ad esempio nella formazione di strutture aeree (spore o corpi fruttiferi) e nell'aderenza delle strutture fungine alle superfici idrofobiche durante le interazioni simbiotiche o patogene.

Le idrofobine sono una famiglia di piccole proteine (circa 100 aminoacidi), e rappresentano un esempio di fibrille amiloidi funzionali prodotte a diversi stadi di crescita da funghi filamentosi, in cui sembrano avere un ruolo chiave. Queste proteine possiedono la caratteristica di auto-assemblare spontaneamente alle interfacce idrofiliche-idrofobiche in strati anfipatici che cambiano la bagnabilità delle superfici. Tradizionalmente sono state divise in idrofobine di classe I e II. Quelle di classe I sono prodotte sia da funghi Basidiomiceti che Ascomiceti, invece quelle di classe II sono state isolate solo da Ascomiceti. Le proteine di questa famiglia hanno bassa identità di sequenza, ma sono caratterizzate da un motivo ben conservato di otto cisteine implicate nella formazione di quattro ponti disolfurici (Cys1-Cys6, Cys2-Cys5, Cys3-Cys4, Cys7-Cys8). Questi otto residui conservati stabilizzano il nucleo proteico e definiscono un modello di idrofobicità tipico di queste proteine. Gli spazi

inter-cisteina in quelle di classe I sono meno conservati rispetto a quelle di classe II. La differenza sostanziale tra le due classi risiede nella stabilità dei film anfifilici che formano. Le idrofobine di classe I formano film molto stabili e resistenti ai lavaggi con solventi e detergenti, come ad esempio l'etanolo al 60% e il sodio dodecil solfato (SDS) caldo al 2%; dissociabili solo in presenza di acidi forti come l'acido formico o l'acido trifluoroacetico (TFA), condividendo molte proprietà strutturali con le fibrille amiloidi. Al contrario i film formati dalle idrofobine di classe II sono poco stabili, possono essere più facilmente disciolti in detergenti o solventi organici, e mancano di strutture amiloidi. Entrambe le classi di idrofobine, per le loro interessanti proprietà, sono state sfruttate in molte applicazioni biotecnologiche:

| Applicazioni	Esempi
Applicazioni Industriali	
Emulsionanti	Biotensioattivi o emulsionanti, per migliorare la solubilità di preparati
Applicazioni ad alto valore aggiunto	
Nanotecnologia e diagnostica	Biosensori, come componenti per *lab-on-chip* e per il *drug delivery*
Anti-biofilm	Rivestimento di dispositivi medici, come cateteri, per ridurre la possibilità di legame da parte di batteri patogeni
Purificazioni	Purificazione di proteine di interesse, opportunamente fuse alle idrofobine

Queste capacità delle idrofobine possono essere sfruttate come un'interessante alternativa ai metodi convenzionali per la funzionalizzazione di superfici sviluppando dispositivi ibridi. Per l'ottenimento di uno strato bio-ibrido omogeneo possono essere utilizzate tecniche di ingegneria genetica in cui è possibile fondere le caratteristiche delle idrofobine con le proprietà specifiche delle proteine *target*. Seguendo questo approccio, le proteine fuse ingegnerizzate possono essere utilizzate direttamente per funzionalizzare le superfici con vantaggi in termini di tempo e di sostanze chimiche consumate.

Nel gruppo di ricerca presso cui è stato svolto Il mio progetto di PhD, è da tempo oggetto di studio il fungo basidiomicete *Pleurotus ostreatus*, ampiamente caratterizzato ed utilizzato come fonte di proteine di interesse industriale. In questo fungo sono stati identificati diversi geni codificanti idrofobine, espressi in differenti stadi del ciclo vitale. In particolare, è stata purificata dal brodo di coltura di questo fungo l'idrofobina di classe I Vmh2, ampiamente caratterizzata sia in forma solubile che aggregata, che è in grado di formare biofilm stabili su superfici solide. Sfruttando le competenze acquisite dal mio gruppo di ricerca, il presente lavoro verte sullo sviluppo di sistemi versatili e semplici di funzionalizzazione di superfici attraverso l'immobilizzazione di proteine chimeriche auto-immobilizzanti e il loro uso in diversi campi, che vanno dalle applicazioni biomediche, quali rivestimento di dispositivi medici per la sua attività anti-biofilm, a quelle industriali come emulsionante, incluso il *biosensing,* immobilizzando diversi enzimi nella loro forma attiva. Quindi, sfruttando tecniche di ingegneria genetica, Vmh2 è stata fusa a proteine *target* di interesse biotecnologico ed espressa in due diversi microrganismi (*Pichia pastoris* ed *Escherichia coli*). In particolare, tre classi di proteine *target*, un enzima ossidativo (laccasi), un peptide antimicrobico (LL37) e un anticorpo (anticorpo anti mesotelina),

sono state utilizzate per progettare, produrre, caratterizzare diverse proteine chimeriche utilizzate come *case studies* per la funzionalizzazione di superfici.

- **LACCASI**

Le laccasi (EC 1.10.3.2) sono enzimi ubiquitari che sono presenti in natura nei funghi (Ascomiceti, Duteromiceti e Basidiomiceti), nelle piante superiori e, in misura minore, nei batteri e negli insetti. Appartengono alla famiglia delle "*blue copper*" ossidasi, cioè enzimi ossidativi che contengono rame. Questi enzimi ad attività *p*-difenolossidasica, in particolare, utilizzano ossigeno atmosferico come accettore finale di elettroni e lo convertono in acqua con contemporanea trasformazione del substrato in prodotto.
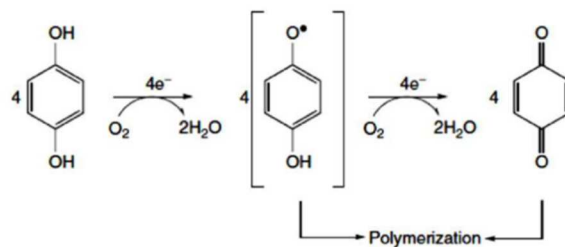
Le laccasi sono enzimi molto versatili; catalizzano l'ossidazione di diverse specie chimiche (quali para-difenoli, polifenoli, metossifenoli, amminofenoli, diammine, poliammine, arilammine, pesticidi, idrocarburi policiclici aromatici, coloranti). La capacità di questi enzimi di ossidare un ampio spettro di substrati li rende particolarmente interessanti per le loro potenziali applicazioni biotecnologiche. Di fatto, questa classe di enzimi trova attualmente largo uso in numerosi settori industriali che includono la delignificazione della pasta di cellulosa, la decolorazione di tessuti, la detossificazione di acque reflue, la trasformazione di antibiotici e steroidi, l'utilizzo come componenti di detersivi. Le laccasi inoltre, possono essere immobilizzate su supporti appropriati per il loro utilizzo sia come biocatalizzatori che per il biosensing.

Immobilizzazione facile e diretta della proteina chimerica laccasi-idrofobina e sviluppo di una piattaforma analitica per il monitoraggio di composti fenolici

I fenoli sono tra le impurità organiche più abbondanti che penetrano nell'ambiente a seguito del loro uso in un gran numero di processi, dall'industria cartiera alla sintesi di materie plastiche e farmaceutiche. Per monitorare questi composti è quindi necessario un processo rapido e affidabile. Per raggiungere questo obiettivo, è stato sviluppata piattaforma analitica basata sulla proteina chimerica laccasi-idrofobina. L'interesse per questa proteina chimerica consiste nell'avere una proteina bifunzionale in cui si associano le proprietà dell'idrofobina Vmh2 di aderire alle superfici, alle proprietà enzimatiche della laccasi, utilizzando un approccio di fusione genetica. Si ottiene, così, una proteina auto-assemblante, autoadesiva e con attività catalitica. Quindi, la prima proteina che è stata fusa con l'idrofobina è stato l'enzima POXA1b. Tra gli isoenzimi prodotti da *P. ostreatus* la laccasi POXA1b è stata scelta per le sue peculiari caratteristiche: *i)* stabilità e attività in un ampio intervallo di pH (3-9) e temperature (25 ° -65 ° C); *ii)* alto potenziale redox (+0,650 V); *iii)* alto livello di produzione in ospiti eterologhi.

La proteina chimerica POXA1b-Vmh2 è stata espressa in *Pichia pastoris* e ritrovata secreta nel mezzo di coltura. Il surnatante della coltura grezza è stato direttamente utilizzato per rivestire piastre multi-pozzetto in polistirene senza ulteriori passaggi di purificazione. Vantaggi della fusione rispetto all'enzima libero prodotto nelle stesse condizioni, sono stati riscontrati sia nella percentuale di immobilizzazione che nella stabilità. La piastra multi-pozzetto così funzionalizzata è stata utilizzata per monitorare due composti fenolici, L-dopa *((S) -2-Amino-3- (3,4-diidrossifenil) propanoico)* e acido caffeico *(Acido 3- (3,4-diidrossifenil) -2-propenoico)*, la cui stima è di interesse per i settori farmaceutico e alimentare. Il metodo si basa sull'uso degli analiti come inibitori in competizione all'ossidazione dell'ABTS mediata dalla laccasi. I principali vantaggi di questa metodologia di monitoraggio sono la facilità di preparazione, l'uso di piccoli volumi di campioni e l'analisi simultanea di più campioni su un'unica piattaforma. I risultati di questi esperimenti sono oggetto di un lavoro scientifico sottomesso alla rivista "Applied Microbiology and Biotechnology" per la pubblicazione.

Immobilizzazione di enzimi chimerici su nanomateriali

I nanomateriali a base di grafene (GBM) sono materiali nanostrutturati particolarmente utili che sono di grandi prospettive in campo biotecnologico e biomedico. I GBM sono estremamente interessanti perché possono combinare proprietà di elevato rapporto superficie / volume, biocompatibilità, stabilità chimica ed elettrochimica e buona conduttività elettrica. Recentemente, è stato messo a punto un processo per la produzione di GBM biofunzionalizzati in miscele di etanolo-acqua, utilizzando ultrasuoni in sinergia con l'idrofobina di classe I Vmh2. Sia il POXA1b che la proteina chimerica POXA1b-Vmh2 sono stati sfruttati per la funzionalizzazione di nanomateriali (NM) attraverso un approccio *"one-step"*. L'obiettivo principale è stato l'ottenimento di nuovi nanobio-catalizzatori, sfruttando le proprietà caratteristiche di Vmh2, dei NM e di POXA1b. In particolare, la miglior resa di bio-funzionalizzazione (11%) del grafene con PoxA1b-Vmh2 è stata ottenuta con l'aggiunta dell'enzima negli ultimi 10 minuti dell'esfoliazione. I dati ottenuti confermano che la fusione genica migliora la stabilità e l'adesione della proteina rispetto alla controparte libera. Inoltre, durante il periodo trascorso all'estero presso il laboratorio del Dr. Alan Le Goff (Department of Molecular Chemistry, Groupe Biosystèmes Electrochimiques et Analytiques, Université Grenoble Alpes, Francia), il grafene bio-funzionalizzato è stato depositato su GCE (*Glassy Carbon Electrode*) e utilizzato come elettrodo di lavoro per test cronometrici per la rivelazione di catecolo. Il risultato di questi esperimenti ha dimostrato che questa tecnica potrebbe rappresentare un'alternativa valida per il rilevamento di questo analita in campioni reali come l'acqua di rubinetto.

La laccasi POXC da *Pleurotus ostreatus*: un enzima ad alte prestazioni per la reazione diretta di riduzione dell'ossigeno in *fuel cell*

Le MCO (*Multicopper Oxidases*) sono una valida opzione come bio-catodi nelle *enzymatic biofuel cells* (EBFC), una sottoclasse di celle a combustibile in cui gli enzimi sostituiscono i catalizzatori convenzionali. A tale scopo, è stata studiata l'elettrochimica diretta di POXC, la laccasi canonica e più abbondante da *P. ostreatus*. Grazie all'interazione favorevole tra questa laccasi nativa e i nanotubi di carbonio (CNT) opportunamente modificati in modo covalente con sali di antrachinone e naftoato di diazonio, POXC presenta un ORR (*Oxygen Reduction Reaction*) ad alto potenziale / alta corrente in un ampio intervallo di pH (da 2 a 8), superando le prestazioni della più nota laccasi commerciale da *Trametes versicolor*

(TvLAC), immobilizzata sugli stessi elettrodi nanostrutturati. Per queste prestazioni uniche, questo enzima è stato in grado di operare all'interfaccia dello strato microporoso, aria umidificata ed elettrolita polimerico, come il nafion®, in una *fuel cell* convenzionale a scambio di protoni H_2 / aria, superando i problemi riscontrati fin qui con altri enzimi della stessa famiglia. I risultati di questi esperimenti sono oggetto di un lavoro scientifico recentemente pubblicato sulla rivista ChemElectroChem.

- **PRODUZIONE RICOMBINANTE DI PROTEINE CHIMERICHE IN *Escherichia coli***

La produzione ricombinante in *E. coli* delle proteine chimeriche è stata eseguita utilizzando il protocollo ottimizzato per altri tipi di proteine di fusione riportati da Piscitelli e coautori. In queste proteine chimeriche, Vmh2 è stata fusa con altre due proteine *target*, un peptide antimicrobico, LL37, e un anticorpo, HN1 ScFv, che simula l'attività dell'anticorpo umano anti-mesotelina, una glicoproteina sovra espressa in diversi tumori umani.

Proteina chimerica peptide antimicrobico-idrofobina

L'interesse crescente verso i peptidi antimicrobici nasce dall'aumentare della resistenza agli antibiotici di molti microrganismi patogeni. Tra questa classe di peptidi, LL37 è stato intensamente studiato poiché è l'unica catelicidina ritrovata nell'uomo. La proteina chimerica LL37-Vmh2 è stata prodotta e purificata con successo; e le sue capacità adesive e di antibiofilm contro *Staphylococcus epidermidis* sono state testate su superfici di polistirene. I risultati più importanti ottenuti sono stati una buona resa di immobilizzazione (circa 40%) e un'efficiente attività anti-biofilm e antimicrobica

Proteina chimerica anticorpo-idrofobina

L'immobilizzazione dell'anticorpo su una superficie solida è stata studiata estesamente per una serie di applicazioni tra cui immuno-dosaggi, biosensori e cromatografia di affinità. Per la maggior parte di queste applicazioni, un aspetto critico è l'orientamento del sito di legame dell'antigene rispetto alla superficie. Con l'obiettivo di superare questo problema, in questa sezione è stata effettuata la produzione ricombinante in *E. coli* della proteina chimerica in cui l'idrofobina è fusa alla parte funzionale dell'anticorpo anti-mesotelina. La mesotelina è una glicoproteina di superficie cellulare che è fisiologicamente espressa sulla superficie cellulare delle cellule mesoteliali e sovra espressa in diversi tumori umani, tanto che si possono trovare forme solubili di mesotelina nei fluidi di pazienti affetti da questi tumori. Quindi, la misurazione della mesotelina nel sangue può essere utile per la diagnosi, ma anche per la terapia mirata, data la sua limitata espressione nei tessuti normali e l'alta espressione in diversi tumori. Questa proteina chimerica è stata prodotta in *E. coli.*

- **CONCLUSIONI**

Il principale vantaggio della fusione genica consiste nel combinare le proprietà adesive e auto-assemblanti dell'idrofobina Vmh2 con le proprietà di diverse proteine *target* di interesse biotecnologico per sviluppare metodi di immobilizzazione semplici, arrivando ad ottenere superfici ibride con caratteristiche uniche, che dipendono dalla scelta della proteina *target*. Di seguito sono riportati i principali risultati conseguiti in questo progetto:

✓ Vmh2-PoxA1b è stata prodotta e secreta nel brodo di coltura del lievito *P. pastoris*. L'enzima fuso immobilizzato è stato utilizzato per sviluppare una superficie funzionale per rilevare composti fenolici in matrici reali di interesse alimentare e biomedico.

✓ È stata sviluppata una procedura *one-step* di esfoliazione e bio-funzionalizzazione del grafene con Vmh2-PoxA1b. Il grafene funzionalizzato è stato depositato su GCE, e può rappresentare una valida alternativa per la rivelazione di catecolo in campioni reali con metodi elettrochimici.

✓ La laccasi POXC ha dimostrato di essere di grande interesse come biocatodo per nuove applicazioni bioelettrocatalitiche.

✓ "l*ayers*" assemblanti di LL37-Vmh2 sono stati utilizzati per inibire i bio-films microbici per produrre superfici di polistirene funzionalizzate per lo sviluppo di dispositivi medici.

✓ La proteina HN1-Vmh2 è stata prodotta nel citoplama di *E. coli* e potrà essere utilizzata per l'immobilizzazione su diverse superfici per immunodosaggi (Elisa Kit) and *drug delivery*.

SUMMARY

During recent years the demand of valuable scaffolds to biofunctionalize nanomaterials has been rapidly increasing. Self-assembling proteins, such as amyloid fibrils, are promising candidates for the functionalization of nanomaterials due to their chemical and mechanical stability. These fibrillar structures are typically associated to neurodegenerative diseases. However, it has been recently observed that many organisms, such as fungi and some bacteria, take advantage of the ability of polypeptides to form amyloids. Hydrophobins represent an example of functional amyloid fibrils produced at different growth stages by filamentous fungi. They are a large family of very active surface proteins and can be grouped into two distinct classes based on the stability of the amphipathic layers that they form. In particular, layers formed by class I share many structural properties with amyloid fibrils, solubilized only after harsh acid treatments Immobilization of active proteins on the hydrophobin layer has been proven as a simple approach for the functionalization of different surfaces useful in biotechnological applications. For most of these applications, a critical aspect concerns protein orientation with respect to the surface. To overcome this problem, design and recombinant production of fused engineered proteins combining the adhesive moiety of hydrophobins to target proteins can be a valuable choice. This PhD project has been focused on recombinant production in different hosts (*Pichia pastoris* and *Escherichia coli*) of chimera proteins built by selected target proteins (laccase, antimicrobial peptides and antibody) fused to an adhesive self-assembling class I hydrophobin, and on their exploitation in some application fields. The selected class I hydrophobin was Vmh2, extracted from the mycelium of the fungus *Pleurotus* ostreatus, one of the most hydrophobic hydrophobin able to spontaneously form stable and homogeneous layers on hydrophilic or hydrophobic surfaces, changing their wettability. As a first goal, the hydrophobin Vmh2 was fused to the laccase POXA1b from *P. ostreatus*, a high redox potential oxidase endowed with a remarkable stability at high temperature and at alkaline pH. The resulting fusion enzyme was secreted into the culture medium by the heterologous yeast *P. pastoris* and directly used for coating different surfaces, *i.e.* graphene and polystyrene, without additional purification steps. The immobilized enzyme was exploited to develop innovative optical and electrochemical biosensing platform for the detection of phenolic compounds. Subsequently, two chimeric proteins were recombinantly expressed in *E. coli*: in the first case, Vmh2 was fused to the antimicrobial peptide LL37, a small cationic amphiphilic peptide belonging to the family of cathelicidins which has an effective activity against a wide range of bacteria and fungi. The LL37-Vmh2 chimeric protein was successfully produced and its adhesive and antibiofilm capabilities, against *Staphylococcus epidermidis*, tested by coating polystyrene surfaces. The chimera HN1-Vmh2, the fusion between the hydrophobin and the anti-mesothelin ScFv antibody, was produced in the soluble fraction of *E. coli* whilst its purification and exploiation needs to be optimized.

In conclusion, chimeric proteins obtained by the genetic fusion of the hydrophobin Vmh2 to target proteins represent a proof of concept of versatile and straightforward solutions of surface functionalizations that could be explored in several fields.

Moreover, during the six months stay at the CNRS of Grenoble, the work was focused on carbon nanotubes (CNT) functionalization using the native laccase POXC from *P. ostreatus*. POXC is a promising biocathode for enzymatic biofuel cells (EBFCs), since it shows efficient ORR (Oxygen Reduction Reaction) performances and it is capable to operate in a conventional H_2/air proton-exchange membrane fuel cell.

1. INTRODUCTION

The design and the realization of bionanomaterials with specific properties and performances are key features in bio-device development. The potential applications of these bionanomaterials strongly depend on the bio-functionalization of device surfaces [1]. Biological molecules fully integrated with micro or nano technological platforms are useful tools to fabricate hybrid devices, showing physical, chemical and/or biological characteristics different from those originally found on the surface. Self-assembled systems are promising candidates for designing novel biomaterials, due to the chemical and mechanical stability of their structures [2,3]. In particular, self-assembly is the inherent ability of numerous multimeric biological structures to assemble from their component parts through random movements of molecules and formation of weak chemical bonds between surfaces with complementary shapes. This phenomenon is mainly governed by weak noncovalent bonds like electrostatic interactions (ionic bonds), hydrogen bonds, hydrophobic and hydrophilic interactions, water-mediated hydrogen bonds, and van der Waals interactions [4]. Although these forces are weak, their collective interactions can produce molecules that are structurally and chemically stable. For all those characteristics, molecular self-assembly is a powerful phenomenon borrowed from nature by scientists for fabricating novel supramolecular architectures. Cellular events like amyloid fibril formation, antigen–antibody recognition, chromatin assembly, and phospholipid membrane self-assembly are excellent examples of molecular self-assembly.

1.1 Amyloid fibrils

Amyloid proteins are a large class of proteins that may undergo a structural transformation from their native, functional folded state, into highly organized, insoluble fibrillar structures (Fig.1).
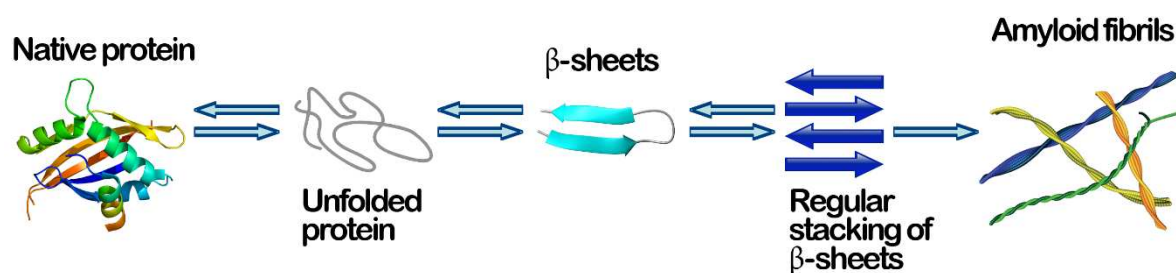

Fig. 1 – A schematic representation of a possible amyloid fibril self-assembly process

During this transformation, the proteins lose their native form and functionality. Additionally, unlike native protein states, the stability of amyloid fibrils is largely attributed to intermolecular interactions. Mature fibrils adopt a more rigid structure than their monomeric and oligomeric precursors, which can be attributed to the high β-sheet content of the fibrils [5–7]. These sheets form a "cross-β" motif, in which β-strand segments run perpendicular to the fibril axis and van der Waals interactions

between side chains promote hydrogen bonding parallel to the fibril [8,9]. Regardless of their amino acid sequence or native structure, amyloid fibrils display a characteristic cross-β pattern in X-ray diffraction experiments, indicating the orthogonal orientation of individual b-strands with respect to the fibril axis [10,11] (Fig.2).
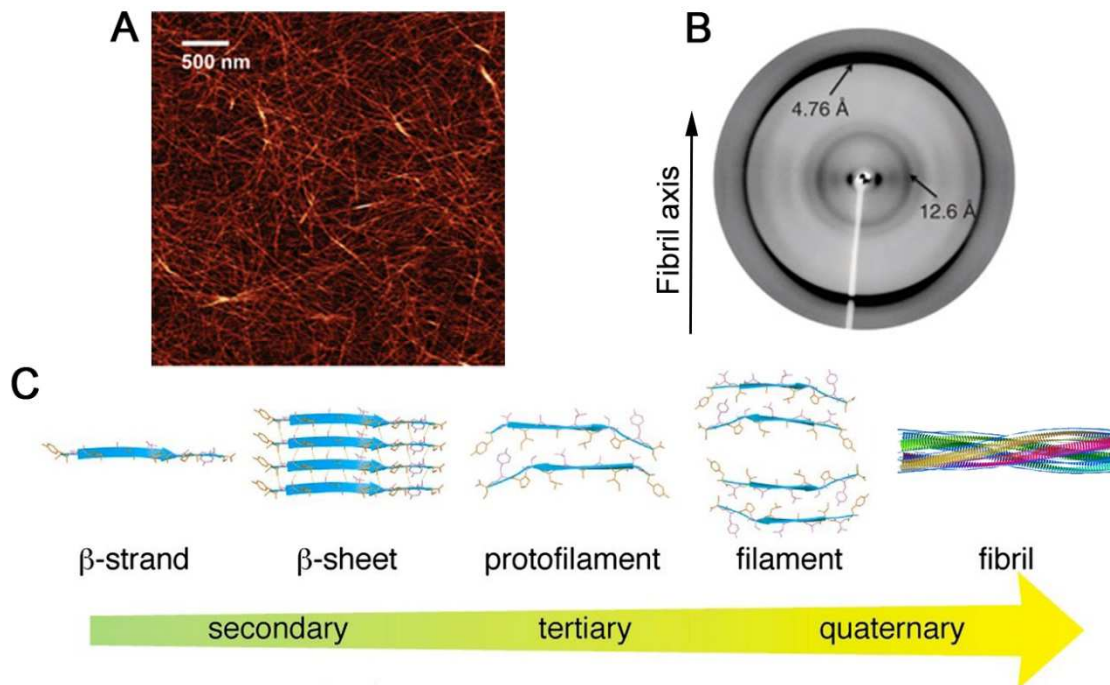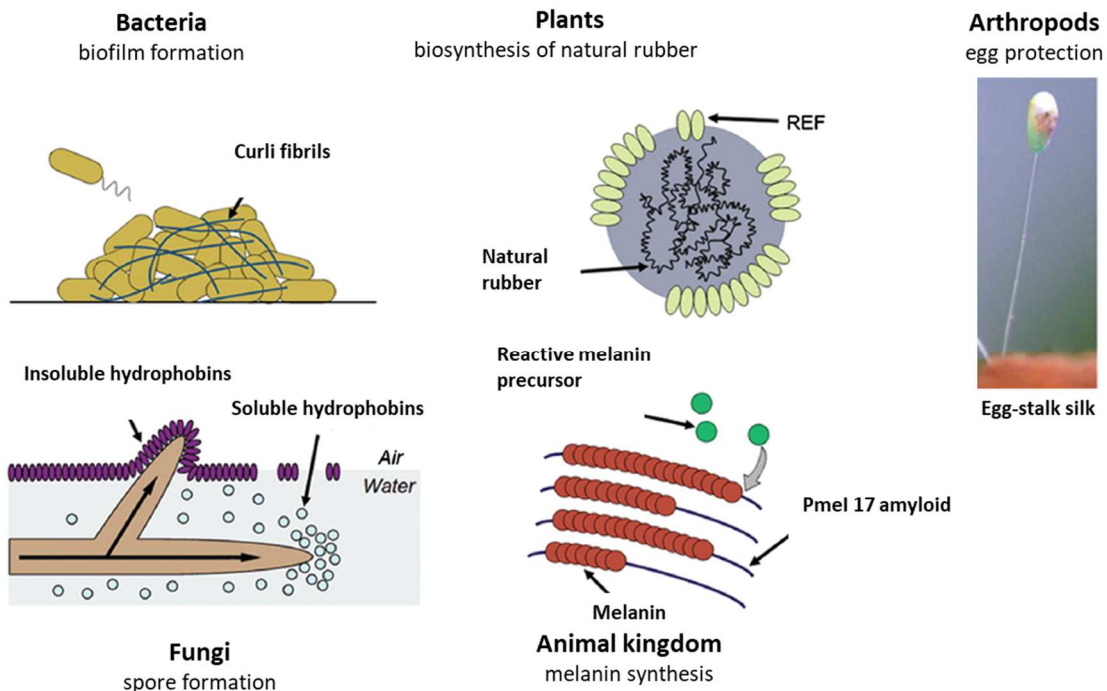

Fig. 2 ‒ **A**: atomic force microscopy (AFM) of amyloid fibrils generated by the PSMa1 peptide from *S. aureus*; **B**: the typical ''cross-b'' X-ray diffraction pattern for amyloid fibrils and **C**: atomic models for secondary, tertiary, and quaternary structure (adapted from [8])

The unique molecular organization of amyloid fibrils endows them with remarkable mechanical properties as well as persistent structural integrity in the presence of high temperatures, proteases, denaturants, and physical forces [12].

Functional amyloids

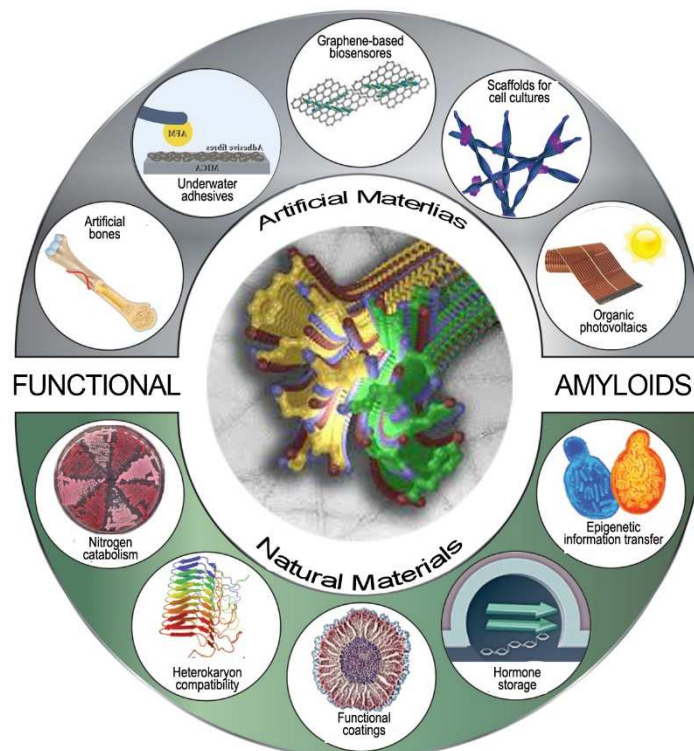These fibrillar structures are typically associated to neurodegenerative diseases such as Alzheimer's and Parkinson's diseases. However, more recently it has been observed that they can also fulfill important physiological roles in a variety of biological processes [13,14]. Many organisms, such as fungi and some bacteria, take advantage of the ability of polypeptides to form amyloids [15,16] (Fig.3).

Bacteria
biofilm formation

Curli fibrils

Plants
biosynthesis of natural rubber

REF

Natural rubber

Arthropods
egg protection

Egg-stalk silk

Insoluble hydrophobins

Soluble hydrophobins

Air
Water

Fungi
spore formation

Reactive melanin precursor

Pmel 17 amyloid

Melanin

Animal kingdom
melanin synthesis

Fig. 3 – Functional and structural diversity of amyloid proteins (adapted from [17]).

Amyloid fibrils are known to display impressive material properties, including high deformation resistance, elasticity, and persistence under extreme conditions. These unique properties make them excellent candidate materials for the design of functional biomaterials (Fig.4).

Graphene-based biosensores

Scaffolds for cell cultures

Underwater adhesives

Artificial bones

Organic photovoltaics

FUNCTIONAL

AMYLOIDS

Artificial Materials

Nitrogen catabolism

Epigenetic information transfer

Heterokaryon compatibility

Functional coatings

Hormone storage

Natural Materials

Fig. 4 – Roadmap to the diversity in functions in amyloids-based materials (adapted from [18]).

Hydophobins

In filamentous fungi, amyloids are involved in numerous processes, e.g., in the formation of aerial structures (spores or fruiting bodies) [19] and in the adherence of fungal structures to hydrophobic surfaces. This adherence can occur on the surface of a host organism, thereby facilitating pathogenesis and playing a role in symbiosis [20]. Hydrophobins, a large family of small proteins (about 100 aminoacids), represent an example of functional amyloid fibrils produced at different growth stages by filamentous fungi (Fig.5). Their biological functions seem to be diverse, these proteins self-assemble at hydrophobic/hydrophilic interfaces into amphipathic layers changing the wettability of surfaces, they are very active surface and play a role as coating/protective agents, in adhesion, surface modification, or other types of functions that require surfactant-like properties [21].
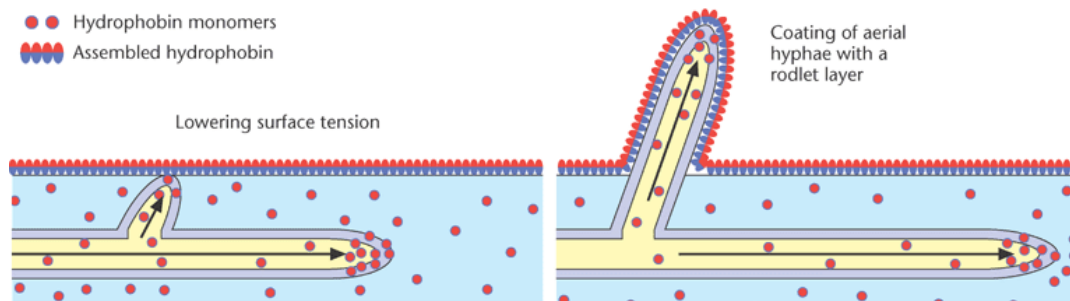

Fig. 5 – Models showing the role of hydrophobins in the emergence of aerial hyphae (adapted from [22])

Hydrophobins are characterized by a β-barrel motif in the 3D structure and the presence of eight conserved cysteine residues that form four disulphide bonds (Cys1–Cys6, Cys2–Cys5, Cys3–Cys4, Cys7–Cys8). These eight conserved residues stabilize the protein core and define a hydrophobicity pattern typical of these proteins.

**A**

Class I hydrophobins

```
SC4   CNSG-PVQ--CCNETTT--VANAQ-KQGLLGG----LLGVVV----GPITGLVGLNCSP----ISVVGV----LTGNSCTA-QTVCCDHVTQNG-----LVN--VGC
PRI2  CNNG-SLQ--CCNSSMTQDRGNLQIAQGVLGGLLGGLLGLGGLLDLVDLNALIGVQCSP----ISIVG------NANTCTQ-QTVCCSNNNFNG-----LIA--LGC
SC3   CTTG-SLS--CCNQVQS---ASSSPVTALLG-----LLGIV-----LDLNVLVGISCSP----LTVIG-----VGGSGCSA-QTVCCENTQFNG-----LIN--IGC
ABH1  CDVG-EIH--CCDTQQT-----PDHTSAAASG----LLGVP-----INLGAFLGFDCTP----ISVLG-----VGGNNCAA-QPVCCTGNQFTA-----LINA-LDC
EAS   CSID-DYKPYCCQSMSG-----PAGSPGL-------LNLIP-----VDLSASLG--C---------VVG----VIGSQCGA-SVKCCKDDVTNTGNSFLIINA-ANC
HCF1  CAVGSQIS--CCTTNSS-------GSD---------ILGNV-----------LGGSCLLDN--VSLISSLN-----SNCPAGNTFCCPS-NQDG-----TLNINVSC
MPG1  CGAEKVVS--CCNSKELK--NSKSGAE---------IPIDV----------LSGECKNIPINILTINQLI--PINNFCSD-TVSCCSGEQIG------LVN--IQC
RODA  CGDQAQLS--CCNKATYAG-DVTDIDEGILAGTLKNLIGGGS----GTEGLGLFNQCSKLDLQIPVIGIPIQALVNQKCKQ-NIACCQNSPSDASG--SLIGLGLPC
```

Class II hydrophobins

```
HFBI  CPPG-LFSNPQCCATQVLGLIGLDCKVPSQNVYDGTDFRNVCAKTGA-QPLCCVAP-VAGQALLC
HFBII CPTG-LFSNPLCCATNVLDLIGVDCKTPTIAVDTGAIFQAHCASKGS-KPLCCVAP-VADQALLC
SRH1  CPNG-LYSNPQCCGANVLGVAALDCHTPRVDVLTGPIFQAVCAAEGGKQPLCCVVP-VAGQDLLC
CU    CTGL-LQKSPQCCNTDILGVANLDCHGPPSVPTSPSQFQASCVADGGRSARCCTLS-LLGLALVC
CRP   CSST-LYSEAQCCATDVLGVADLDCETVPETPTSASSFESICATSG-RDAKCCTIP-LLGQALLC
MGP   CSG--LYGSAQCCATDILGLANLDCGQPSDAPVDADNFSEICAAIG-QRARCCVLP-ILDQGILC
HCF6  CPAN---RVPQCCQLSVLGVADVTCASPSSGLTSVSAFEADCANDG-TTAQCCLIP-VLGLGLFC
HYD4  CPDGGLIGTPQCCSLDLVGVLSGECSSPSKTPNSAKEFQEICAASG-QKARCCFLSEVFTLGAFC
```

B
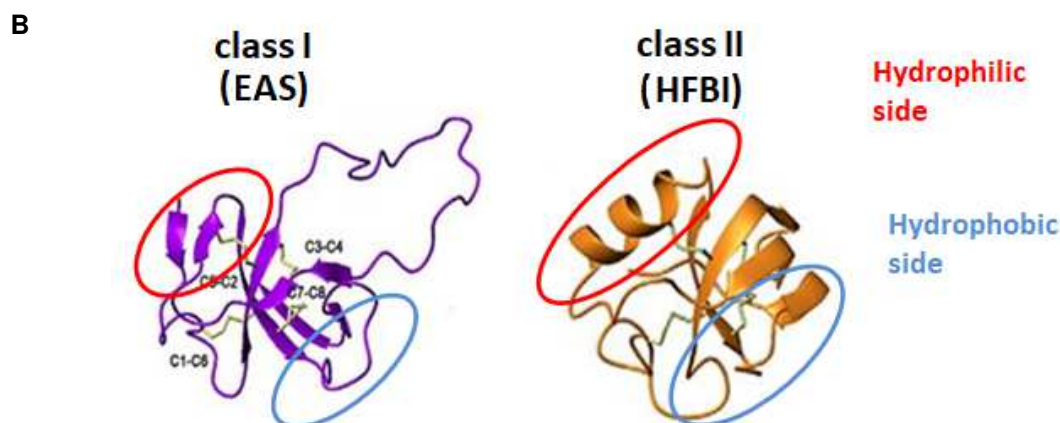
Fig. 6 — A: Amino acid sequence comparison of class I and II hydrophobins. The conserved Cys residues are highlighted with the conserved disulphide-bonding pattern indicated with brackets. **B**: Comparative models between class I (EAS from *Neurospora crassa*) and class II (HFBI from *Trichoderma reesei*) hydrophobin. The blue circle highlights the hydrophobic domains and the red circle the hydrophilic ones

Hydrophobin family can be divided into two distinct classes based on their structural differences, such as lengths of the inter-cysteine spaces and the stability of the amphipathic monolayers that they form. In particular, class I hydrophobins are produced in both ascomycetes and basidiomycetes species and the inter-cysteine space is more variable; class II hydrophobins are observed only in the ascomycetes and have a conserved length of the inter-cysteine spaces (Fig.6A). Moreover, fibrillar structures formed by class I hydrophobins, share many structural properties with amyloid fibrils. They assemble into insoluble polymeric layers, known as rodlets, extremely stable (resisting to hot 2% sodium dodecyl sulphate) and soluble only after harsh acid treatment (pure formic acid or trifluoroacetic acid (TFA))[23]. Class II aggregates are nonfibrillar and less stable, they can be more easily dissolved in detergent or organic solvents (i.e, ethanol or sodium dodecyl sulphate) [24]. Both classes of Hydrophobin for their intriguing properties have been exploited in many biotechnological applications [25], summarized in Table 1.

Table 1 – Biotechnological applications of hydrophobins

Application	Example
Industrial applications	
Emulsions	Personal care product, Food industry, Drug delivery
High-value applications	
Nanotechnology and diagnostic	Biosensors, Electrodes, DNA/protein Microarrays, Immunological assays
Tissue engineering	Biocompatibility of medical implants and devices
Separation technologies	Co-purification of hybridized protein of interest

The layers of hydrophobins can be exploited as an attractive platform to immobilize proteins on different surfaces, due to their adhesive abilities. Immobilization of proteins has been widely studied and several methods are used to functionalize surface [26]. For example, the adsorption method is the easiest and oldest

immobilization techniques [27]. The interaction between the target protein and the surface of the matrix occurs by various weak interactions such as electrostatic, hydrophobic/hydrophilic and van der waals forces. The cross-linking/covalent method is a conventional method for immobilization. It can be achieved by direct attachment between the protein and the material through a covalent linkage [28]. In the entrapment method target proteins are occluded in a permeable membrane (gel, fibre and microcapsule [29]) which allows the substrates and the products to pass, but it retains the target protein inside the network. In affinity binding, the target protein is linked to the matrix through specific interactions [30]. In most of these cases, immobilization leads to the reduction of the biological activity. The loss in activity could be due to changes in the protein conformation after immobilization, structural modification of the protein during immobilization, or changes in the protein microenvironment resulting from the interaction between the support and the protein.

Protein immobilization mediated by hydrophobin layer is a valid alternative to conventional methods and two main approaches have been carried out: deposition on a preformed self-assembled film [31–35], or genetical fusion to the self-assembling protein [36,37]. Protein immobilization by deposition on a preformed self-assembled film may depend on the characteristics of the adhering protein and has to be optimized varying pH and ionic strength [31]. A step forward the obtainment of a homogeneous biohybrid layer is the exploitation of genetic engineering techniques to combine the hydrophobins features with the specific properties of target proteins. Following this approach, the engineered fused proteins can be straightly used to functionalize surfaces with advantage in terms of time required and chemicals consumed.

Among surfaces functionalized by class I hydrophobins, it is worth underlining the possibility of functionalization of nanomaterials:

1.2 Nanotechnology and Nanomaterials

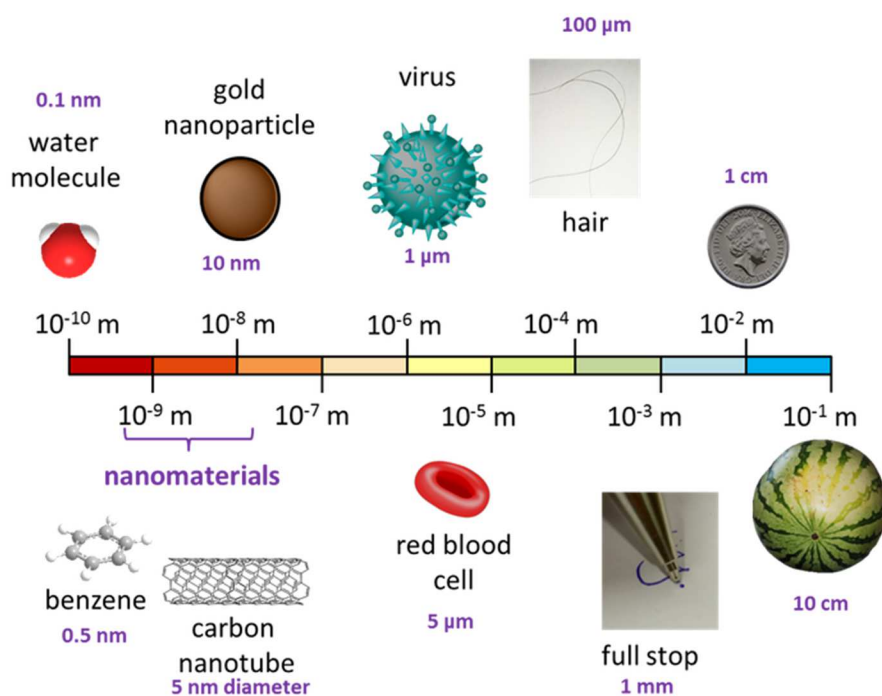The definition of a nanomaterial is an aggregate of atoms bonded together with a radius between 1 and 100 nm. (Fig.7)

Fig. 7 – Nanoscale

Nano system components are fabricated using top-down approach, that starts with a bulk or thin film material and removes selective regions to fabricate nanostructures, or bottom-up approach, that is based on molecular recognition and self-assembly to fabricate nanostructures out of smaller building blocks (molecules, colloids, and clusters).

When the dimension of a material is reduced from a large size, the properties remain the same at first, then small changes occur, until finally when the size drops below 100 nm, dramatic changes in properties can occur. If only one length of a three-dimensional nanostructure is of Nano dimension, the structure is referred to as a quantum well; if two sides are of nanometer length, the structure is referred to as a quantum wire. A quantum dot has all three dimensions in the nano range. The term *quantum* is associated with these three types of nanostructures because the changes in properties depend from the quantum-mechanical nature of physics in the domain of the ultrasmall. Thus physical, chemical e biological properties of nanomaterials are different from those of bulk matter. For instance, nanomaterials show *i)* high surface to volume ratio that makes them more chemically reactive; *ii)* optical properties that depend on parameters such as feature size, shape and surface characteristics; *iii)* magnetic properties that increase for particles small in size, in fact a paramagnetic bulk matter become a ferromagnetic cluster.

Hence, the advancement of nanomaterial research plays an essential role in the exploration of the biochemical and nanotechnological fields [38].

Graphene

Carbon materials are known to be more environmentally and biologically friendly than inorganic materials, since the carbon is one of the most common elements in our ecosystem. In particular, graphite is a naturally occurring material that has been used in our daily lives for hundreds of years without critical toxicity issues.

Graphene is the name given to a two-dimensional sheet of sp^2-hybridized carbon. Its extended honeycomb network is the fundamental building block of other important allotropes; it can be stacked to form 3D graphite, rolled to form 1D nanotubes, and wrapped to form 0D fullerenes [39] (Fig.8).
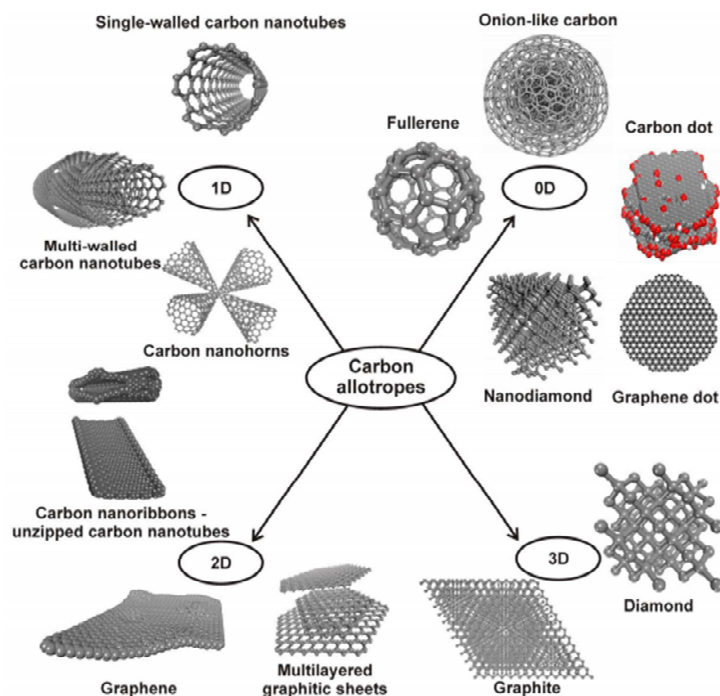

Fig. 8 – Carbon's allotropic forms

Graphene exhibits unparalleled properties such as high planar surface, superlative mechanical strength, remarkable thermal and electrical conductivity, high absorption of incident white light and highly efficient fluorescence quenching. Due to its extraordinary structure and fascinating properties, graphene is definitely the most studied nanomaterial [40]. Consequently, it can be integrated as the core of cutting-edge technologies and devices related to photonics, electronics, composite materials, environment, energy, biotechnology, biomedicine and biosensors [41]. Since the innovative discovery of the surprising properties of graphene, the industrial and scientific communities have focused their attention on the development of new graphene synthesis methods enabling a variety of options in terms of oxidation grade, number of layers, edge and basal defects, lateral size, quality, and cost for any particular application. According to the literature [42,43], the most relevant methods for graphene generation are the chemical vapor deposition, mechanical cleavage, wet chemical synthesis, and exfoliation of graphite [44]. Generally, liquid-phase exfoliation of graphite entails the use of ultrasonication as a key method which promotes the generation of laminated material that is subsequently bound to aggregate due to the lack of hydrophilic groups onto the exfoliated material. In fact, re/aggregation is one of the main challenges to address during the exfoliation procedure and the stabilization of solvent-dispersed graphene flakes [45]. However, re/aggregation is typically minimized by using organic solvents with suitable characteristics or surfactant–water solutions. Biological interfacing of graphene has become crucial to improve its biocompatibility and selectivity toward various applications in the biotechnological and biomedical fields [46]. Although graphene

modification and biofunctionalization are under active research, the *in situ* production of biofunctionalized graphene has been still little explored. However, fungal biosurfactants have been recently exploited to disperse and stabilize few-layered graphene in ethanol-water mixtures [47].

Carbon Nanotubes (CNT)

Carbon Nanotubes have sparked much excitement in recent years. These intriguing structures are an example of true nanotechnology: they are less than 100 nanometers in diameter and can be as thin as 1 or 2 nm, while they can be up to 18 centimeters in length [48]. Nanotubes have a very broad range of electronic, thermal, and structural properties that change depending on the different kinds of nanotube (defined by its diameter, length, and chirality, or twist). CNTs are made by rolling up of sheet of graphene into a cylinder. Depending on the number of concentrically rolled-up graphene sheets, they are also classified to single-walled (SWNT), double-walled (DWNT), and multiwalled (MWNT) (Fig.9). The structure of SWNT can be conceptualized by rolling-up layer of graphene into a seamless cylinder [49]. MWNT consists of two or more numbers of rolled-up concentric layers of graphene. DWNT is considered as a special type of MWNT where only two concentrically rolled up graphene sheets are present.
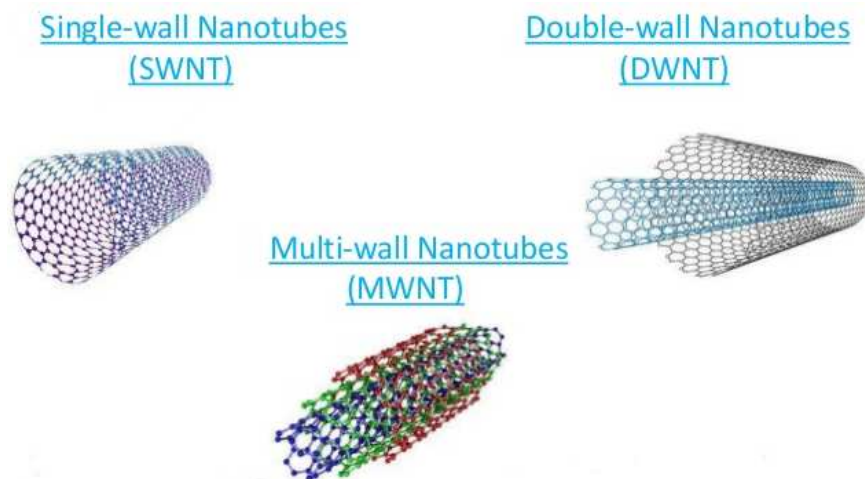
Fig. 9 – Basic structures of a single-walled, double-walled and multi-walled CNTs

CNTs have not only unique atomic arrangements but also have unique properties. These extraordinary properties of CNTs qualifies them exciting prospects and variety of applications. Particularly, in the area of microelectronics/nanoelectronics [50], CNTs and graphene nanoribbons (GNRs) demonstrates wide range of applications such as energy storage devices; energy conversion devices that includes thermoelectric [51] and photovoltaic [52] devices; field emission displays and radiation sources [53]; nanometer semiconductor transistors [54], nanoelectromechanical systems (NEMS) [55], electrostatic discharge (ESD) protection (Hyperion Catalysis), interconnects [56,57], and passives.

1.3 Applications of Functional Amyloids from Fungi: Surface Modification by Class I Hydrophobins

As a general introduction about functionalization of different surfaces with class I hydrophobins, the review published in 2017 on "Biomolecules" is reported below.

Applications of Functional Amyloids from Fungi: Surface Modification by Class I Hydrophobins

Alessandra Piscitelli [1] (iD)**, Paola Cicatiello [1], Alfredo Maria Gravagnuolo [1,2], Ilaria Sorrentino [1], Cinzia Pezzella [1] and Paola Giardina [1,*]**

[1]   Department of Chemical Sciences, Università degli Studi di Napoli Federico II, Complesso Universitario Monte S. Angelo, Via Cintia 4, 80126 Naples, Italy; apiscite@unina.it (A.P.); paola.cicatiello@unina.it (P.C.); alfredo.gravagnuolo@manchester.ac.uk (A.M.G.); ilaria.sorrentino@unina.it (I.S.); cpezzella@unina.it (C.P.)

[2]   Division of Pharmacy and Optometry, Faculty of Biology, Medicine and Health, The University of Manchester, M13 9PT Manchester, UK

*   Correspondence: giardina@unina.it; Tel.: +39-081-674-319

Abstract: Class I hydrophobins produced from fungi are amongst the first proteins recognized as functional amyloids. They are amphiphilic proteins involved in the formation of aerial structures such as spores or fruiting bodies. They form chemically robust layers which can only be dissolved in strong acids. These layers adhere to different surfaces, changing their wettability, and allow the binding of other proteins. Herein, the modification of diverse types of surfaces with Class I hydrophobins is reported, highlighting the applications of the coated surfaces. Indeed, these coatings can be exploited in several fields, spanning from biomedical to industrial applications, which include biosensing and textile manufacturing.

1. Introduction

In the last decade, several papers have reported that amyloids can fulfill important functional roles in a variety of biological processes of taxonomically distant organisms. Many organisms take advantage of the ability of polypeptides to form amyloids [1,2]. In filamentous fungi, amyloids are involved in numerous processes, e.g., in signal transduction mechanism, in which Nod-like receptors control the induction of programmed cell death [3]; controlling the translation termination by Sup35 [4] and the nitrogen catabolism by Ure2 [5]; and in the formation of aerial structures (spores or fruiting bodies) by amphipathic proteins known as hydrophobins (HFBs) [6]. HFBs self-assemble into an amphipathic membrane at hydrophilic : hydrophobic interfaces fulfilling many other fungal functions, such as the adherence of fungal structures to hydrophobic surfaces, including the surface of a host organism, thereby facilitating pathogenesis and playing a role in symbiosis [7]. Analysis of fungal genomes indicates that HFBs exist as gene families. Different HFBs are expressed at different stages in the fungal life cycle accomplishing specific functions [8].

The HFB family is composed of small proteins (<20 kDa) with high sequence variability, however they share a β-barrel motif in the 3D structure and a pattern of eight cysteine residues forming four disulfide bonds that stabilize the protein core [8]. These proteins are divided into two main classes based on their structural differences, such as the lengths of the inter-cysteine spaces, which determine their different properties. Class I HFBs assemble into insoluble polymeric layers composed of fibrillar structures known as rodlets and have a morphology like amyloid fibrils associated with diseases states [9–11]. These layers are extremely stable (resistant to treatment with hot 2% sodium

dodecyl sulfate), can only be solubilized with harsh acid treatments (very concentrated formic acid or trifluoroacetic acid) and the soluble forms can polymerize back into rodlets under appropriate conditions [12]. Conversely, the layers formed by class II hydrophobins lack the fibrillary rodlet morphology and can be solubilized with organic solvents and detergents [13].

Only class I HFBs belong to the functional amyloid family, since the structural and morphological similarities between rodlets and amyloid fibrils have been confirmed many times. Indeed, rodlets bind amyloid-specific dyes (Congo Red, Thioflavin T) and their diffraction pattern displays typical reflections of amyloid structures (4.8 and 10–12 Å). [9].

The propensity of class I HFBs to self-assemble and the presence of disorder portions in their soluble forms, has precluded the achievement of crystals suitable for X-ray crystallography. However 3D structures of soluble class I HFBs have been obtained by nuclear magnetic resonance (NMR) studies for the EAS from *Neurospora crassa* [9], DewA from the fungus *Aspergillus nidulans* [14], MPG1 from the fungus *Magnaporthe oryzae* [15], and very recently for SC16 from *Schizophyllum commune* [16].

Both classes of HFBs have been exploited in many biotechnological applications [17]. Bioinspired coatings based on HFBs can offer novel opportunities for surface modification [13]. Over the last decade the surfaces coated with the layers of HFBs have been employed to immobilize several enzymes of industrial interest, and several materials coated with HFBs and their engineered variants have been proven effective for a wide range of biotechnological applications. Taking into consideration the topic of this special issue, this review is focused on the recent advances in the use of the functional amyloids class I HFBs in surface coating, organizing the reported results based on the typology of the surfaces.

2. Metal and Metalloid Functionalization

Thin films of titanium show unique chemical, optical, and electrical properties [18]. The interest on their fabrication is increasing due to their attractive applications (i.e., microelectronic devices, photonic materials, high-efficiency catalysts, environmental remediation, optical devices, and medical treatments). Santhiya et al. [19] set up a novel method for the aqueous phase deposition of smooth, nanocrystalline TiO_2 thin films using a self-assembled HFB layer on a silicon substrate. In this report, the class I HFB used was H*Protein B, an engineered protein based on the class I HFB DewA from *A. nidulans*. A HFB layer on the silicon surface was prepared and used to deposit highly uniform nanocrystalline TiO_2 thin films. Resistance and elasticity properties of the developed films were compatible with implant coatings and other biomedical devices.

Boeuf et al. [20] engineered DewA from *A. nidulans* by inserting the RGD sequence or the laminin globular domain (LG3 binding motif) at surface-accessible sites of the protein to functionalize the surfaces of orthopedic implants made of titanium. The purified proteins were used to produce surfaces that can enhance the adhesion of the human cells, while the adhesion of *Staphylococcus aureus* did not increase, thus minimizing the risk of bacterial infection.

Vmh2 from *Pleurotus ostreatus* was used to functionalize different surfaces, such as silicon, steel and gold. Vmh2 forms a chemically and mechanically stable layer of self-assembled proteins on crystalline silicon. This biomolecular film was exploited as a masking material, since the protein film perfectly protected the coated silicon surface during the standard KOH etching process [21]. The protein-modified silicon surface exhibited also an improvement in wettability and suitability for the immobilization of other proteins, such as BSA or the enzyme laccase, improving its stability [22].

The self-assembled Vmh2 layer also changed the wettability of the Porous silicon (PSi) structures and protected this nanocrystalline material from the basic dissolution process. PSi is a versatile material owing to its peculiar morphological, physical, and chemical properties [23] The major drawback of the "as etched" PSi is its chemical instability, since it is oxidized at room temperature by atmospheric oxygen [24]. The Vmh2 coating added chemical stability to PSi (Figure 1), without altering the sensing ability of this optical transducer, which can be a key tool for biomolecular experiments.
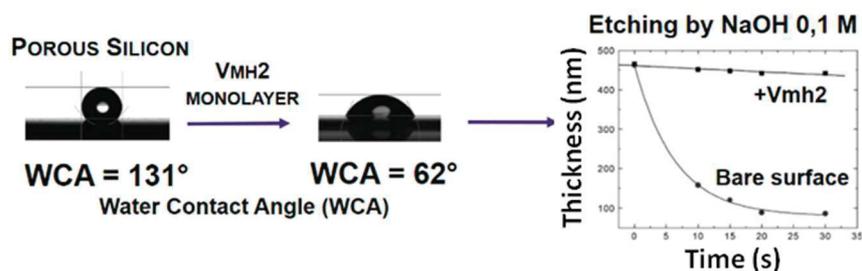
Figure 1. Change of wettability of PSi by Vmh2 and variation of PSi thickness with time, showing protection from etching by Vmh2.

The sample-loading steel plate used in matrix-assisted laser desorption/ionization time-of-flight mass spectrometry (MALDI-TOF MS) was stably coated by the Vmh2 layer and the functionalized support can be reused, since Vmh2 can be de-polymerized and solubilized. The hybrid surface was able to homogenously adsorb peptides and proteins whereas salts or denaturants could be washed away with water, allowing fast and high-throughput on-plate desalting prior to MS analysis [25]. Moreover, the function of the Vmh2 coating was expanded by immobilizing enzymes of interest in proteomics (trypsin, V8 protease, PNGaseF, and alkaline phosphatase) on the steel surface. High sequence coverage of model proteins and analysis of a whole proteome (whey milk) were achieved by rapid and efficient multiple enzyme digestions, serially performed on plate (Figure 2) [26]. The same procedure provided the opportunity to discriminate blood provenance even when two different blood sources were present in a mixture [27]. Phosphatases or deglycosidase were also immobilized on-plate, allowing the study of proteins with post-translational modifications [26].

The spontaneous self-assembling of Vmh2 on the gold surface was verified by using the quartz crystal-microbalance (QCM) and confirmed by spectroscopic ellipsometry [28]. The Vmh2 layer stably assembled on the gold QCM electrode was also used to perform a quantitative analysis of the Vmh2-glucose interaction.
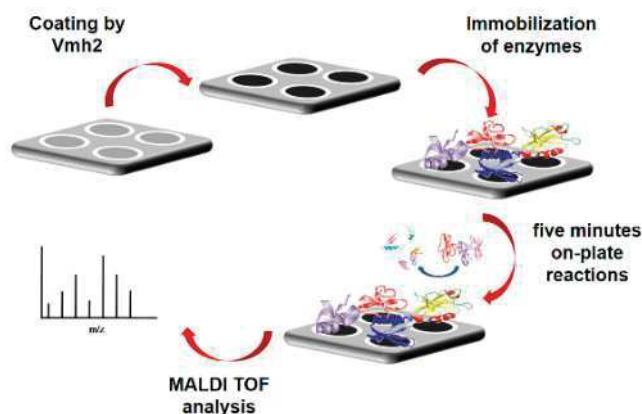
Figure 2. In situ reaction of trypsin immobilized on Vmh2 coated matrix-assisted laser desorption/ionization time-of-flight mass spectrometry (MALDI-TOF-MS) sample plate.

Additionally, gold nanoparticles (AuNPs) were synthesized, by a simple and novel process, in the presence of polyethylene-glycol (PEG), using Vmh2 to produce stable hybrid protein–metal nanoparticles, with outer surface rich in functional chemical groups [29]. Even though in the hybrid system the Vmh2 proteins were intrinsically bonded to the gold core, Vmh2-glucose interaction was confirmed, and the PEG-HFB-AuNPs was used in glucose monitoring [30].

3. Plastic Functionalization

Different plastic materials were modified using class I HFBs from both native and recombinant sources (Table 1). When heterologously produced, fused proteins composed of the HFB moiety and target proteins were successfully exploited. The modified materials were mainly used in the development of biomedical devices, examples of applications in biosensing and protein immobilization were demonstrated.

Platforms for protein immobilization were developed by using HGFI from *Grifola frondosa* native [31] and recombinant source [32]. On the other hand, the HFBs DewA and DewB from *A. nidulans* were fused to the laccase LccC from the same fungal source, developing an efficient system for laccase immobilization on polystyrene multiwell plates [33].

Table 1. Class I hydrophobins used in functionalization of plastic materials.

Application	HFB	Source	Surface	Refs.
Medical	eng SC3 [1] SC3—RGD [2] eng SC3—RGD [1,2]	*S. commune*	Teflon	[34–36]
	eng SC3 [1] SC3—RGD [2]	*S. commune*		[34–36]
	SC3 SC4	*S. commune*		[34–36]
	SC3	*S. commune*	Polystyrene Copolymer of benzoyl-1,4 phenylene and 1,3-phenylene	[37]
	eng DewA [1]	*A. nidulans*	Plastic biliary stent	[38]
	DewA DewA–RGD [2] DewA–LG3 [2]	*A. nidulans*	Polystyrene	[20]
	HGFI—TPS [2] HGFI—VGF [2] HGFI—VGF [2] HGFI—PA1 [2]	*G. frondosa* *G. frondosa* *G. frondosa* *G. frondosa*	Polycaprolattone	[39] [40] [41] [42]
	Vmh2 Pac3	*P. ostreatus* *Acremonium sclerotigenum*	Polystyrene	[43]
Biosensing	EAS EAS-α [2] Vmh2-GST [2] Vmh2-GFP [2]	*N. crassa* *P. ostreatus* *P. ostreatus*	Polystyrene	[44] [45] [46]
Immobilization	HGFI rHGFI [3] DewA–LccC [2] DewB–LccC [2]	*G. frondosa* *G. frondosa* *A. nidulans*	Polystyrene	[31] [32] [33]

[1] Recombinant engineered protein; [2] Recombinant fused protein; [3] Recombinant protein.

The exploitation of plastic surfaces coated with class I HFBs for biomedical devices was started by the pioneering work of Scholtmeijer et al. and Janssen and coworkers, who exploited the class I HFBs SC3 and SC4 (either native or recombinant engineered fused HFBs) in the functionalization of Teflon surfaces [34–36]. In that work, as well as in other examples, the main interest was in the development of biocompatible surfaces that allow both adhesion of human cells and tissue regeneration. Indeed, the HFBs were fused to different cell adhesion-mediating motifs and proved to be effective in the design of materials for regenerative medicine [20,39]. Moreover, Wang et al. and Zhao et al. [31,40] fused the HGFI to the vascular endothelial growth factor (VEGF), an effective molecule able to regulate the proliferation, migration, and survival pathways of endothelial cells [41].

Other examples of medical applications are the development of antibacterial devices [42] by the fusion of the bacteriocin pediocin PA-1 to HGFI. Furthermore, the layers formed by two fungal hydrophobins (Vmh2 and Pac3 from *A. sclerotigenum* [47]) reduce the biofilm formed by different strains of *Staphylococcus epidermidis* on polystyrene surfaces, without affecting the cell vitality [43]. Polymeric surfaces with enhanced lubricity and reduced surface friction were obtained using SC3 by Misra and coworkers [37]. Biliary plastic stents with delayed clogging process were developed thanks to the coating with the HFB, alone or in combination with heparin [38].

Considering biosensing applications, the EAS HFB from *N. crassa* fused to the yeast peptide pheromone α-factor was used in the detection and quantification of this pheromone [44]. Upon functionalization of polystyrene multiwell plate with a combination of HFBs either lacking or exposing the α-factor, an inverted enzyme-linked immunosorbent assay (ELISA) approach was developed yielding a novel kind of biosensor with the lowest limit of detection reported at the time of publication. Vmh2 from *P. ostreatus* fused to the enzyme glutathione-S-transferase (Vmh2-GST) was exploited for the quantification of the pesticides molinate and captan, acting as inhibitors of the enzymatic activity [45]. The fused protein efficiently functionalized the polystyrene multiwell plate for the development of high throuput analyses (Figure 3).
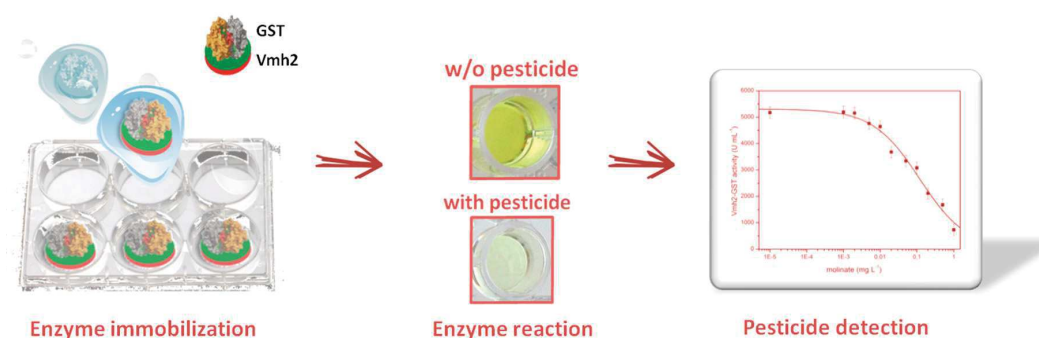
Figure 3. Pesticide biosensor developed on polystyrene multiwell plate coated with Vmh2-GST fused proteins

Vmh2 adhesion ability was also combined with the fluorescence emission of the Green Fluorescent Protein (GFP) by genetic fusion [46]. Vmh2-GFP was proven to be a smart and effective tool for the study of Vmh2 self-assembling and was used as the active biological element in the realization of an ultrasensitive thrombin biosensor. Since the two proteins were linked by the specific cutting site of the thrombin, a decrease in the fluorescence intensity of the sample was observed due to the cleavage of the linker by thrombin and the subsequent desorption of the GFP from the surface (Figure 4).
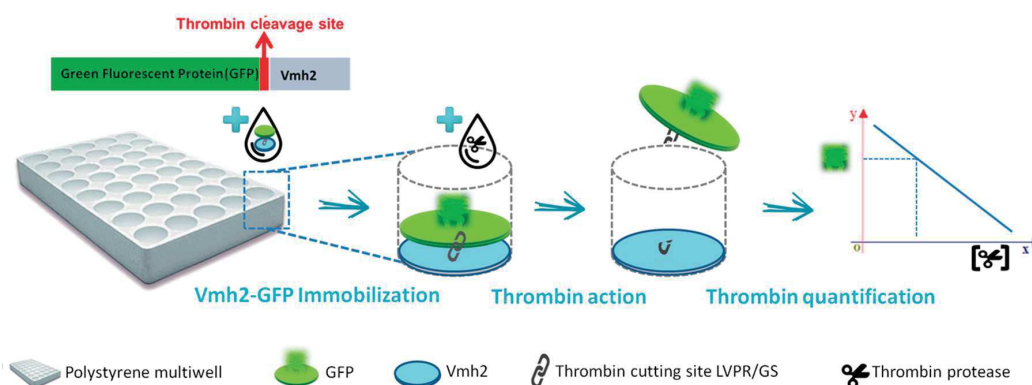
Figure 4. Thrombin biosensor developed on polystyrene multiwell plate coated with Vmh2-GFP fused proteins.

4. Carbon Nanotubes and 2D Materials Functionalization

Since 2D materials possess high surface area to volume ratio, they can be exploited in enzyme immobilization, obtaining high enzyme loading and increasing the reaction kinetics, thus improving biocatalytic efficiency for industrial applications. Carbon nanotubes (CNT), graphene, and the semiconducting transition metal dichalcogenides MoS_2 and WS_2 were dispersed and coated by class I HFBs [48–51]. Few layer microsheets of graphene were produced and dispersed by ultrasonic wave exfoliation of low-cost graphite in the presence of Vmh2 in water-ethanol solutions (Figure 5) [49]. Notably, the non-covalent nature of the amphiphilic protein–carbon interactions preserved the band structure of sp^2-carbon lattice. The functionalized bio-hybrid material was endowed with the self-assembling properties of Vmh2 (including the ability to form homogeneous films), controlled by environmental factors, and is a valuable material for biotechnological applications, such as sensing, nanomedicine, and bioelectronic technologies.

hydrophilic side
hydrophobic side
Vmh2
Graphite
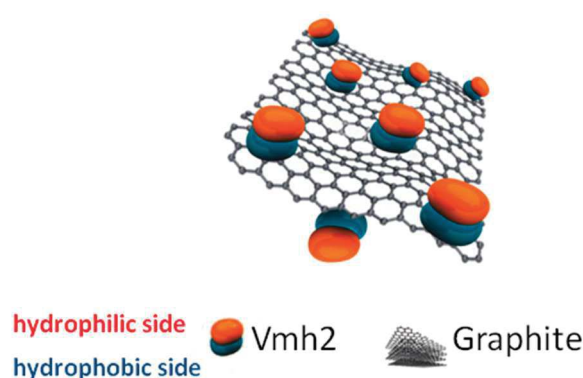
Figure 5. Biofunctionalized graphene produced by in situ exfoliation of graphite in the presence of Vmh2.

When Vmh2 was interfaced to MoS_2 and WS_2 nanosheets their ζ-potential could be tuned to control the stability of the dispersions. Stable liquid dispersions of high quality few-layered, photoluminescent and bio-functionalized nanosheets of 2D materials were produced [50].

5. Functionalization of Other Materials

5.1. Biosensing and Biomedical Applications

The recombinant HFB of the fungus *Pisolithus tinctorius* HYDPt-1 was used to immobilize small, electroactive molecules on three different electrode substrates: glassy carbon electrode (GCE), thin mercury film electrode (TMFE) and hydrophilic surfaces such as a gold electrode (GE) [52]. These promising results were evolved in the settings of stable, enzyme-based catalytic surfaces for applications in biosensing [53]. Two redox enzymes, glucose oxidase and horseradish peroxidase, which are utilized in biosensing, were immobilized on SC3 HFB coated GCE and were active for more than one month.

The applications of HGFI in surface wettability conversion on mica (patterning applications), glass (cell culture and protein fixation) and polydimethylsiloxane (biomedical devices), were investigated by Hou et al. [54]. The coated surfaces were used as platform for antibody immobilization to set up an immunoassay system, thus showing a feasible strategy for biosensor device fabrication.

The ability of class I HFB to functionalize glass surface was demonstrated by Rieder and coworkers [55]. Recently, the spontaneous self-assembling of Vmh2 at liquid–solid interfaces was exploited to achieve the highly homogeneous glass functionalization in 4 min, coating 1880 cm^2 of glass per mg of protein [56]. The Vmh2-coated glass slides were proven to immobilize not only proteins, but also nanomaterials such as graphene oxide (GO) and cadmium telluride (CdTe) quantum dots (QDs).

This novel glass substrate can be amenable for optical biosensing applications in the microarray format. Moreover, two HFB proteins were exploited in dental repair applications. DewA_4 and DewA_5 showed binding abilities to hydroxyapatite in a mouthwash formulation and an increased nucleation in artificial saliva [57].

5.2. Textiles Finishing Processes

The non-toxic and biodegradable properties of HFBs can have great potential in textile surface modification, changing properties such as wettability, and flame resistance. After HFB deposition, hydrophobic fabrics resulted in a significant hydrophilization, while hydrophilic textiles attained strong hydrophobic character [58]. Cotton fabrics coated by the H*Protein B HFB displayed an enhanced flame resistance, suggesting that the use of these proteins can be an alternative strategy for the design of sustainable and green flame retardants [59]. The normal finishing agents that confer the anti-microbial resistance to textiles have low adherence and poor uniformity. The use of H*Protein A and H*Protein B avoided these drawbacks and the formed uniform layer of HFBs and antimicrobial agents (Ag and ZnO) on cotton/poly ester fabrics inhibited different bacterial species [60].

5.3. Biocatalytic Transformations

Palomo et al. [61] used *P. ostreatus* HFBs to build a functionalized agarose support to immobilize different lipases. The immobilized lipases underwent the typical mechanism of interfacial activation on hydrophobic supports. Hence the time required for the immobilization procedure was offset by the improvement of the catalytic activity, stability and enantioselectivity of the enzyme.

More recently, the physiological role of HFBs to cover the wall of mycelium was used to change the surface characteristics of *Pichia pastoris* cells, opening the frontiers to the development of new high efficiency cell catalysts [62]. Surface display of fungal HFBs SC3 successfully modified the hydrophobicity of the surface of yeast cells.

6. Conclusion

HFBs can represent robust and reliable green alternatives to chemical strategies in surface functionalization. Albeit the number of applications of Class I HFBs is quite large in laboratory scale, the full potential of these proteins is yet to be realized. The main bottleneck for their utilization is the lack of production systems at industrial level. Most HFBs cannot yet be produced in gram per liter quantities, thus limiting their use. Currently, only BASF succeeded in the production of the two recombinant class I HFBs, H*Protein A and B, in quantities sufficient for large-scale applications [63]. This result suggests that industrial applications of hydrophobins are expected in the near future.

Author Contributions: A. P., P.C., A. M. G. and P. G. wrote the review. C. P. and I. S. were involved in the literature search.

Conflicts of Interest: The authors declare no conflicts of interest.

References

1. Fowler, D.M.; Koulov, A.V.; Balch, W.E.; Kelly, J.W. Functional amyloid—From bacteria to humans. *Trends. Biochem. Sci.* **2007**, *32*, 217–224. [CrossRef] [PubMed]
2. Chapman, M.R.; Robinson, L.S.; Pinkner, J.S.; Roth, R.; Heuser, J.; Hammar, M.; Normark, S.; Hultgren, S.J. Role of *Escherichia coli* curli operons in directing amyloid fiber formation. *Science* **2002**, *295*, 851–855. [CrossRef] [PubMed]
3. Loquet, A.; Saupe, S. Diversity of Amyloid Motifs in NLR Signaling in Fungi. *Biomolecules* **2017**, *7*, 38. [CrossRef] [PubMed]

4.　Shorter, J.; Lindquist, S. Prions as adaptive conduits of memory and inheritance. *Nat. Rev. Genet.* **2005**, *6*, 435–450. [CrossRef] [PubMed]

5.　Wickner, R.B. [URE3] as an altered URE2 protein: Evidence for a prion analog in *Saccharomyces cerevisiae*. *Science* **1994**, *264*, 566–569. [CrossRef] [PubMed]

6.　Zampieri, F.; Wösten, H.A.B.; Scholtmeijer, K. Creating surface properties using a palette of hydrophobins. *Materials (Basel)* **2010**, *3*, 4607–4625. [CrossRef]

7.　Whiteford, J.R.; Spanu, P.D. Hydrophobins and the interactions between fungi and plants. *Mol. Plant Pathol.* **2002**, *3*, 391–400. [CrossRef] [PubMed]

8.　Sunde, M.; Kwan, A.H.Y.; Templeton, M.D.; Beever, R.E.; Mackay, J.P. Structural analysis of hydrophobins. *Micron* **2008**, *39*, 773–784. [CrossRef] [PubMed]

9.　Kwan, A.H.Y.; Winefield, R.D.; Sunde, M.; Matthews, J.M.; Haverkamp, R.G.; Templeton, M.D.; Mackay, J.P. Structural basis for rodlet assembly in fungal hydrophobins. *Proc. Natl. Acad. Sci. USA* **2006**, *103*, 3621–3626. [CrossRef] [PubMed]

10.　Macindoe, I.; Kwan, A.H.; Ren, Q.; Morris, V.K.; Yang, W.; Mackay, J.P.; Sunde, M. Self-assembly of functional, amphipathic amyloid monolayers by the fungal hydrophobin EAS. *Proc. Natl. Acad. Sci. USA* **2012**, *109*, E804–E811. [CrossRef] [PubMed]

11.　Houmadi, S.; Rodriguez, R.D.; Longobardi, S.; Giardina, P.; Fauré, M.C.; Giocondo, M.; Lacaze, E. Self-Assembly of Hydrophobin Protein Rodlets Studied with Atomic Force Spectroscopy in Dynamic Mode. *Langmuir* **2012**, *28*, 2551–2557. [CrossRef] [PubMed]

12.　Lo, V.; Ren, Q.; Pham, C.; Morris, V.; Kwan, A.; Sunde, M. Fungal Hydrophobin Proteins Produce Self-Assembling Protein Films with Diverse Structure and Chemical Stability. *Nanomaterials* **2014**, *4*, 827–843. [CrossRef] [PubMed]

13.　Linder, M.B. Hydrophobins: Proteins that self assemble at interfaces. *Curr. Opin. Colloid Interface Sci.* **2009**, *14*, 356–363. [CrossRef]

14.　Morris, V.K.; Kwan, A.H.; Sunde, M. Analysis of the Structure and Conformational States of DewA Gives Insight into the Assembly of the Fungal Hydrophobins. *J. Mol. Biol.* **2013**, *425*, 244–256. [CrossRef] [PubMed]

15.　Pham, C.L.L.; Rey, A.; Lo, V.; Soulès, M.; Ren, Q.; Meisl, G.; Knowles, T.P.J.; Kwan, A.H.; Sunde, M. Self-assembly of MPG1, a hydrophobin protein from the rice blast fungus that forms functional amyloid coatings, occurs by a surface-driven mechanism. *Sci. Rep.* **2016**, *6*, 25288. [CrossRef] [PubMed]

16.　Gandier, J.-A.; Langelaan, D.N.; Won, A.; O'Donnell, K.; Grondin, J.L.; Spencer, H.L.; Wong, P.; Tillier, E.; Yip, C.; Smith, S.P.; Master, E.R. Characterization of a Basidiomycota hydrophobin reveals the structural basis for a high-similarity Class I subdivision. *Sci. Rep.* **2017**, *7*, 45863. [CrossRef] [PubMed]

17.　Wösten, H.A.B.; Scholtmeijer, K. Applications of hydrophobins: Current state and perspectives. *Appl. Microbiol. Biotechnol.* **2015**, *99*, 1587–1597. [CrossRef] [PubMed]

18.　Chen, X.; Mao, S.S. Titanium Dioxide Nanomaterials: Synthesis, Properties, Modifications, and Applications. *Am. Chem. Rev.* **2007**, *107*, 2891–2959. [CrossRef] [PubMed]

19.　Santhiya, D.; Burghard, Z.; Greiner, C.; Jeurgens, L.P.H.; Subkowski, T.; Bill, J. Bioinspired Deposition of TiO_2 Thin Films Induced by Hydrophobins. *Langmuir* **2010**, *26*, 6494–6502. [CrossRef] [PubMed]

20.　Boeuf, S.; Throm, T.; Gutt, B.; Strunk, T.; Hoffmann, M.; Seebach, E.; Mühlberg, L.; Brocher, J.; Gotterbarm, T.; Wenzel, W.; et al. Engineering hydrophobin DewA to generate surfaces that enhance adhesion of human but not bacterial cells. *Acta Biomater.* **2012**, *8*, 1037–1047. [CrossRef] [PubMed]

21.　De Stefano, L.; Rea, I.; Armenante, A.; Giardina, P.; Giocondo, M.; Rendina, I. Self-assembled biofilm of hydrophobins protects the silicon surface in the KOH wet etch process. *Langmuir* **2007**, *23*, 7920–7922. [CrossRef] [PubMed]

22.　De Stefano, L.; Rea, I.; De Tommasi, E.; Rendina, I.; Rotiroti, L.; Giocondo, M.; Longobardi, S.; Armenante, A.; Giardina, P. Bioactive modification of silicon surface using self-assembled hydrophobins from *Pleurotus ostreatus*. *Eur. Phys. J. E* **2009**, *30*, 181–185. [CrossRef] [PubMed]

23.　Canham, L.K. *Properties of Porous Silicon*; Canham, L., Ed.; The Institution of Electrical Engineers: London, UK, 1997.

24.　De Stefano, L.; Rea, I.; Giardina, P.; Armenante, A.; Rendina, I. Protein-Modified Porous Silicon Nanostructures. *Adv. Mater.* **2008**, *20*, 1529–1533. [CrossRef]

25. Longobardi, S.; Gravagnuolo, A.M.; Rea, I.; De Stefano, L.; Marino, G.; Giardina, P. Hydrophobin-coated plates as matrix-assisted laser desorption/ionization sample support for peptide/protein analysis. *Anal. Biochem.* **2014**, *449*, 9–16. [CrossRef] [PubMed]

26. Longobardi, S.; Gravagnuolo, A.M.; Funari, R.; Della Ventura, B.; Pane, F.; Galano, E.; Amoresano, A.; Marino, G.; Giardina, P. A simple MALDI plate functionalization by Vmh2 hydrophobin for serial multi-enzymatic protein digestions. *Anal. Bioanal. Chem.* **2015**, *407*, 487–496. [CrossRef] [PubMed]

27. Patel, E.; Cicatiello, P.; Deininger, L.; Clench, M.R.; Marino, G.; Giardina, P.; Langenburg, G.; West, A.; Marshall, P.; Sears, V.; et al. A proteomic approach for the rapid, multi-informative and reliable identification of blood. *Analyst* **2016**, *141*, 191–198. [CrossRef] [PubMed]

28. Della Ventura, B.; Rea, I.; Caliò, A.; Giardina, P.; Gravagnuolo, A.M.; Funari, R.; Altucci, C.; Velotta, R.; De Stefano, L. Vmh2 hydrophobin layer entraps glucose: A quantitative characterization by label-free optical and gravimetric methods. *Appl. Surf. Sci.* **2016**, *364*, 201–207. [CrossRef]

29. Politi, J.; De Stefano, L.; Longobardi, S.; Giardina, P.; Rea, I.; Methivier, C.; Pradier, C.M.; Casale, S.; Spadavecchia, J. The amphiphilic hydrophobin Vmh2 plays a key role in one step synthesis of hybrid protein-gold nanoparticles. *Coll. Surf. B Biointerfaces* **2015**, *136*, 214–221. [CrossRef] [PubMed]

30. Politi, J.; De Stefano, L.; Rea, I.; Gravagnuolo, A.M.; Giardina, P.; Methivier, C.; Casale, S.; Spadavecchia, J. One-pot synthesis of a gold nanoparticle-Vmh2 hydrophobin nanobiocomplex for glucose monitoring. *Nanotechnology* **2016**, *27*, 195701. [CrossRef] [PubMed]

31. Wang, Z.; Huang, Y.; Li, S.; Xu, H.; Linder, M.B.; Qiao, M. Hydrophilic modification of polystyrene with hydrophobin for time-resolved immunofluorometric assay. *Biosens. Bioelectron.* **2010**, *26*, 1074–1079. [CrossRef] [PubMed]

32. Niu, B.; Li, B.; Wang, H.; Guo, R.; Liang, H.; Qiao, M.; Li, W. Preparing bioactive surface of polystyrene with hydrophobin for trypsin immobilization. *Mater. Res. Express* **2016**, *3*, 055402. [CrossRef]

33. Fokina, O.; Fenchel, A.; Winandy, L.; Fischer, R. Immobilization of LccC Laccase from *Aspergillus nidulans* on Hard Surfaces via Fungal Hydrophobins. *Appl. Environ. Microbiol.* **2016**, *82*, 6395–6402. [PubMed]

34. Scholtmeijer, K.; Janssen, M.I.; Gerssen, B.; de Vocht, M.L.; van Leeuwen, B.M.; van Kooten, T.G.; Wösten, H.A.B.; Wessels, J.G.H. Surface modifications created by using engineered hydrophobins. *Appl. Environ. Microbiol.* **2002**, *68*, 1367–1373. [CrossRef] [PubMed]

35. Janssen, M.I.; van Leeuwen, M.B.M.; Scholtmeijer, K.; van Kooten, T.G.; Dijkhuizen, L.; Wösten, H.A.B. Coating with genetic engineered hydrophobin promotes growth of fibroblasts on a hydrophobic solid. *Biomaterials* **2002**, *23*, 4847–4854. [CrossRef]

36. Janssen, M.I.; van Leeuwen, M.B.; van Kooten, T.G.; de Vries, J.; Dijkhuizen, L.; Wösten, H.A. Promotion of fibroblast activity by coating with hydrophobins in the β-sheet end state. *Biomaterials* **2004**, *25*, 2731–2739. [CrossRef] [PubMed]

37. Misra, R.; Li, J.; Cannon, G.C.; Morgan, S.E. Nanoscale reduction in surface friction of polymer surfaces modified with SC3 hydrophobin from *Schizophyllum commune*. *Biomacromolecules* **2006**, *7*, 1463–1470. [CrossRef] [PubMed]

38. Weickert, U.; Wiesend, F.; Subkowski, T.; Eickhoff, A.; Reiss, G. Optimizing biliary stent patency by coating with hydrophobin alone or hydrophobin and antibiotics or heparin: An in vitro proof of principle study. *Adv. Med. Sci.* **2011**, *56*, 138–144. [CrossRef] [PubMed]

39. Huang, Y.; Zhang, S.; Niu, B.; Wang, D.; Wang, Z.; Feng, S.; Xu, H.; Kong, D.; Qiao, M. Poly(ε-caprolactone) modified with fusion protein containing self-assembled hydrophobin and functional peptide for selective capture of human blood outgrowth endothelial cells. *Coll. Surf. B Biointerfaces* **2013**, *101*, 361–369. [CrossRef] [PubMed]

40. Zhao, L.; Ma, S.; Pan, Y.; Zhang, Q.; Wang, K.; Song, D.; Wang, X.; Feng, G.; Liu, R.; Xu, H.; et al. Functional Modification of Fibrous PCL Scaffolds with Fusion Protein VEGF-HGFI Enhanced Cellularization and Vascularization. *Adv. Healthc. Mater.* **2016**, *5*, 2376–2385. [CrossRef] [PubMed]

41. Wang, K.; Zhang, Q.; Zhao, L.; Pan, Y.; Wang, T.; Zhi, D.; Ma, S.; Zhang, P.; Zhao, T.; Zhang, S.; et al. Functional Modification of Electrospun Poly(ε-caprolactone) Vascular Grafts with the Fusion Protein VEGF–HGFI Enhanced Vascular Regeneration. *ACS Appl. Mater. Interfaces* **2017**, *9*, 11415–11427. [CrossRef] [PubMed]

42. Wang, X.; Mao, J.; Chen, Y.; Song, D.; Gao, Z.; Zhang, X.; Bai, Y.; Saris, P.E.J.; Feng, H.; Xu, H.; et al. Design of antibacterial biointerfaces by surface modification of poly (ε-caprolactone) with fusion protein containing hydrophobin and PA-1. *Coll. Surf. B Biointerfaces* **2017**, *151*, 255–263. [CrossRef] [PubMed]

43.   Artini, M.; Cicatiello, P.; Ricciardelli, A.; Papa, R.; Selan, L.; Dardano, P.; Tilotta, M.; Vrenna, G.; Tutino, M.L.; Giardina, P.; et al. Hydrophobin coating prevents *Staphylococcus epidermidis* biofilm formation on different surfaces. *Biofouling* **2017**, in press.

44.   Hennig, S.; Rödel, G.; Ostermann, K. Hydrophobin-Based Surface Engineering for Sensitive and Robust Quantification of Yeast Pheromones. *Sensors (Basel)* **2016**, *16*, 602. [CrossRef] [PubMed]

45.   Piscitelli, A.; Pennacchio, A.; Longobardi, S.; Velotta, R.; Giardina, P. Vmh2 hydrophobin as a tool for the development of self-immobilizing enzymes for biosensing. *Biotechnol. Bioeng.* **2017**, *114*, 46–52. [CrossRef] [PubMed]

46.   Piscitelli, A.; Pennacchio, A.; Cicatiello, P.; Politi, J.; De Stefano, L.; Giardina, P. Rapid and ultrasensitive detection of active thrombin based on the Vmh2 hydrophobin fused to a Green Fluorescent Protein. *Biosens. Bioelectron.* **2017**, *87*, 816–822. [CrossRef] [PubMed]

47.   Cicatiello, P.; Dardano, P.; Pirozzi, M.; Gravagnuolo, A.M.; De Stefano, L.; Giardina, P. Self-assembly of two hydrophobins from marine fungi affected by interaction with surfaces. *Biotechnol. Bioeng.* **2017**. [CrossRef] [PubMed]

48.   Wang, Z.; Wang, Y.; Huang, Y.; Li, S.; Feng, S.; Xu, H.; Qiao, M. Characterization and application of hydrophobin-dispersed multi-walled carbon nanotubes. *Carbon N. Y.* **2010**, *48*, 2890–2898. [CrossRef]

49.   Gravagnuolo, A.M.; Morales-Narvaez, E.; Longobardi, S.; Da Silva, E.T.; Giardina, P.; Merkoci, A. In situ production of biofunctionalized few-layer defect-free microsheets of graphene. *Adv. Funct. Mater.* **2015**, *25*, 2771–2779. [CrossRef]

50.   Kaur, J.; Gravagnuolo, A.M.; Maddalena, P.; Altucci, C.; Giardina, P.; Gesuele, F. Green synthesis of luminescent and defect-free bio-nanosheets of MoS 2: Interfacing two-dimensional crystals with hydrophobins. *RSC Adv.* **2017**, *7*, 22400–22408. [CrossRef]

51.   Yang, W.; Ren, Q.; Wu, Y.-N.; Morris, V.K.; Rey, A.A.; Braet, F.; Kwan, A.H.; Sunde, M. Surface functionalization of carbon nanomaterials by self-assembling hydrophobin proteins. *Biopolymers* **2013**, *99*, 84–94. [CrossRef] [PubMed]

52.   Bilewicz, R.; Witomski, J.; Van der Heyden, A.; Tagu, D.; Béatrice Palin, A.; Rogalska, E. Modification of Electrodes with Self-Assembled Hydrophobin Layers. *J. Phys. Chem. B* **2001**, *105*, 9772–9777. [CrossRef]

53.   Corvis, Y.; Walcarius, A.; Rink, R.; Mrabet, N.T.; Rogalska, E. Preparing Catalytic Surfaces for Sensing Applications by Immobilizing Enzymes via Hydrophobin Layers. *Anal. Chem.* **2005**, *77*, 1622–1630. [CrossRef] [PubMed]

54.   Hou, S.; Li, X.; Li, X.; Feng, X.-Z.; Wang, R.; Wang, C.; Yu, L.; Qiao, M.-Q. Surface modification using a novel type I hydrophobin HGFI. *Anal. Bioanal. Chem.* **2009**, *394*, 783–789. [CrossRef] [PubMed]

55.   Rieder, A.; Ladnorg, T.; Wöll, C.; Obst, U.; Fischer, R.; Schwartz, T. The impact of recombinant fusion-hydrophobin coated surfaces on E. coli and natural mixed culture biofilm formation. *Biofouling* **2011**, *27*, 1073–1085. [CrossRef] [PubMed]

56.   Gravagnuolo, A.M.; Morales-Narvaez, E.; Matos, C.R.S.; Longobardi, S.; Giardina, P.; Merkoci, A. On-the-Spot Immobilization of Quantum Dots, Graphene Oxide, and Proteins via Hydrophobins. *Adv. Funct. Mater.* **2015**, *25*, 6084–6092. [CrossRef]

57.   Melcher, M.; Facey, S.J.; Henkes, T.M.; Subkowski, T.; Hauer, B. Accelerated Nucleation of Hydroxyapatite Using an Engineered Hydrophobin Fusion Protein. *Biomacromolecules* **2016**, *17*, 1716–1726. [CrossRef] [PubMed]

58.   Opwis, K.; Gutmann, J.S. Surface modification of textile materials with hydrophobins. *Text. Res. J.* **2011**, *81*, 1594–1602. [CrossRef]

59.   Alongi, J.; Carletto, R.A.; Bosco, F.; Carosio, F.; Di Blasio, A.; Cuttica, F.; Antonucci, V.; Giordano, M.; Malucelli, G. Caseins and hydrophobins as novel green flame retardants for cotton fabrics. *Polym. Degrad. Stab.* **2014**, *99*, 111–117. [CrossRef]

60.   Dumitrescu, I.; Iordache, O.G.; Mocioiu, A.M.; Nicula, G. Antimicrobial functionalization of textile materials with hydrophobins and Ag/ZnO composite nanopowders. *Ind. Text.* **2013**, *64*, 303–312.

61.   Palomo, J.M.; Peñas, M.M.; Fernández-Lorente, G.; Mateo, C.; Pisabarro, A.G.; Fernández-Lafuente, R.; Ramírez, L.; Guisán, J.M. Solid-Phase Handling of Hydrophobins: Immobilized Hydrophobins as a New Tool To Study Lipases. *Biomacromolecules* **2003**, *4*, 204–210. [CrossRef] [PubMed]

62.　Wang, P.; He, J.; Sun, Y.; Reynolds, M.; Zhang, L.; Han, S.; Liang, S.; Sui, H.; Lin, Y. Display of fungal hydrophobin on the *Pichia pastoris* cell surface and its influence on *Candida antarctica* lipase B. *Appl. Microbiol. Biotechnol.* **2016**, *100*, 5883–5895. [CrossRef] [PubMed]

63.　Wohlleben, W.; Subkowski, T.; Bollschweiler, C.; von Vacano, B.; Liu, Y.; Schrepp, W.; Baus, U. Recombinantly produced hydrophobins from fungal analogues as highly surface-active performance proteins. *Eur. Biophys. J.* **2010**, *39*, 457–468. [CrossRef] [PubMed]

1.4   Vmh2: A Class I Hydrophobin from *Pleurotus ostreatus*

In this project the development of new hybrid devices is explored by exploiting the properties of Vmh2, a hydrophobin extensively studied by our research group. This protein is extracted and purified from the mycelium of the basidiomycete fungus *Pleurotus ostreatus* [58]. *P. ostreatus* is a commercially important edible fungus, used as a source of proteins and other chemicals for industrial applications [59]. The family of genes coding for its hydrophobins is large and complex, and the function of these proteins depends on different growth stages [60]. Vmh2 appears to be the most hydrophobic hydrophobin characterized so far, and shows an unconventional conversion presenting predominantly β-sheet forms which is modulated by protein concentration and the environmental conditions (Fig.10). This process is promoted by increase in temperature, acidic pH, or by the presence of Ca^{2+} ions [61,62]. In the latter conditions it spontaneously self-assembles forming aggregates and isolated, micrometer long, and twisted amyloid fibrils. However, the pure protein is soluble in ethanol solution, or in aqueous buffers at pH higher than 7.
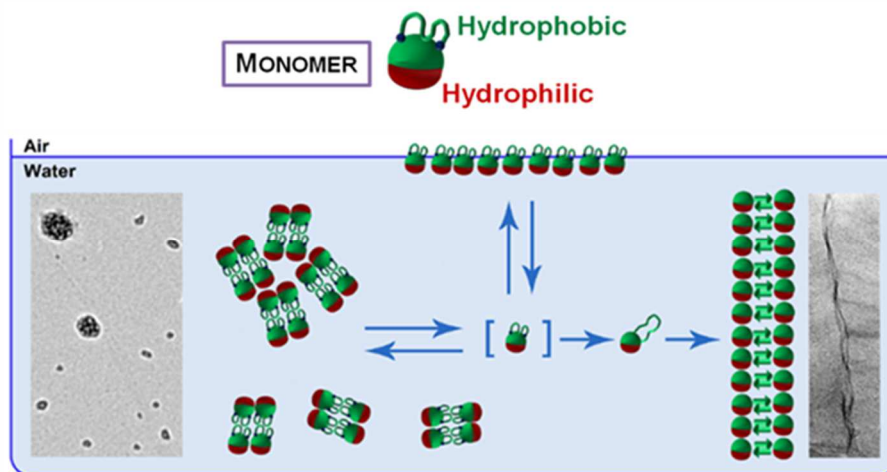

Fig. 10 – Schematic representation of the Vmh2 behavior in solution (adapted from [62])

More recently, to clarify the molecular determinants which play a key role in Vmh2 self-assembly, five mutants were produced by site-directed mutagenesis and then characterized. The obtained results were explained on the basis of a reliable 3D model built using the structure of another class I hydrophobin Sc16 from *Schizophyllum commune* as template (Fig.11A), and a possible mechanism of formation of amyloids was proposed [63]. In the proposed model (Fig.11B), part of the loop L1 (red), the region identified as the most prone towards aggregation, changes conformation forming a β-hairpin, which represents the β-spine of the fibrils, whereas the bulk of the protein is accommodated externally.
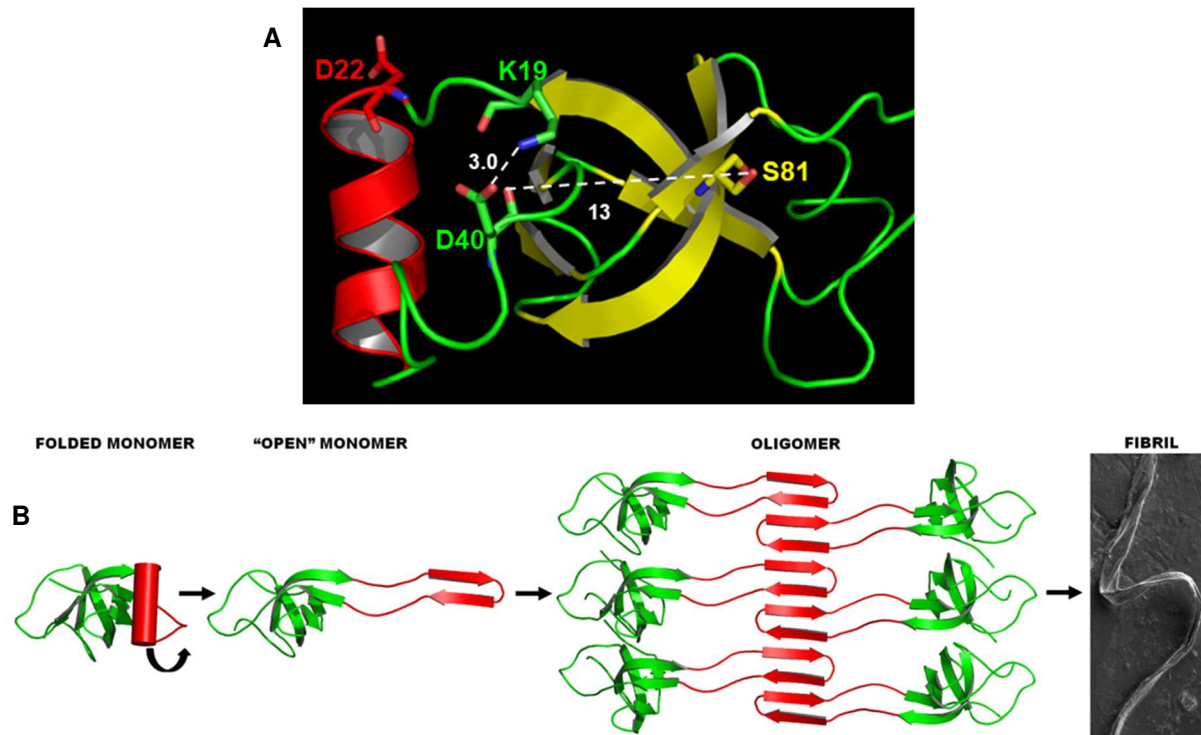
Fig. 11 – A: Vmh2 model based on Sc16, ribbons are coloured by secondary structure (red, helices; green, loops; yellow, strands); **B**: A model for the formation of fibrils proposed after site-directed mutagenesis studies (adapted from [63])

Taking advantage by genetic engineering techniques, two systems of Vmh2 of genetical fusion have been set up and promising results were obtained in both cases. The first system is based on the recombinant production in *Escherichia coli* as inclusion bodies of Vmh2 fused to the enzyme Glutathione-S-Transferase (GST) to develop a biosensor to quantify toxic compounds in aqueous environmental samples [36]. In the second system recombinant Vmh2 fused to the Green Fluorescent Protein (GFP) has been expressed and secreted by the yeast *Pichia pastoris* [37]. The Vmh2-GFP fusion protein has proven to be an effective tool for the study of Vmh2 self-assembling and for the development of a high sensitivity biosensor to monitor the thrombin in plasma samples.

These attractive results make the hydrophobin-protein chimera a highly interesting platform for the development of new biodevices. In this case, the main advantage of the genetic fusion is to combine both adhesive and self-assembling properties of the hydrophobin Vmh2 with the properties of the target protein. Indeed, versatile and simple immobilization methods able to functionalize a wide range of surfaces, can be developed selecting suitable target proteins to be fused to Vmh2.

1.5 Aim of this thesis: work description

The main purpose of this PhD project is to develop versatile and straightforward systems of surface functionalization through immobilization of hydrophobin-protein chimera to expand their use in several fields, spanning from biomedical to industrial applications, including biosensing. Thus, taking advantage by genetic engineering techniques, Vmh2 has been expressed in two different microorganisms fused to target proteins for the development of self-immobilizing chimera proteins. In these new proteins the Vmh2 moiety anchor the target protein onto a surface in its active

form obtaining a bio / non-bio hybrid surface with unique characteristics. In particular, three classes of target proteins, such as an oxidative enzyme (laccase), an antimicrobial peptides (LL37), and an antibody (anti-mesothelin antibody), have been used to design, produce and characterize different chimeric proteins for surface functionalization and lay the foundation of their applications.
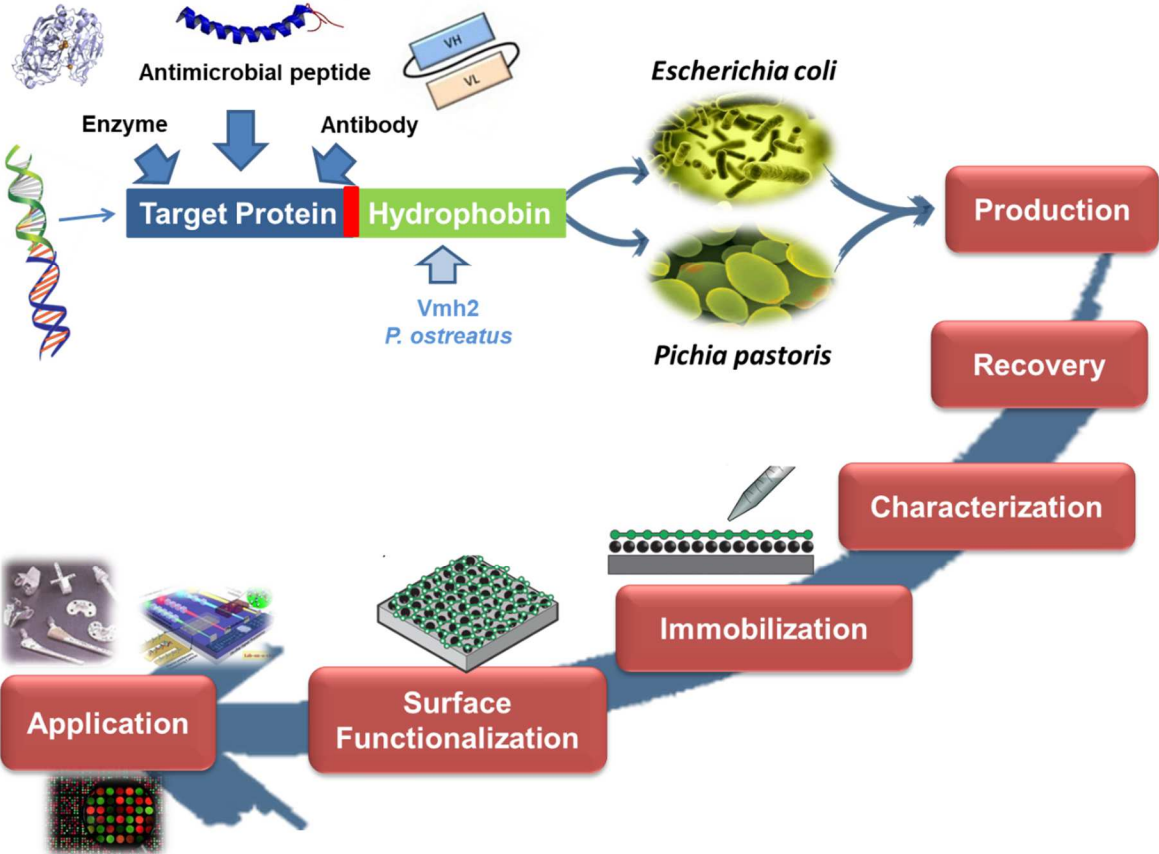
Fig. 12 – Aim of my PhD project: target proteins will be fused to Vmh2 hydrophobin to develop functionalized surfaces

1.6 References

1. Serra, P. A. *Biosensors-Emerging Materials and Applications Edited*. (2011).

2. Humenik, M. & Scheibel, T. Nanomaterial building blocks based on spider silk-oligonucleotide conjugates. *ACS Nano* **8,** 1342–1349 (2014).

3. Dehsorkhi, A., Castelletto, V. & Hamley, I. W. Self-assembling amphiphilic peptides. *J. Pept. Sci.* **20,** 453–467 (2014).

4. Hosseinkhani, H., Hong, P. Da & Yu, D. S. Self-assembled proteins and peptides for regenerative medicine. *Chem. Rev.* **113,** 4837–4861 (2013).

5. Knowles, T. P. *et al.* Role of intermolecular forces in defining material properties of protein nanofibrils. *Science* **318,** 1900–3 (2007).

6. Nagel-Steger, L., Owen, M. C. & Strodel, B. An Account of Amyloid Oligomers: Facts and Figures Obtained from Experiments and Simulations. *ChemBioChem* **17,** 657–676 (2016).

7. Ruggeri, F. S. *et al.* Infrared nanospectroscopy characterization of oligomeric and fibrillar aggregates during amyloid formation. *Nat. Commun.* **6,** 7831 (2015).

8. Fitzpatricka, A. W. P. *et al. Atomic structure and hierarchical assembly of a cross-β amyloid fibril. Proc Natl Acad Sci U S A* **5590,** (2013).

9. Tycko, R. & Wickner, R. B. Molecular Structures of Amyloid and Prion Fibrils: Consensus versus Controversy. *Acc. Chem. Res.* **46,** 1487–1496 (2013).

10. EANES, E. D. & GLENNER, G. G. X-RAY DIFFRACTION STUDIES ON AMYLOID FILAMENTS. *J. Histochem. Cytochem.* **16,** 673–677 (1968).

11. Sunde, M. *et al.* Common core structure of amyloid fibrils by synchrotron X-ray diffraction 1 1Edited by F. E. Cohen. *J. Mol. Biol.* **273,** 729–739 (1997).

12. Schleeger, M. *et al.* Amyloids: From molecular structure to mechanical properties. *Polym. (United Kingdom)* **54,** 2473–2488 (2013).

13. Blanco, L. P., Evans, M. L., Smith, D. R., Badtke, M. P. & Matthew, R. NIH Public Access. **20,** 66–73 (2013).

14. Gebbink, M. F. B. G., Claessen, D., Bouma, B., Dijkhuizen, L. & Wösten, H. A. B. Amyloids — a functional coat for microorganisms. *Nat. Rev. Microbiol.* **3,** 333–341 (2005).

15. Fowler, D. M., Koulov, A. V., Balch, W. E. & Kelly, J. W. Functional amyloid - from bacteria to humans. *Trends Biochem. Sci.* **32,** 217–224 (2007).

16. Chapman, M. R. *et al.* Role of Escherichia coli Curli Operons in Directing Amyloid Fiber Formation. *Science (80-.).* **295,** 851–855 (2002).

17. Bleem, A. & Daggett, V. Structural and functional diversity among amyloid proteins: Agents of disease, building blocks of biology, and implications for

molecular engineering. *Biotechnol. Bioeng.* **114,** 7–20 (2017).

18. Knowles, T. P. J. & Mezzenga, R. Amyloid Fibrils as Building Blocks for Natural and Artificial Functional Materials. *Adv. Mater.* **28,** 6546–6561 (2016).

19. Zampieri, F., Wösten, H. A. B. & Scholtmeijer, K. Creating Surface Properties Using a Palette of Hydrophobins. *Materials (Basel).* **3,** 4607–4625 (2010).

20. Whiteford, J. R. & Spanu, P. D. Hydrophobins and the interactions between fungi and plants. *Mol. Plant Pathol.* **3,** 391–400 (2002).

21. Linder, M. B. Hydrophobins: Proteins that self assemble at interfaces. *Curr. Opin. Colloid Interface Sci.* **14,** 356–363 (2009).

22. De Vocht, M. L. *et al.* Self-assembly of the hydrophobin SC3 proceeds via two structural intermediates. *Protein Sci.* **11,** 1199–1205 (2002).

23. Kwan, A. H. Y. *et al.* Structural basis for rodlet assembly in fungal hydrophobins. *Proc. Natl. Acad. Sci.* **103,** 3621–3626 (2006).

24. Bayry, J., Aimanianda, V., Guijarro, J. I., Sunde, M. & Latgé, J.-P. Hydrophobins—Unique Fungal Proteins. *PLoS Pathog.* **8,** e1002700 (2012).

25. Wösten, H. A. B. & Scholtmeijer, K. Applications of hydrophobins: current state and perspectives. *Appl. Microbiol. Biotechnol.* **99,** 1587–1597 (2015).

26. Datta, S., Christena, L. R. & Rajaram, Y. R. S. Enzyme immobilization: an overview on techniques and support materials. *3 Biotech* **3,** 1–9 (2013).

27. Brady, D. & Jordaan, J. Advances in enzyme immobilisation. *Biotechnol. Lett.* **31,** 1639–1650 (2009).

28. Wong, L. S., Thirlway, J. & Micklefield, J. Direct Site-Selective Covalent Protein Immobilization Catalyzed by a Phosphopantetheinyl Transferase. *J. Am. Chem. Soc.* **130,** 12456–12464 (2008).

29. BERNFELD, P. & WAN, J. ANTIGENS AND ENZYMES MADE INSOLUBLE BY ENTRAPPING THEM INTO LATTICES OF SYNTHETIC POLYMERS. *Science* **142,** 678–9 (1963).

30. Porath, J. Immobilized metal ion affinity chromatography. *Protein Expr. Purif.* **3,** 263–81 (1992).

31. Wang, Z., Lienemann, M., Qiau, M. & Linder, M. B. Mechanisms of protein adhesion on surface films of hydrophobin. *Langmuir* **26,** 8491–8496 (2010).

32. De Stefano, L. *et al.* Bioactive modification of silicon surface using self-assembled hydrophobins from Pleurotus ostreatus. *Eur. Phys. J. E* **30,** 181–185 (2009).

33. Qin, M. *et al.* Bioactive Surface Modification of Mica and Poly(dimethylsiloxane) with Hydrophobins for Protein Immobilization. *Langmuir* **23,** 4465–4471 (2007).

34. Zhao, Z.-X. *et al.* Amperometric glucose biosensor based on self-assembly

hydrophobin with high efficiency of enzyme utilization. *Biosens. Bioelectron.* **22,** 3021–3027 (2007).

35. Longobardi, S. *et al.* A simple MALDI plate functionalization by Vmh2 hydrophobin for serial multi-enzymatic protein digestions. *Anal. Bioanal. Chem.* **407,** 487–496 (2015).

36. Piscitelli, A., Pennacchio, A., Longobardi, S., Velotta, R. & Giardina, P. Vmh2 hydrophobin as a tool for the development of "self-immobilizing" enzymes for biosensing. *Biotechnol. Bioeng.* **114,** 46–52 (2017).

37. Piscitelli, A. *et al.* Rapid and ultrasensitive detection of active thrombin based on the Vmh2 hydrophobin fused to a Green Fluorescent Protein. *Biosens. Bioelectron.* **87,** 816–822 (2017).

38. Bechet, D. *et al.* Nanoparticles as vehicles for delivery of photodynamic therapy agents. *Trends Biotechnol.* **26,** 612–621 (2008).

39. Allen, M. J., Tung, V. C. & Kaner, R. B. Honeycomb Carbon: A Review of Graphene. *Chem. Rev.* **110,** 132–145 (2010).

40. Geim, A. K. Graphene: status and prospects. *Science* **324,** 1530–4 (2009).

41. Morales-Narváez, E. & Merkoçi, A. Graphene Oxide as an Optical Biosensing Platform. *Adv. Mater.* **24,** 3298–3308 (2012).

42. Novoselov, K. S. *et al.* A roadmap for graphene. *Nature* **490,** 192–200 (2012).

43. Ferrari, A. C. *et al.* Science and technology roadmap for graphene, related two-dimensional crystals, and hybrid systems. *Nanoscale* **7,** 4598–4810 (2015).

44. Eigler, S. & Hirsch, A. Chemistry with Graphene and Graphene Oxide-Challenges for Synthetic Chemists. *Angew. Chemie Int. Ed.* **53,** 7720–7738 (2014).

45. Park, S. & Ruoff, R. S. Chemical methods for the production of graphenes. *Nat. Nanotechnol.* **4,** 217–224 (2009).

46. Chung, C. *et al.* Biomedical Applications of Graphene and Graphene Oxide. *Acc. Chem. Res.* **46,** 2211–2224 (2013).

47. Gravagnuolo, A. M. *et al.* In Situ Production of Biofunctionalized Few-Layer Defect-Free Microsheets of Graphene. *Adv. Funct. Mater.* **25,** 2771–2779 (2015).

48. Javey, A. & Kong, J. *Carbon nanotube electronics.* (Springer, 2009).

49. Majumder, M., Chopra, N. & Hinds, B. J. Mass Transport through Carbon Nanotube Membranes in Three Different Regimes: Ionic Diffusion and Gas and Liquid Flow. *ACS Nano* **5,** 3867–3877 (2011).

50. Avouris, P., Chen, Z. & Perebeinos, V. Carbon-based electronics. *Nat. Nanotechnol.* **2,** 605–615 (2007).

51. Wei, P., Bao, W., Pu, Y., Lau, C. N. & Shi, J. Anomalous Thermoelectric Transport of Dirac Particles in Graphene. *Phys. Rev. Lett.* **102,** 166808 (2009).

52. Ago, H., Petritsch, K., Shaffer, M. S. P., Windle, A. H. & Friend, R. H. Composites of Carbon Nanotubes and Conjugated Polymers for Photovoltaic Devices. *Adv. Mater.* **11,** 1281–1285 (1999).

53. Choi, W. B. *et al.* Electrophoresis deposition of carbon nanotubes for triode-type field emission display. *Appl. Phys. Lett.* **78,** 1547–1549 (2001).

54. Collins, P. G., Arnold, M. S. & Avouris, P. Engineering carbon nanotubes and nanotube circuits using electrical breakdown. *Science* **292,** 706–9 (2001).

55. Dadgour, H., Cassell, A. M. & Banerjee, K. Scaling and variability analysis of CNT-based NEMS devices and circuits with implications for process design. in *2008 IEEE International Electron Devices Meeting* 1–4 (IEEE, 2008). doi:10.1109/IEDM.2008.4796742

56. Kreupl, F. *et al.* Carbon nanotubes in interconnect applications. *Microelectron. Eng.* **64,** 399–408 (2002).

57. Banerjee, K. *et al.* Carbon Nanomaterials for Next-Generation Interconnects and Passives: Physics, Status, and Prospects. *IEEE Trans. Electron Devices* **56,** (2009).

58. Armenante, A. *et al.* The Pleurotus ostreatus hydrophobin Vmh2 and its interaction with glucans. *Glycobiology* **20,** 594–602 (2010).

59. Giardina, P. *et al.* The gene, protein and glycan structures of laccase from Pleurotus ostreatus. *Eur. J. Biochem.* **235,** 508–515 (1996).

60. Peñas, M. M., Rust, B., Larraya, L. M., Ramírez, L. & Pisabarro, A. G. Differentially regulated, vegetative-mycelium-specific hydrophobins of the edible basidiomycete Pleurotus ostreatus. *Appl. Environ. Microbiol.* **68,** 3891–8 (2002).

61. Longobardi, S. *et al.* Environmental Conditions Modulate the Switch among Different States of the Hydrophobin Vmh2 from Pleurotus ostreatus. *Biomacromolecules* **13,** 743–750 (2012).

62. Gravagnuolo, A. M. *et al.* Class i Hydrophobin Vmh2 Adopts Atypical Mechanisms to Self-Assemble into Functional Amyloid Fibrils. *Biomacromolecules* **17,** 954–964 (2016).

63. Pennacchio, A., Cicatiello, P., Notomista, E., Giardina, P. & Piscitelli, A. New clues into the self-assembly of Vmh2, a basidiomycota class I hydrophobin. *Biol. Chem.* **399,** 895–901 (2018).
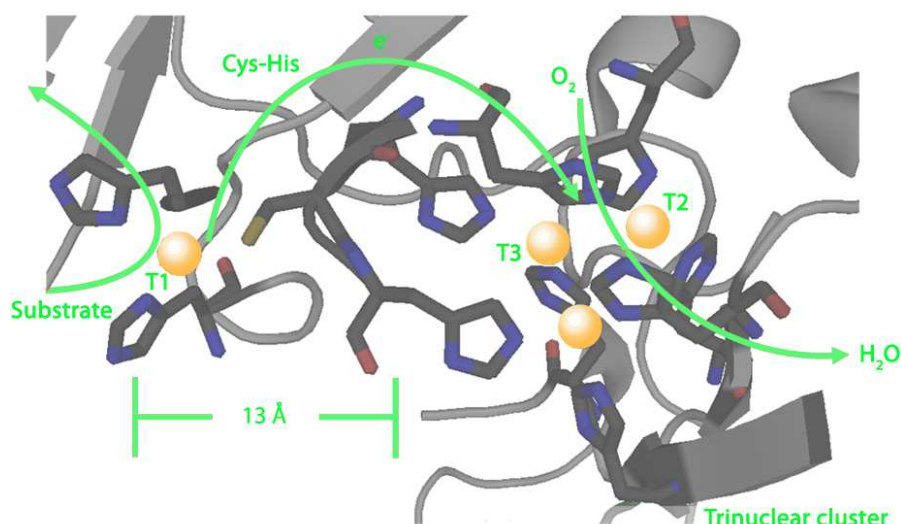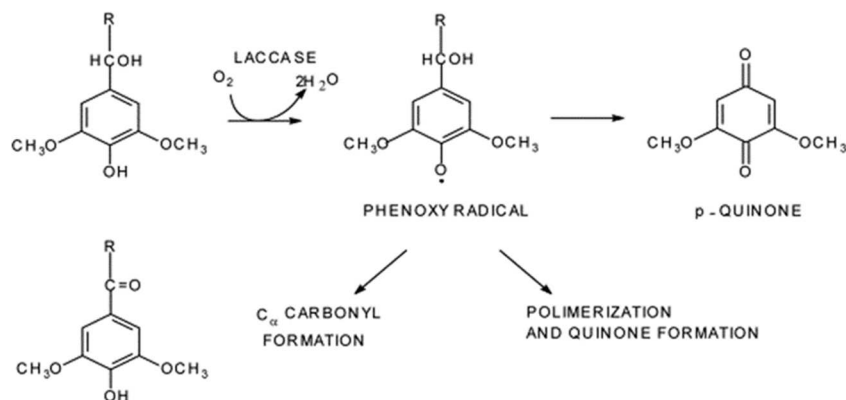
2. LACCASE
2.1 Introduction

Laccases (EC 1.10.3.2, p-diphenol dioxigen oxidoreductase) are one of the very few enzymes that have been studied since the end of 19th century and extensively exploited for many industrial purposes. During recent years this class of oxidative enzymes, being energy-saving and biodegradable, is attracting increasing interest for eco-friendly industries. Laccases represent the largest subgroup of Multicopper Oxidases (MCO). They are ubiquitary enzymes, the presence of laccase-like enzyme has been reported in bacteria (*Azospirillum lipoferum*)[1], plant, fungi and insects (*Bombix sp*)[2]. The functions of the enzyme differ from organism to organism and typify the diversity of laccase in nature. Laccases can be mainly divided into two groups: laccases from higher plants and those from fungi. Fungal laccases are widely distributed in ascomycetes, duteromycetes, and basidiomycetes. Expression of different patterns of laccase isoenzymes coded by gene families is differentially regulated, depending on growth conditions and physiological states[3]. Several studies indicated that the expression of most fungal laccase genes is affected by metal ions, such as copper and cadmium, and by aromatic compounds[3]. Although many studies on laccase activity have been conducted, its biological role in fungi is not yet completely defined. Fungal laccases are suggested to carry out a variety of physiological roles including morphogenesis, lignocellulose degradation, soil organic matter recycling, fruiting body formation, different pathways of pigment production, fungal plant-pathogen/host interaction, defense, stress response to diverse environmental challenges[4]. Most of fungal laccases are monomeric glycoproteins of approximately 60–70 kDa with an acidic isoelectric point (pI) around pH 4.0, even if several exceptions exist[4]. Their glycosydic moiety generally accounts for 10-25% of their molecular weight, rarely for more than 30%[5]. Glycosylation of fungal laccases is one of the main problems for the heterologous production of the enzyme. Laccases couple single-electron oxidations of various substrates to the four-electron reduction of dioxygen to water. The catalysis is guaranteed by the presence of different copper centers in the active site. In particular, typical metal content of laccases includes one type-1 (T1) copper, and one type-2 (T2) and two type-3 (T3) copper ions, these last arranged in a trinuclear cluster (TNC)[4] (Fig.13). Copper Type 1 is involved in the oxidation of four reducing substrates by catalyzing four-electron extraction. These four electrons are transferred to T2/T3, where molecular oxygen is reduced to water[6]. Two histidines and one cysteine serve as ligands for type-1 Cu. Type 2 center is 3-coordinate with two histidines and water as ligands. Type 3 copper ions are 4-coordinate, having three histidines as ligands[7,8]. The histidines and the cysteine are spread over four highly conserved amino acid regions. These regions are considered fungal laccase signature sequences (L1-L4) and include not only residues involved in copper binding, but also residues responsible to maintain a local three-dimensional fold[9]. The different copper centers can be identified on the basis of their spectroscopic properties. The T1 copper is characterized by a strong absorption around 600 nm, whereas the T2 copper exhibits only weak absorption in the visible region. The T2 site is electron paramagnetic resonance (EPR)-active, whereas the two copper ions of the T3 site are EPR-silent due to an antiferromagnetic coupling mediated by a bridging ligand.

Fig. 13 – Structure of the laccase active site with arrows marking the flow of substrates, electrons (e⁻) and O_2 (adapted from [4])

The wide range of laccase substrates includes aromatic compounds (ortho- and para-diphenols, methoxysubstituted phenols, diamines, benzenethiols), metal ions (Mn^{2+}), organometallic compounds (e.g. $[W(CN)8]^{4-}$, $[Fe(EDTA)]^{2+}$), organic redox compounds (e.g. 2,2′-azino-bis(3-ethylbenzothiazoline6-sulphonic acid), ABTS; 1-hydroxybenzotriazole, HBT) and the iodide anion[10,11]. Laccases use oxygen as the electron acceptor to oxidize phenolic hydroxyl groups. This reaction gives rise to radicals that can spontaneously rearrange, leading to fission of C-C or C-O bonds of the alkyl side chains, or to cleavage of aromatic rings [12] (Fig.14).

Fig. 14 – General reaction of oxidation of phenolic hydroxyl groups by laccases

Frequently, however, substrates of interest cannot be oxidized directly by laccases, either because they are too large to penetrate into the enzyme active site or because they have a particularly high redox potential. By mimicking nature, it is possible to overcome this limitation with the addition of so-called 'chemical mediators', which are suitable compounds that act as intermediate substrates for the laccase, whose oxidized radical forms are able to interact with the bulky or high redox-potential substrate targets (Fig.15). Then, in the presence of both natural and synthetic redox mediators, the catalytic activity of these enzymes may be expanded to non-phenolic substrates (e.g. polycyclic aromatic hydrocarbons (PAH), polychlorinated biphenyls, azodyes or organophosphate pesticides)[13].
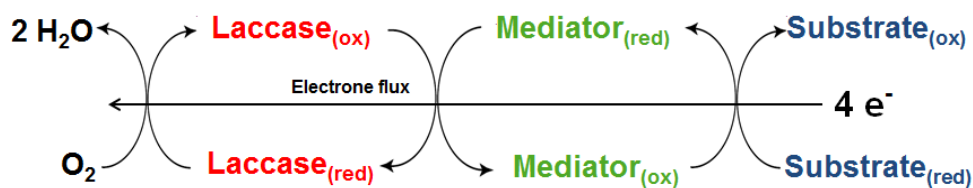
Fig. 15 – General scheme of laccases chemical mediator

Laccases have been subject of intensive research in the last decades due to their non-specific substrate and consequently oxidation of a broad spectrum of structurally different substrates. Their uses span in several fields like food industry, textile and petrochemical industries, bioremediation processes. Recently, laccases have also been applied in nanobiotecnology and in the design of biosensors and biofuel cells. Thus, electrode-based biosensors using a monolayer of laccase as bio-element have been developed for the determination of phenolic compounds in several real matrix [14,15].

Laccases from *Pleurotus ostreatus*

The white-rot fungus *P. ostreatus*, belonging to basidiomycetes, has been widely exploited for its abilities in bioremediation processes[16–19] and can be considered an invaluable source of oxidases. In particular, six different laccases isoenzymes have been isolated and characterised according to the culture conditions. These isoenzymes represent a variegated group of laccases endowed with peculiar properties. POXC is a canonical laccase, most abundantly produced under different growth conditions[20]. POXA1b is a neutral blue laccase very stable at alkaline pH[21] and with a high redox potential[22], POXA3 is an atypical heterodimeric laccase, constituted by a large subunit, clearly homologous to other fungal laccases, and a small subunit ssPOXA3, probably involved in the stabilization of the complex[23–25]. LACC12 is a laccase isolated from *P. ostreatus* fruiting body[26]. Finally, Pox3, Pox4 and Pox5 coding genes have been identified in this fungus, although their corresponding proteins have never been isolated in the culture broth.

2.2 Straightforward laccase immobilization by means of a laccase-hydrophobin chimera

Phenols are among the most abundant organic impurities penetrating into the environment as a result of their use in a large number of processes, from paper industry to synthesis of plastics and pharmaceuticals. Because most phenolic compounds exhibit a high degree of toxicity, they have been included in the list of high priority pollutants by several countries. To monitor these compounds, a rapid and reliable process for their determination is therefore necessary. In order to achieve this objective, multi-well plate with immobilized chimera protein was used to develop fast and easy-to-use biosensing platform to monitor phenols which is significantly advantageous in terms of sensitivity, surface bioconjugation, chemical stability and nontoxicity. Then, the first protein to be fused to the hydrophobin has been a laccase enzyme, to combine the adhesive self-assembling properties of Vmh2 to the catalytic abilities of POXA1b. Among the laccases from *P. ostreatus* POXA1b was chosen for fusion to hydrophobin for its peculiar characteristics: *i)* stability and activity in a wide range of pHs (3–9) and temperatures (25°–65 °C); *ii)* high redox potential (+0.650 V); *iii)* high production level in heterologous hosts. Such

an attractive enzyme enlarges the range of its potential biotechnological applications. This enzyme has been successfully used as template for the selection of random mutants with further improved features[27–29]. Indeed, PoxA1b has been already successfully expressed and produced in the yeast *P. pastoris* in a consolidated process with a competitive cost[30]. Moreover, laccase immobilization on solid surface has already been proven as a useful tool to develop efficient applications[31], either as biosensors[32] or in bioconversion processes [33,34].

The developments and the biosensing applications of this new fusion protein are described below (submitted to "Applied Microbiology and Biotechnology").

2.3 Immobilization of chimeric enzymes on graphene surfaces

Introduction

Recently in our laboratory, a process for production of biofunctionalized Graphene-based nanomaterials (GBMs) in ethanol-water mixtures have been set out, using ultrasonic waves in synergy with class I hydrophobin Vmh2[35]. Herein, both POXA1b and the chimera protein POXA1b-Vmh2 were exploited to functionalize nanomaterials (NMs) through a one-step approach (Fig.16). The main goal is the achievement of new nanobiocatalysts, exploiting the singular properties of Vmh2, NMs and POXA1b.
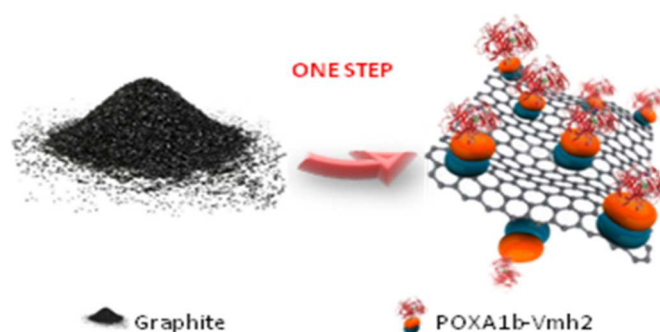
Fig. 16 – Biofunctionalized graphene produced by in situ exfoliation of graphite in the presence of Vmh2 and POXA1b.

Ultrasonication of graphite powder in different conditions was explored to produce biofunctionalized graphene, and the obtained nanomaterials were characterized in terms of graphene concentration and laccase loaded. The results of the concentration of graphene are in agreement with the literature.

Conclusions

The immobilization of enzymes on the nanomaterial surface to develop novel biosensing platforms has been carried out, exploiting the properties of the hydrophobin Vmh2, the graphene and the laccase PoxA1b. This enzyme from *P. ostreatus* displays a high redox potential and is endowed with a remarkable stability at high temperature and at alkaline pH, thus it can be used to detect phenolic compounds in different matrices. The fusion with Vmh2 allowed to use the enzyme for coating different surfaces without additional purification steps, thanks to the self-assembling property of the hydrophobin. The achieved results were listed below:

- The bio-functionalization of graphene with PoxA1b-Vmh2 was achieved with the addition of 4 Utot of the enzyme in the last 10 minutes of the exfoliation. An immobilization yield of 11% was calculated by laccase activity assay.
- The t½ and the specific activity on graphene (26 days and 0.4 U/mg) were estimated and the results showed that PoxA1b-Vmh2 was more stable and more active than PoxA1b.
- The biofunctionalized graphene with the fused enzyme was deposited on GCE and used as working electrode for a chronoamperometric test for the revelation of catechol. The result of these experiments demonstrated that this technique could represent a feasible option for the detection of catechol in real sample systems such as tap water.

2.4 POXC laccase from *Pleurotus ostreatus*: a high-performance multicopper enzyme for direct Oxygen Reduction Reaction operating in a proton-exchange membrane fuel cell

MCOs have been used to elaborate enzymatic biofuel cells (EBFCs), a sub-class of fuel cells in which enzymes replace the conventional catalysts. For this purpose, the direct electrochemistry of both recombinant laccases POXA1b and POXA1b-Vmh2 has been studied. However, both laccases did not show Direct Electron Transfer (DET), maybe because the distance between the electrode and the T1 of the trinuclear copper center (TNC) was higher than the electron-tunneling distance. This can be explained either by a non-optimal protein orientation on the electrode surface and/or by the hyper glycosylation of the protein due to the recombinant production in *P. pastoris*. In order to overcome these poor performances, the electrochemistry of POXC, the canonical and more abundant laccase from *P. ostreatus*, has been explored. In this case, thanks to a favorable interaction between this native laccase and covalently-modified carbon nanotubes (CNTs) and its ability to operate in a conventional H_2/air proton-exchange membrane fuel cell, POXC has proven to be of great interest as a biocathode for new bioelectocatalytic applications. The specific results of these experiments are discussed in more detail below.

POXC Laccase from *Pleurotus ostreatus*: A High-Performance Multicopper Enzyme for Direct Oxygen Reduction Reaction Operating in a Proton-Exchange Membrane Fuel Cell

Ilaria Sorrentino,[b] Solène Gentil,[a, c] Yannig Nedellec,[a] Serge Cosnier,[a] Alessandra Piscitelli,[b] Paola Giardina,[b] and Alan Le Goff*[a]

In this work, POXC, a laccase from *Pleurotus ostreatus*, was immobilized on carbon nanotubes (CNTs) modified by electrografting anthraquinone and naphthoate diazonium salts. Thanks to a favorable interaction between laccase and covalently modified CNTs, this laccase exhibits high-potential/high-current oxygen reduction reaction (ORR) performances, surpassing the performances of the well-known laccase from *Trametes versicolor* (TvLAC) immobilized on the same nanostructured electrodes. Furthermore, immobilized POXC demonstrates high ORR activity over a wide range of pH (2 to 8), being also highly active at a gas-diffusion electrode. Finally, owing to these unique performances, this enzyme was able to operate at the interface of the microporous layer, humidified air and a polymer electrolyte, that is, Nafion®, in a conventional H_2/air proton-exchange membrane fuel.

The development of hydrogen fuel cells, in particular proton-exchange membrane fuel (PEMFC), at an industrial scale requires to tackle major challenges. The $4H^+/4e^-$ Oxygen Reduction Reaction (ORR) occurs at the cathode side. For now, ORR requires a high amount of platinum catalysts to be efficient. And no competitive, base-metal catalysts have been proven to represent a viable alternative yet.[1,2] One of this alternative is the development of ORR catalysts based on multicopper oxidases (MCOs)[3–5] or their synthetic models.[6–8] In enzymatic fuel cells, a subcategory of fuel cells in which electrocatalytic reactions are performed by immobilized enzymes, ORR mostly relies on MCOs.[3,5,9–11] Thanks to high potential ORR, laccases and bilirubin oxidases have been most exclusively used in enzymatic fuel cells. The MCO active site is based on a set of two copper-containing centers: a Type 1 (T1)

copper center located at the surface of the protein and at which the phenolic substrate is activated and a trinuclear copper center (TNC) at which O_2 is activated and reduced into H_2O. In most cases where MCOs are immobilized on an electrode, electrons are transferred to the TNC via the T1 relay center, which has to be at electron-tunneling distance of the surface of the electrode in order to achieve a so-called Direct Electron Transfer (DET). In particular, different strategies have been studied in order to maximize amount of electroactive enzymes and minimize distance between the T1 center and the surface of the electrode. Several studies have been performed on laccase from *Trametes versicolor* (TvLAC), which exhibits one the lowest overpotential towards ORR in the MCO family and comparable to Pt/C, around 100 mV. F. A. Armstrong and colleagues have shown that grafted polycyclic aromatics were able to promote the favorable immobilization of TvLAC on modified graphitic electrodes.[12,13] In order to increase the enzyme surface coverage, this strategy was transferred to nanostructured electrodes. Carbon nanotubes (CNTs) or graphene sheets were modified by non-covalent[14–17] and covalent [18–21] methods to introduce anthraquinone, anthracene or naphthalene molecules to favor TvLAC orientation. This strategy has led to the design of highly-efficient oxygen-reducing biocathodes for fuel cell applications. However, the ORR studies of these enzymes have been exclusively limited to near-neutral-pH buffered solutions, at which the enzymatic activity is optimal. However, a functional PEMFC has to rely on solid, "unbuffered" and acidic polymer electrolytes such as Nafion®. The enzymatic activity of most enzymes is strongly inhibited in such acidic and low-water content medium. The only example of such enzyme operating in a PEMFC has been shown by Minteer and colleagues using laccase from *Rhus vernificera* entrapped in neutralized tetrabutylammonium-bromide-modified-Nafion® and operating in H_2/O_2 fuel cell.[22] Unfortunately, the fuel cell exhibited low cell voltages of 0.6 V despite high current densities, which were reached at low voltages under O_2.

In this work, we studied the direct electrochemistry of POXC, a laccase from *Pleurotus ostreatus*, which has not been investigated on electrodes yet. POXC is the most abundantly secreted laccase under all growth conditions examined until now, and seems to play a major role during vegetative growth.[23] The enzyme has been extensively characterized in solution: it is a high redox potential laccase with an acidic pI.[24,25] Multi-walled carbon-nanotube (MWCNT)-coated glassy

[a] Dr. S. Gentil, Y. Nedellec, Dr. S. Cosnier, Dr. A. Le Goff
Univ. Grenoble Alpes, CNRS, DCM, 38000 Grenoble
E-mail: alan.le-goff@univ-grenoble-alpes.fr
[b] I. Sorrentino, Dr. A. Piscitelli, Dr. P. Giardina
Department of Chemical Sciences
University Federico II, Naples, Italy
[c] Dr. S. Gentil
Univ. Grenoble Alpes, CEA, CNRS, BIG-LCBM
38000 Grenoble, France

carbon and gas-diffusion electrodes (GCE and GDE respectively) were modified by electrografting of 6-carboxynaphthalenediazonium and 2-diazoniumanthraquinone tetrafluoroborate salts according to previously-described procedures.[26] We have already demonstrated that such functionalization strategy leads to the formation of a thin organic layer on the surface of CNT sidewalls. The synergistic effect of grafted functional groups and CNT graphene sidewalls induces a favorable and specific interaction with metalloenzymes such as bilirubin oxidases,[26,27] promoting direct electron transfer between MWCNTs and the enzyme active site or electron relay. Here, we show that this covalent functionalization strategy favors both POXC immobilization and DET. The behavior of this enzyme was, for the first time, exhaustively investigated towards ORR by Cyclic Voltammetry (CV) and electrochemical models. Furthermore, the comparison between POXC and *Tv*LAC at the same functionalized electrodes was investigated, underlining the similar overpotentials towards ORR for both laccases and the higher current densities obtained for POXC as compared to *Tv*LAC. Finally, high current densities over a wide range of pH (between 2 and pH 8) make POXC, a promising enzyme able to operate at the triple phase boundary between a polymer electrolyte, i.e. Nafion®, the MWCNT-coated GDE and the gas phase in a conventional PEMFC.

POXC was immobilized on pristine MWCNTs and MWCNTs modified with 6-carboxynaphthalenediazonium and 2-diazoniumanthraquinone tetrafluoroborate salts according to a previously-described procedure.[26] Figure 1 displays the 3D representation of the enzyme and CV performed under saturated O_2 purging for pristine MWCNT, naphthoate-modified MWCNT and anthraquinone-modified MWCNT electrodes ($[O_2] = 0.72\ mmol\ L^{-1}$)
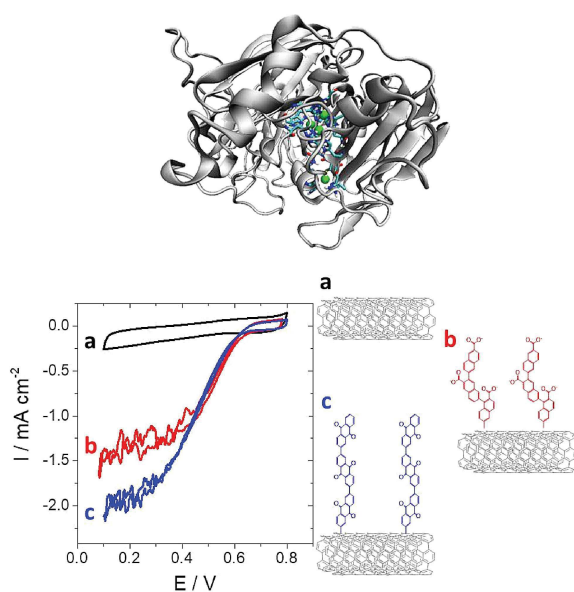

Figure 1. 3D representation of POX (top); CV curves (left) and structures (right) of POXC-functionalized MWCNT electrodes under O_2 for a) pristine MWCNTs, b) naphthoate-modified MWCNTs and c) anthraquinone-modified MWCNTs (stirred and oxygen-purged citrate-phosphate buffer pH 3, $v = 10\ mV\ s^{-1}$). ■■ok?■■

For all MWCNT electrodes, an irreversible electrocatalytic reduction wave is unambiguously attributed to the electroenzymatic reduction of O_2 into H_2O by immobilized POXC. For naphthoate- and anthraquinone-modified MWCNT, a respective 23-fold and 35-fold increase, as compared to pristine MWCNTs, are observed in terms of current density, reaching $2\ mA\ cm^{-2}$. As it has been demonstrated for *Tv*LAC in the case of anthraquinone-modified electrodes,[13] this can be attributed to the favorable hydrophobic interactions between anthraquinone and the hydrophobic substrate cavity of POXC. Furthermore, this is the first time that a similar observation can be made with naphthoate groups for these enzymes. However, this type of functional groups has already been shown to improve DET for bilirubin oxidases from *Myrothecium verrucaria*, owing to a combination of hydrophobic interactions and electrostatic interactions via negatively-charged carboxylate groups.[26,28] In order to confirm these hydrophobic interactions and to directly compare POXC with *Tv*LAC in the same conditions, the same experiments were performed by using commercially-available TvLAC. As expected, modification of MWCNTs with hydrophobic molecules such as anthraquinone or naphthoate groups also led to an important increase in current density for *Tv*LAC, reaching $0.7\ mA\ cm^{-2}$ at pH 5 (Figure S1). According to previous studies,[13,14,21] this is in good agreement with the presence of a favorable interaction between the cavity of both POXC or *Tv*LAC and naphthoate- and anthraquinone-modified MWCNTs.

Long-term stability experiments were performed by one-hour chronoamperometric discharge at 0.2 V almost every day during 20 days (Figure S2). POXC immobilized on both anthraquinone- or naphthoate-modified MWCNTs shows similar and excellent activity over weeks. The bioelectrodes still achieve 65% of their activity after 7 days and 38% after 20 days, namely $0.4\ mA\ cm^{-2}$. This stability is superior to bioelectrodes based on entrapment of laccases in redox hydrogels (66% of the activity is lost after 5 days for laccase from *Coriolus hirsutus*)[29,30] and falls in the same range as previously-described nanostructured electrodes based on laccases from *Trametes sp*.[14,31] *Trametes hirsuta* laccases immobilized at gold nanoparticle-based electrodes exhibited maximum current densities of $1\ mA\ cm^{-2}$, with a 40% loss of activity after 5 days of continuous operation.[32] The same laccase was immobilized at anthraquinone-modified CNTs which exhibited current densities up to $3.5\ mA\ cm^{-2}$ with 21% loss of activity after 7 days.[18] Pyrene-modified laccases from *Trametes sp C30* immobilized at both MWCNT and gold-nanoparticle-based electrodes exhibited maximum current density of $3\ mA\ cm^{-2}$, losing 60% of its activity after one month.[31] *Tv*Lac immobilized at adamantane- or pyrene-modified MWCNTs[14,17] exhibited maximum current densities of $2\ mA\ cm^{-2}$ keeping 66% and 50% of its initial activity after one month. TvLAC immobilized at Anthracene-modified MWCNTs exhibited maximum current density of $140\ \mu A\ cm^{-2}$ accompanied with loss of activity of 25% after 24 h.[19]

In order to get more insights into the difference between nonmodified MWCNTs, naphthoate- and anthraquinone-modified MWCNTS towards POXC and to extract kinetic parameters, the model developed by Armstrong and Léger was applied to the faradaic electrocatalytic wave.[33,34] This model takes into

account the random distribution of redox-active enzyme on the electrode surface. This distribution of orientation is taking into account in the βd_0 tunneling factor. βd_0 is the product of the exponential decay constant β and d_0, the minimal distance between the enzyme electron entry point or electrochemical relay center and the electrode. This factor accounts for the existence of an apparent cone of electron transfer rate distribution, arising from different statistical orientations of POXC. Figure 2 displays the experimental background-sub-
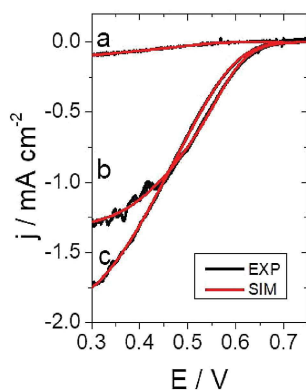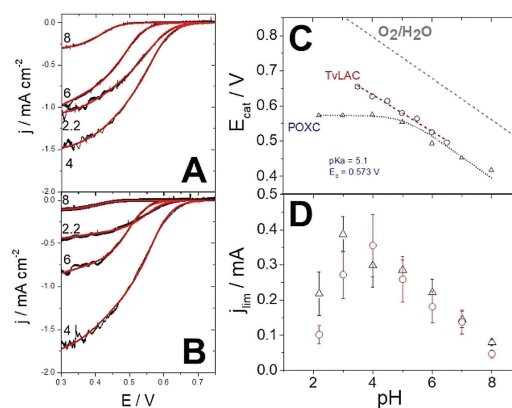

Figure 2. Background-subtracted CV curves of POXC-functionalized a) MWCNT, b) naphthoate-MWCNT, and c) anthraquinone-MWCNT electrodes under O_2. The simulated red trace considers the average between the backward and forward scan.

tracted CV curve accompanied by its simulated counterpart after fitting of the CV curve for each MWCNT electrodes under O_2 at pH = 3. It is noteworthy that, beyond immobilization of the enzyme, mass transfer contributions were minimized through stirring the solution and maintaining a constant oxygen flow. By increasing stirring speed (or by increasing Rotating Disk Electrode rate above 1000 rpm[31]), no increase of electrocatalytic currents (indicative of mass-transport limitations) was observed with any of the tested bioelectrodes.

It is noteworthy that this model takes into account that the electrocatalysis has to be limited by the kinetics of the electroenzymatic reaction. In this case, diffusion limitations, arising from the highly porous structure of the MWCNT film, might influence the electrocatalytic response, especially at high overpotentials. This underlines the fact that this model has to be considered as an approximation of the experimental response. However, models fit well with experimental curves for all tested conditions with R^2 of 0.99 in most cases (see supplementary materials for details). This fit gives access to constant parameters, i.e. the catalysis redox potential (E_{cat}), the ratio between catalytic rate constant k_{cat} and heterogenous electron transfer rate constant at minimal distance k_0^{max} and the electron transfer tunneling factor βd_0. High βd_0 value is observed for pristine MWCNTs ($\beta d_0 = 26$), arising from the high randomization of orientation on MWCNT sidewalls. As expected, much smaller values of 5.0 and 5.3 are observed for anthraquinone-modified and naphthoate-modified MWCNTS respectively, underlining that the orientation of POXC is favored at these modified surfaces. As previously mentioned, this effect

has been already observed for TvLAC on different type of functionalized electrodes[13,14,19,35] and can be extended to POXC. The electrocatalytic waveshape for ORR performed by POXC was also modeled between pH 2 and pH 8 for MWCNTs modified with anthraquinone and naphthoate groups (Figure 3). First, these fits allow the access to E_{cat} between pH 2 and


Figure 3. Background-subtracted CV of POXC-functionalized A) anthraquinone-MWCNT and B) naphthoate-MWCNT between pH 2 and 8. The simulated red traces consider the average between the backward and forward scan. C) Evolution of E_{cat} and D) j_{lim} estimated from simulated CV curves performed between pH 2.2 and 8.

8, allowing the calculation of the dependence of E_{cat} towards pH (figure 3C). This dependence was well fitted using eq. (1):

$$E_{cat} = E_{cat(acid)} + \frac{2.3RT}{nF} * \log(1 + \frac{[K_a]}{[H^+]}) \qquad (1)$$

where R is the gas constant, T the temperature, F the Faraday constant and n the number of electrons involved in the redox system. K_a is the proton dissociation constant for the oxidized form of the enzyme and $E_{cat(acid)}$ is the limiting value of E_{cat} at pH below pKa. Using n = 1, the fit gives access to an E_{cat}(acid) of 0.57 ± 0.01 V and a pKa of 5.1 ± 0.2 ($R^2 = 0.96$). This equation accounts for a $1e^-/1H^+$ accompanied with an acid-base couple with a pKa of 5.1. First, the redox potential of E_{cat} of 0.55 V vs. Ag/AgCl (or 0.75 V vs. NHE) at pH 5 matches very well with the redox potential of POXC measured by redox titration (0.74 V at pH 5[36]). This unambiguously confirms that the electrochemical redox center is controlled by DET to the T1 copper center. Furthermore, this particular pH dependence has already been observed for other copper enzymes such as azurin[37] CueO[38] or BODs.[39] The monoelectronic T1 Cu(II)/Cu(I) proton-coupled electron transfer (PCET) is thus influenced by the acid/base couple of an amino acid such as histidine which induces a structural rearrangement of the T1 copper center upon the reduction/oxidation process.[38,40] This also implies that this protonation causes an increase in ORR overpotentials below pH 5 when comparing with the evolution of the standard redox potential of the O_2/H_2O couple (gray line, figure 3C). This dependence was also compared with the evolution of the catalytic potential of TvLAC obtained by the same procedure.

These are not the final page numbers! ↗↗
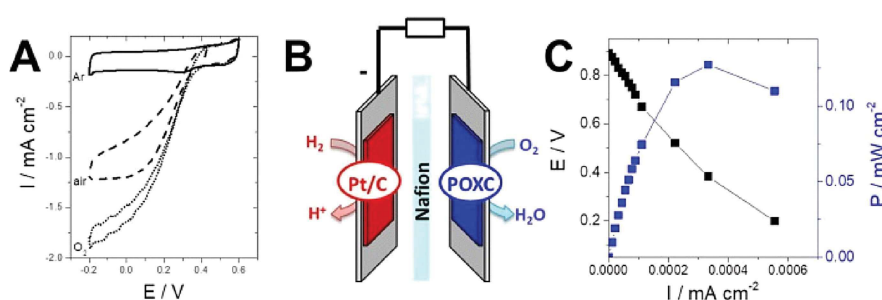
Figure 4. CV curves of a POXC-functionalized AQ-MWCNT GDE under humidified argon, air, and O_2 ($v = 10$ mV s^{-1}, pH 3, 25 °C. B) Schematic representation of the H_2/air fuel cell; C) polarization (▲, black) and power (□, blue) curves for the fuel cell.

The E_{cat} for *Tv*LAC follows a typical linear trend towards pH (slope of 52 mV, red line, figure 3C) corresponding to a typical 1e$^-$/1H$^+$. By comparing the two laccases, it is noteworthy that *Tv*LAC and POXC exhibit closed redox potential above pH 5. This implies that *Tv*LAC and POXC likely share the same electrocatalytic mechanism involving electron transfers at the T1 center, the only striking difference being the involvement of an amino acid protonation step below pH 5 in the case of POXC. When looking at maximum current densities for both types of modified MWCNT electrodes, POXC shows an electrocatalytic activity over a wide pH range between pH 2 and pH 8, reaching maximum current density of 1. 97 mA cm^{-2} at pH 3. Naphthoate- or anthraquinone-modified MWCNTS exhibit similar behavior over this pH range. The decrease of current densities below pH 3 for naphthoate might be attributed to an influence of the protonation of naphthoate groups (pKa ~ 4) on a partial desorption of POXC or on an unfavorable orientation of the enzyme.

POXC was integrated in a GDE. GDE is used in PEMFC technology, allowing the catalyst to operate at the interface between the catalytic layer, the humidified gas phase and the polymer electrolyte. We and others have successfully adapted this technology for the integration of enzymes in fuel cells.[41,42,42–47] Anthraquinone was electrografted on a GDE modified with a thin layer of MWCNTs. Half-cell experiments were performed at pH 3 under Ar, humidified air and O_2 (figure 4A). POXC exhibits similar behavior at both MWCNT-coated GDE and GCE. This confirms that POXC can operate at the interface between the electrolyte, the gas phase and the electrode. Maximum current densities of 1.2 and 1.9 mA cm^{-2} were obtained under air and O_2 at MWCNT-coated GDE respectively in quiescent solution. Similar current densities between GCE and GDE indicate that electrocatalysis is likely limited by the kinetics of the enzymatic reaction. The performance of this POXC-based GDE is among the best performances for a laccase-based GDE, surpassing GDE based on laccases from *Trametes hirsuta* or *Rhus vernificera*, which delivers maximum current densities of 0.5 to 1 mA cm^{-2} under O_2.[42,43]

Since one of the main advantage of POXC is its ability to efficiently operate at acidic pH, this prompted us to integrate POXC in a conventional PEMFC. Figure 4C displays the polarization and power curves measured for this POXC/Pt PEMFC, obtained by successive constant current discharges. A commercial Pt/C GDE was used at the anode for H_2 oxidation. The fuel cell was operated at 25 °C with humidified streams of H_2 and air at atmospheric pressure. The fuel cell delivers a maximum power density of 0.12 mW cm^{-2} at 0.38 V, accompanied with an open-circuit voltage (OCV) of 0.90 V. High cell voltage of 0.90 V confirms that POXC is still active at the interface between the MWCNT layer, air and the polymer electrolyte.

The presence of an important slope in the ohmic region of the polarization curve is indicative of the fact that proton conduction through the Nafion® membrane is hindered by the low amount of produced water. However, the OCV of 0.90 V of this POXC/Pt PEMFC is closed to the OCV (around 1.0 V) observed for conventional Pt/Pt PEMFC, despite lower power densities.[1,48] In a control experiment in which the cathode is based on pristine MWCNTs (without immobilization of POXC), low voltages of 0.7 V and power densities of 45 μW cm^{-2} underline the poor catalytic activity of MWCNTs (figure S3). For comparison, a full Pt/C PEMFC delivers 100 mW cm^{-2} approximately in the same test cell at 60 °C.[48] Furthermore, this is the highest OCV reported so far for a fuel cell based on an enzyme operating in a Nafion®-based PEMFC. A previous example has been shown by Minteer and colleagues with *Tv*LAC. However, low OCV of 0.6 V were observed for this enzyme, despite high current densities of 10 mA cm^{-2} at low voltages of 0.2 V. Furthermore, we have recently shown that bilirubin oxidase from *Myrothecium verrucaria* was particularly efficient in a non-noble metal fuel cell running in a pH 5 phosphate buffer but was not able to operate in Nafion®-based PEMFC.[48]

This work thus demonstrates that DET of POXC is promoted at naphthoate- and anthraquinone-modified MWCNTs. Thanks to its efficient wiring on MWCNT electrodes, direct electrochemistry of POXC can be exhaustively investigated at these electrodes. POXC demonstrates efficient ORR performances over a wide range of pH, surpassing performances of the most well-known laccases towards ORR at both GCE and GDE. This acidophilic laccase is able to work at a three-phase boundary between a solid electrolyte, CNT sidewalls and humidified air. This work demonstrated that the study of novel enzymes by direct electrochemistry can led to the discovery of highly-efficient biocatalyst able to operate in metal-catalyst-based conventional systems which, by design, are unconventional for enzymes This is the reason why its activity might be hindered by the strong acidic nature of sulfonated groups and the low

water content at the interface, despite gas humidification. Therefore, there is still room for improvement, especially in order to design enzyme-specific proton-exchange membranes that would increase water production and retention at the interface between the enzyme, the electrode and the humidified gas. Furthermore, such copper biocatalysts that perform low-overpotential ORR in a PEMFC also pave the way for the development of novel molecular copper catalysts that would perform low-overpotential ORR in a fuel cell.[6,8]

Acknowledgements

Conflict of Interest

The authors declare no conflict of interest.

[1] M. Shao, Q. Chang, J.-P. Dodelet, R. Chenitz, *Chem. Rev.* **2016**, *116*, 3594–3657.
[2] F. Jaouen, E. Proietti, M. Lefèvre, R. Chenitz, J.-P. Dodelet, G. Wu, H. T. Chung, C. M. Johnston, P. Zelenay, *Energy Environ. Sci.* **2010**, *4*, 114–130.
[3] A. Le Goff, M. Holzinger, S. Cosnier, *Cell. Mol. Life Sci.* **2015**, *72*, 941–952.
[4] N. Mano, L. Edembe, *Biosens. Bioelectron.* **2013**, *50*, 478–485.
[5] N. Mano, A. de Poulpiquet, *Chem. Rev.* **2017**, *118*, 2392–2468.
[6] S. Gentil, D. Serre, C. Philouze, M. Holzinger, F. Thomas, A. Le Goff, *Angew. Chem. Int. Ed.* **2016**, *55*, 2517–2520; *Angew. Chem.* **2016**, *128*, 2563–2566.
[7] E. C. M. Tse, D. Schilter, D. L. Gray, T. B. Rauchfuss, A. A. Gewirth, *Inorg. Chem.* **2014**, *53*, 8505–8516.
[8] M. A. Thorseth, C. E. Tornow, E. C. M. Tse, A. A. Gewirth, *Coord. Chem. Rev.* **2013**, *257*, 130–139.
[9] I. Mazurenko, X. Wang, A. de Poulpiquet, E. Lojou, *Sustain. Energy Fuels* **2017**, *1*, 1475–1501.
[10] M. Rasmussen, S. Abdellaoui, S. D. Minteer, *Biosens. Bioelectron.* **2016**, *76*, 91–102.
[11] S. Cosnier, A. J. Gross, A. Le Goff, M. Holzinger, *J. Power Sources* **2016**, *325*, 252–263.
[12] C. F. Blanford, C. E. Foster, R. S. Heath, F. A. Armstrong, *Faraday Discuss.* **2008**, *140*, 319–335.
[13] C. F. Blanford, R. S. Heath, F. A. Armstrong, *Chem. Commun.* **2007**, *0*, 1710–1712.
[14] N. Lalaoui, R. David, H. Jamet, M. Holzinger, A. Le Goff, S. Cosnier, *ACS Catal.* **2016**, *6*, 4259–4264.
[15] M. Bourourou, K. Elouarzaki, N. Lalaoui, C. Agnès, A. Le Goff, M. Holzinger, A. Maaref, S. Cosnier, *Chem. Eur. J.* **2013**, *19*, 9371–9375.
[16] F. Giroud, S. D. Minteer, *Electrochem. Commun.* **2013**, *34*, 157–160.
[17] N. Lalaoui, K. Elouarzaki, A. Le Goff, M. Holzinger, S. Cosnier, *Chem. Commun.* **2013**, *49*, 9281–9283.
[18] M. Sosna, L. Stoica, E. Wright, J. D. Kilburn, W. Schuhmann, P. N. Bartlett, *Phys. Chem. Chem. Phys.* **2012**, 11882.
[19] M. T. Meredith, M. Minson, D. Hickey, K. Artyushkova, D. T. Glatzhofer, S. D. Minteer, *ACS Catal.* **2011**, *1*, 1683–1690.
[20] N. Lalaoui, A. Le Goff, M. Holzinger, M. Mermoux, S. Cosnier, *Chem. Eur. J.* **2015**, *21*, 3198–3201.
[21] K. Stolarczyk, M. Sepelowska, D. Lyp, K. Żelechowska, J. F. Biernat, J. Rogalski, K. D. Farmer, K. N. Roberts, R. Bilewicz, *Bioelectrochemistry* **2012**, *87*, 154–163.
[22] W. Gellett, J. Schumacher, M. Kesmez, D. Le, S. D. Minteer, *J. Electrochem. Soc.* **2010**, *157*, B557–B562.
[23] C. Pezzella, V. Lettera, A. Piscitelli, P. Giardina, G. Sannia, *Appl. Microbiol. Biotechnol.* **2013**, *97*, 705–717.
[24] P. Giardina, V. Aurilia, R. Cannio, L. Marzullo, A. Amoresano, R. Siciliano, P. Pucci, G. Sannia, *Eur. J. Biochem.* **1996**, *235*, 508–515.
[25] G. Palmieri, P. Giardina, L. Marzullo, B. Desiderio, G. Nittii, R. Cannio, G. Sannia, *Appl. Microbiol. Biotechnol.* **1993**, *39*, 632–636.
[26] N. Lalaoui, M. Holzinger, A. L Goff, S. Cosnier, *Chem. Eur. J.* **2016**, *22*, 10494–10500.
[27] N. Lalaoui, A. de Poulpiquet, R. Haddad, A. Le Goff, M. Holzinger, S. Gounel, M. Mermoux, P. Infossi, N. Mano, E. Lojou, *Chem. Commun.* **2015**, *51*, 7447–7450.
[28] L. dos Santos, V. Climent, C. F. Blanford, F. A. Armstrong, *Phys. Chem. Chem. Phys.* **2010**, *12*, 13962–13974.
[29] S. C. Barton, H.-H. Kim, G. Binyamin, Y. Zhang, A. Heller, *J. Phys. Chem. B* **2001**, *105*, 11917–11921.
[30] T. Chen, S. C. Barton, G. Binyamin, Z. Gao, Y. Zhang, H.-H. Kim, A. Heller, *J. Am. Chem. Soc.* **2001**, *123*, 8630–8631.
[31] N. Lalaoui, P. Rousselot-Pailley, V. Robert, Y. Mekmouche, R. Villalonga, M. Holzinger, S. Cosnier, T. Tron, A. Le Goff, *ACS Catal.* **2016**, *6*, 1894–1900.
[32] C. Gutiérrez-Sánchez, M. Pita, C. Vaz-Domínguez, S. Shleev, A. L. De Lacey, *J. Am. Chem. Soc.* **2012**, *134*, 17212–17220.
[33] C. Léger, A. K. Jones, S. P. J. Albracht, F. A. Armstrong, *J. Phys. Chem. B* **2002**, *106*, 13058–13063.
[34] S. V. Hexter, F. Grey, T. Happe, V. Climent, F. A. Armstrong, *Proc. Mont. Acad. Sci.* **2012**, *109*, 11516–11521.
[35] M. S. Thorum, C. A. Anderson, J. J. Hatch, A. S. Campbell, N. M. Marshall, S. C. Zimmerman, Y. Lu, A. A. Gewirth, *J. Phys. Chem. Lett.* **2010**, *1*, 2251–2254.
[36] A. M. Garzillo, M. C. Colao, R. Buonocore, R. Oliva, L. Falcigno, M. Saviano, A. M. Santoro, R. Zappala, R. P. Bonomo, C. Bianco, *J. Protein Chem.* **2001**, *20*, 191–201.
[37] L. J. C. Jeuken, L.-J. Wisson, F. A. Armstrong, *Inorg. Chim. Acta* **2002**, *331*, 216–223.
[38] Y. Miura, S. Tsujimura, S. Kurose, Y. Kamitaka, K. Kataoka, T. Sakurai, K. Kano, *Fuel Cells* **2009**, *9*, 70–78.
[39] N. Lalaoui, A. Le Goff, M. Holzinger, S. Cosnier, *Chem. Eur. J.* **2015**, *21*, 16868–16873.
[40] C. S. St. Clair, W. R. Ellis Jr., H. B. Gray, *Inorg. Chim. Acta* **1992**, *191*, 149–155.
[41] K. So, K. Sakai, K. Kano, *Curr. Opin. Electrochem.* **2017**, *5*, 173–182.
[42] C. Lau, E. R. Adkins, R. P. Ramasamy, H. R. Luckarift, G. R. Johnson, P. Atanassov, *Adv. Energy Mater.* **2012**, *2*, 162–168.
[43] G. Gupta, C. Lau, B. Branch, V. Rajendran, D. Ivnitski, P. Atanassov, *Electrochim. Acta* **2011**, *56*, 10767–10771.
[44] G. Gupta, C. Lau, V. Rajendran, F. Colon, B. Branch, D. Ivnitski, P. Atanassov, *Electrochem. Commun.* **2011**, *13*, 247–249.
[45] N. Lalaoui, A. de Poulpiquet, R. Haddad, A. Le Goff, M. Holzinger, S. Gounel, M. Mermoux, P. Infossi, N. Mano, E. Lojou, *Chem. Commun.* **2015**, *51*, 7447–7450.
[46] K. So, Y. Kitazumi, O. Shirai, K. Nishikawa, Y. Higuchi, K. Kano, *J. Mater. Chem. A* **2016**, *4*, 8742–8749.
[47] K. So, Y. Kitazumi, O. Shirai, K. Kurita, H. Nishihara, Y. Higuchi, K. Kano, *Chem. Lett.* **2014**, *43*, 1575–1577.
[48] S. Gentil, N. Lalaoui, A. Dutta, Y. Nedellec, S. Cosnier, W. J. Shaw, V. Artero, A. Le Goff, *Angew. Chem. Int. Ed.* **2017**, *56*, 1845–1849; *Angew. Chem.* **2017**, *129*, 1871–1875.

These are not the final page numbers! ↗↗

COMMUNICATIONS

Enzyme power: Immobilized at carbon nanotubes modified by aryldiazonium salts, POXC laccase from *Pleurotus ostreatus* demonstrates high-potential/high-current oxygen reduction reaction performances over a wide range of pH values and successfully operates at the cathode side of a proton-exchange membrane fuel cell.
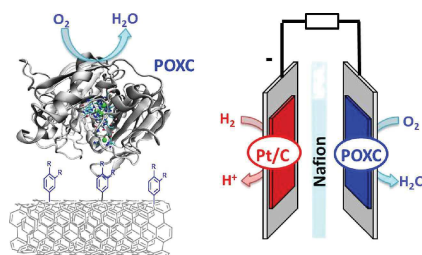
I. Sorrentino, Dr. S. Gentil, Y. Nedellec, Dr. S. Cosnier, Dr. A. Piscitelli, Dr. P. Giardina, Dr. A. Le Goff*

1 – 6

POXC Laccase from *Pleurotus ostreatus*: A High-Performance Multicopper Enzyme for Direct Oxygen Reduction Reaction Operating in a Proton-Exchange Membrane Fuel Cell

SPACE RESERVED FOR IMAGE AND LINK

Share your work on social media! *ChemElectroChem* has added Twitter as a means to promote your article. Twitter is an online microblogging service that enables its users to send and read short messages and media, known as tweets. Please check the pre-written tweet in the galley proofs for accuracy. If you, your team, or institution have a Twitter account, please include its handle @username. Please use hashtags only for the most important keywords, such as #catalysis, #nanoparticles, or #proteindesign. The ToC picture and a link to your article will be added automatically, so the **tweet text must not exceed 250 characters**. This tweet will be posted on the journal's Twitter account (follow us @ChemElectroChem) upon publication of your article in its final (possibly unpaginated) form. We recommend you to re-tweet it to alert more researchers about your publication, or to point it out to your institution's social media team.

ORCID (Open Researcher and Contributor ID)

Please check that the ORCID identifiers listed below are correct. We encourage all authors to provide an ORCID identifier for each coauthor. ORCID is a registry that provides researchers with a unique digital identifier. Some funding agencies recommend or even require the inclusion of ORCID IDs in all published articles, and authors should consult their funding agency guidelines for details. Registration is easy and free; for further information, see http://orcid.org/.

Ilaria Sorrentino
Dr. Solène Gentil
Yannig Nedellec
Dr. Serge Cosnier
Dr. Alessandra Piscitelli
Dr. Paola Giardina
Dr. Alan Le Goff

2.5   Conclusions

In this chapter the fungal laccases, POXA1b-Vmh2 and POXC, have been successfully exploited to develop novel hybrid devices, which are significantly advantageous in terms of high activity, biocompatibility, chemical and electrochemical stability. Aiming at addressing needs in terms of velocity and reliability in the determination of macromolecules in different real matrices, POXA1b-Vmh2 was used to develop fast and easy-to-use optical biosensing platforms to monitor phenols on polystyrene multi-well plate. Furthermore, to combine GBMs properties with enzymatic activity, this chimera protein was used to functionalize NMs through a one-step approach. POXC, the acidophilic laccase was found to be highly promising as a biocathode for EBFCs. Indeed, it shows efficient ORR performances on both modified electrodes GCE and GDE. In addition, it is capable of operating at the interface of the microporous layer, humidified air and a polymer electrolyte, i.e., Nafion®, in a conventional H_2/air proton-exchange membrane fuel cell.

2.6 References

1. Givaudan, A. *et al.* Polyphenol oxidase in Azospirillum lipoferum isolated from rice rhizosphere: Evidence for laccase activity in non-motile strains of Azospirillum lipoferum. *FEMS Microbiol. Lett.* **108,** 205–210 (1993).

2. Yamazaki, H. I. Cuticular phenoloxidase from the silkworm, Bombyx mori: Properties, solubilization, and purification. *Insect Biochem.* **2,** 431–444 (1972).

3. Piscitelli, A. *et al.* Induction and transcriptional regulation of laccases in fungi. *Curr. Genomics* **12,** 104–12 (2011).

4. Giardina, P. *et al.* Laccases: A never-ending story. *Cell. Mol. Life Sci.* **67,** 369–385 (2010).

5. Shleev, S. V. *et al.* Comparison of physico-chemical characteristics of four laccases from different basidiomycetes. *Biochimie* **86,** 693–703 (2004).

6. Messerschmidt, A. *Multi-copper oxidases.* (World Scientific, 1997).

7. Hakulinen, N. *et al.* Crystal structure of a laccase from Melanocarpus albomyces with an intact trinuclear copper site. *Nat. Struct. Biol.* **9,** 601 (2002).

8. Piontek, K., Antorini, M. & Choinowski, T. Crystal structure of a laccase from the fungus Trametes versicolor at 1.90-A resolution containing a full complement of coppers. *J. Biol. Chem.* **277,** 37663–9 (2002).

9. Kumar, S. V. S., Phale, P. S., Durani, S. & Wangikar, P. P. Combined sequence and structure analysis of the fungal laccase family. *Biotechnol. Bioeng.* **83,** 386–394 (2003).

10. Morozova, O. V, Shumakovich, G. P., Gorbacheva, M. A., Shleev, S. V & Yaropolov, A. I. "Blue" laccases. *Biochemistry. (Mosc).* **72,** 1136–50 (2007).

11. Xu, F. Catalysis of novel enzymatic iodide oxidation by fungal laccase. *Appl. Biochem. Biotechnol.* **59,** 221–230 (1996).

12. Karigar, C. S. & Rao, S. S. Role of microbial enzymes in the bioremediation of pollutants: a review. *Enzyme Res.* **2011,** 805187 (2011).

13. Cañas, A. I. & Camarero, S. Laccases and their natural mediators: Biotechnological tools for sustainable eco-friendly processes. *Biotechnol. Adv.* **28,** 694–705 (2010).

14. Rodríguez-Delgado, M. M. *et al.* Laccase-based biosensors for detection of phenolic compounds. *TrAC Trends Anal. Chem.* **74,** 21–45 (2015).

15. Mazlan, S. Z., Lee, Y. H. & Hanifah, S. A. A New Laccase Based Biosensor for Tartrazine. *Sensors (Basel).* **17,** (2017).

16. Olivieri, G. *et al.* Strategies for dephenolization of raw olive mill wastewater by means of Pleurotus ostreatus. *J. Ind. Microbiol. Biotechnol.* **39,** 719–729 (2012).

17.   Gullotto, A. *et al.* Biodegradation of naphthalenesulphonate polymers: the potential of a combined application of fungi and bacteria. *Environ. Technol.* **36,** 538–545 (2015).

18.   Faraco, V., Pezzella, C., Miele, A., Giardina, P. & Sannia, G. Bio-remediation of colored industrial wastewaters by the white-rot fungi Phanerochaete chrysosporium and Pleurotus ostreatus and their enzymes. *Biodegradation* **20,** 209–220 (2009).

19.   Karas, P. A., Perruchon, C., Exarhou, K., Ehaliotis, C. & Karpouzas, D. G. Potential for bioremediation of agro-industrial effluents with high loads of pesticides by selected fungi. *Biodegradation* **22,** 215–228 (2011).

20.   Palmieri, G. *et al.* Stability and activity of a phenol oxidase from the ligninolytic fungus Pleurotus ostreatus. *Appl. Microbiol. Biotechnol.* **39,** 632–6 (1993).

21.   Giardina, P. *et al.* Protein and gene structure of a blue laccase from Pleurotus ostreatus1. *Biochem. J.* **341 (Pt 3),** 655–63 (1999).

22.   Garzillo, A. M. *et al.* Structural and Kinetic Characterization of Native Laccases from Pleurotus ostreatus, Rigidoporus lignosus, and Trametes trogii. *J. Protein Chem.* **20,** 191–201 (2001).

23.   Palmieri, G. *et al.* Atypical laccase isoenzymes from copper supplemented Pleurotus ostreatus cultures. *Enzyme Microb. Technol.* **33,** 220–230 (2003).

24.   Giardina, P. *et al.* Structural characterization of heterodimeric laccases from Pleurotus ostreatus. *Appl. Microbiol. Biotechnol.* **75,** 1293–1300 (2007).

25.   Faraco, V. *et al.* Heterologous expression of heterodimeric laccase from Pleurotus ostreatus in Kluyveromyces lactis. *Appl. Microbiol. Biotechnol.* **77,** 1329–1335 (2008).

26.   Lettera, V. *et al.* Identification of a new member of Pleurotus ostreatus laccase family from mature fruiting body. *Fungal Biol.* **114,** 724–730 (2010).

27.   Festa, G., Autore, F., Fraternali, F., Giardina, P. & Sannia, G. Development of new laccases by directed evolution: Functional and computational analyses. *Proteins Struct. Funct. Bioinforma.* **72,** 25–34 (2008).

28.   Miele, A., Giardina, P., Sannia, G. & Faraco, V. Random mutants of a *Pleurotus ostreatus* laccase as new biocatalysts for industrial effluents bioremediation. *J. Appl. Microbiol.* **108,** 998–1006 (2010).

29.   Giacobelli, V. G. *et al.* Repurposing designed mutants: a valuable strategy for computer-aided laccase engineering – the case of POXA1b. *Catal. Sci. Technol.* **7,** 515–523 (2017).

30.   Pezzella, C. *et al.* A step forward in laccase exploitation: Recombinant production and evaluation of techno-economic feasibility of the process. *J. Biotechnol.* **259,** 175–181 (2017).

31.   Pezzella, C., Guarino, L. & Piscitelli, A. How to enjoy laccases. *Cell. Mol. Life Sci.* **72,** 923–940 (2015).

32. Battista, E. *et al.* Enzymatic sensing with laccase-functionalized textile organic biosensors. *Org. Electron. physics, Mater. Appl.* **40,** 51–57 (2017).

33. Lettera, V. *et al.* Efficient immobilization of a fungal laccase and its exploitation in fruit juice clarification. *Food Chem.* **196,** 1272–1278 (2015).

34. Pezzella, C. *et al.* Green routes towards industrial textile dyeing: A laccase based approach. *J. Mol. Catal. B Enzym.* **134,** 274–279 (2016).

35. Gravagnuolo, A. M. *et al.* In Situ Production of Biofunctionalized Few-Layer Defect-Free Microsheets of Graphene. *Adv. Funct. Mater.* **25,** 2771–2779 (2015).

36. Laaksonen, P. *et al.* Interfacial Engineering by Proteins: Exfoliation and Functionalization of Graphene by Hydrophobins. *Angew. Chemie Int. Ed.* **49,** 4946–4949 (2010).

37. Grieshaber, D., MacKenzie, R., Vörös, J. & Reimhult, E. Electrochemical Biosensors - Sensor Principles and Architectures. *Sensors (Basel).* **8,** 1400–1458 (2008).

38. Hammond, J. L., Formisano, N., Estrela, P., Carrara, S. & Tkac, J. Electrochemical biosensors and nanobiosensors. *Essays Biochem.* **60,** 69–80 (2016).

CHAPTER 3

3. THE RECOMBINANT CHIMERIC PROTEINS PRODUCED IN *Escherichia coli*

Among microorganisms, the available host systems include bacteria, yeast, filamentous fungi, and unicellular algae. All of them have strengths and weaknesses and their choice may be subject to the protein of interest. In this part of the project *E. coli* was chosen as host organism for its well-known advantages. First, it has unparalleled fast growth kinetics in glucose-salts media and, at the optimal environmental conditions, its doubling time is about 20 min. This means that an inoculated culture may reach stationary phase in a few hours. Moreover, high cell density cultures are easily achieved, which could mean high levels of production of recombinant proteins.

In this chapter Vmh2 was fused with two other target proteins, the antimicrobial peptide LL37 and the HN1 ScFv antibody that mimics the activity of anti-mesothelin human antibody. The production of these chimera proteins was performed in *E. coli*, taking into consideration, in addition to the advantages already proposed, that both target proteins and Vmh2 have been already successfully expressed in this host[1–3].

3.1 Chimera protein: Antimicrobial Peptide-Hydrophobin

Antimicrobial peptides (AMPs) are short polycationic peptides (8 to 50 amino acids) of low molecular weight, contain multiple hydrophobic residues, are amphipathic, and exhibit a broad-spectrum of antimicrobial activities, ranging from viruses to parasites. Defensin is the first reported animal-originated AMP; it has been isolated from rabbit leukocytes in 1956[4]. In total, more than 5,000 AMPs have been discovered or synthesized up to date[5]. Natural AMPs can be found in both prokaryotes and eukaryotes (e.g., protozoan, fungi, plants, insects, and animals)[6–8]. In animals, AMPs are mostly found in the tissues and organs that are exposed to airborne pathogens and are believed to be the first line of the innate immune defense[9,10].

Several types of eukaryotic cells such as lymphs, epithelial cells in gastrointestinal and genitourinary systems[11,12], phagocytes[13], and lymphocytes of the immune system[7] are involved in AMP production. In addition to direct involvement in innate immunity, AMPs have also been found to influence host's inflammatory responses during an infection[14,15].

Generally, AMPs exhibit a net positive charge and a high ratio of hydrophobic amino acids, almost 50% of amino acids in the primary sequence of natural AMPs are hydrophobic residues[16]. These are the main factors for the initial interaction with negatively charged cell membranes. Indeed, the ability of AMPs to kill different microbes, usually depends on their ability to interact with bacterial membranes or cell walls, and their selectivity for specific species is due to differences in the membrane composition. Upon their interaction with cell membranes, AMPs can form pores that destroy membrane integrity, promoting lysis of the targeted microbes (Fig.24).
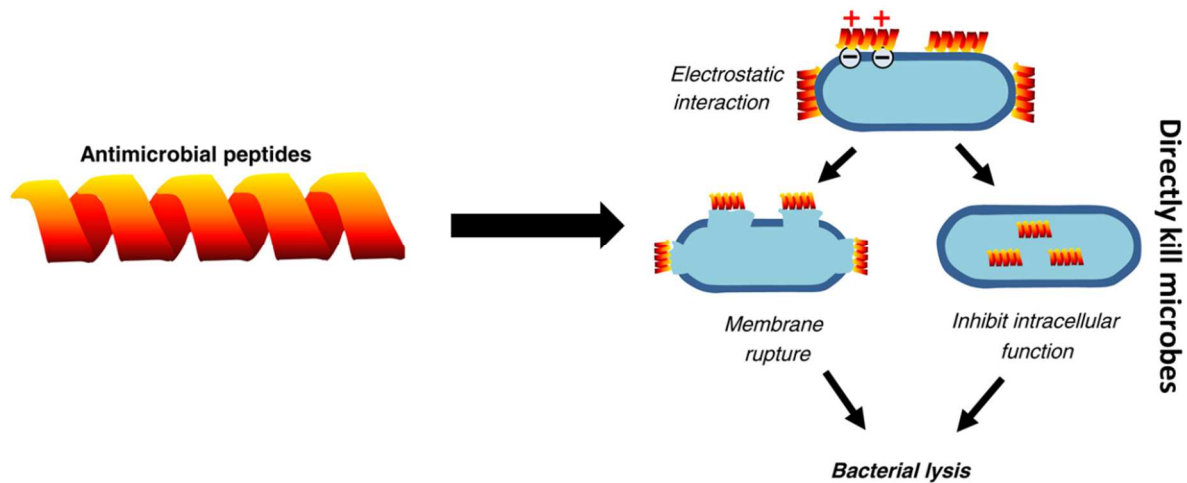
Fig. 24 – Biological function of antimicrobial peptides[17]

In addition, a number of AMPs form a transmembrane channel in the membrane by self-aggregation or polymerization, leading to cytoplasm leakage and cell death. Some AMPs also disrupt bacterial membranes through enzymatic digestion. Nonetheless, some peptides have been described as being able to cross the lipid bilayer without causing any damage but kill bacteria by inhibiting intracellular primary or secondary functions, such as blocking enzyme activity or inhibiting protein and nucleic acid synthesis. Besides to direct antimicrobial activities, some AMPs are also able to inhibit biofilm formation and disrupt existing biofilms.

Based on their secondary structures, AMPs have been classified in different structural groups, being β-sheet and α-helix structures the most common[18]. In mammals, AMPs representative of these two classes are β-defensins and cathelicidins, respectively[19,20]. These peptides are expressed on epithelial surfaces and in neutrophils and have been proposed to provide a first line of defence against invasive bacterial infection by acting as 'natural antibiotics' [9,11]. Whilst the defensins share common structural features, members of the cathelicidin family are characterized by a highly conserved region (cathelin domain) and a highly variable domain[21] (Fig.25).
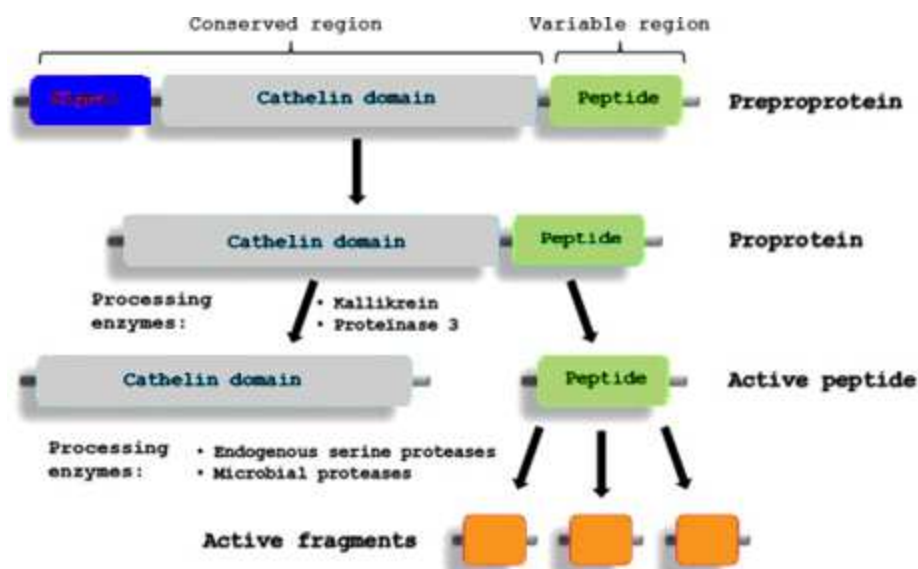

Fig. 25 – Depiction of the typical processing of a cathelicidin protein (adapted from [22])

While there are several gene-encoded defensins, to date the only known member of the cathelicidin family of peptides expressed in humans is LL-37. It is an amphipathic helical peptide composed by 37 residues (Fig.26), it has been found throughout the body. LL-37 peptide is a potent killer of different microorganisms with the ability to prevent immunostimulatory effects of bacterial wall molecules such as lipopolysaccharides. Additional reported activities of LL-37 include chemoattractant function, inhibition of neutrophil apoptosis, and stimulation of angiogenesis, tissue regeneration, and cytokine release (e.g. IL-8).
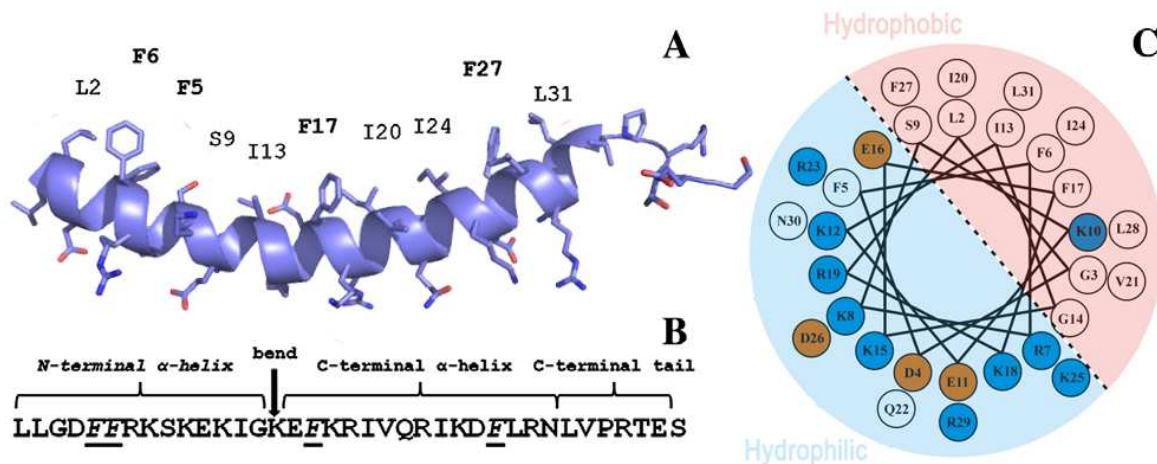
Fig. 26 – 3-dimensional structure of LL-37. **A**: The three-dimensional structure of the human cathelicidin reveals a helix-bend-helix conformation, followed by a C-terminal tail. Note the 4 phenylalanine side chains lying in the concave surface of the peptide. **B**: Sequence of LL-37. Phenylalanines are underscored. **C**: Helical wheel representation of LL-37, illustrating the amphipathic and cationic nature of LL-37 (adapted from [22])

Cellular production of LL-37 is affected by multiple factors, including bacterial products, host cytokines, availability of oxygen, and sun exposure through the activation of CAP-18 gene expression by vitamin D3. At infection sites, the function of LL-37 can be inhibited by charge-driven interactions with DNA and F-actin released from dead neutrophils and other cells lysed as the result of inflammation[23].

The rapid increase in drug-resistant infections represents a serious challenge to antimicrobial therapies and there is an urgent need to develop other control agents. These are the boundaries within which the growing development of natural and synthetic antimicrobial peptides is being handled. In particular, medical devices applied in implant surgery can provide surfaces and environments suitable for colonization by microorganisms, so device-related infections remain a challenge to modern medicine. Therefore, the design of new surfaces, unsuitable for bacterial colonization or inhibiting bacterial growth, is necessary to improve medical devices.

In a previous work[24], Vmh2 was showed to affect the adhesive properties of *S. epidermidis* reducing its biofilm formation, not impairing the cell viability. With the aim to improve the anti-biofilm efficiency of the self-assembled Vmh2 layers against other microorganisms and adding anti-microbial activity to the surfaces, in this section the chimeric LL37-Vmh2 protein was produced in *E. coli* and immobilized on a polystyrene surface.

The fusion protein strategy, as reported by Li and coauthors[25], could mask the peptide lethal effect towards the host, thus overcome the difficulties of its heterologous production.

Materials and Methods

System design

A synthetic gene encoding for LL-37, in frame with the thrombin cleavage site, the linker (Gly₄Ser)₃ and with Vmh2 from *P. ostreatus*, was designed (445 bp) and optimized according to *E. coli* codon usage. The gene product was restricted with *NdeI* and *XhoI* and ligated into the corresponding sites of the pET22b(+) vector under the control of the T7 promoter, thus obtaining the recombinant plasmid pET22b_LL37-Vmh2 (Fig.27). The recombinant plasmid was transformed into *E. coli* BL21 (DE3) to be easily expressed in functional form.
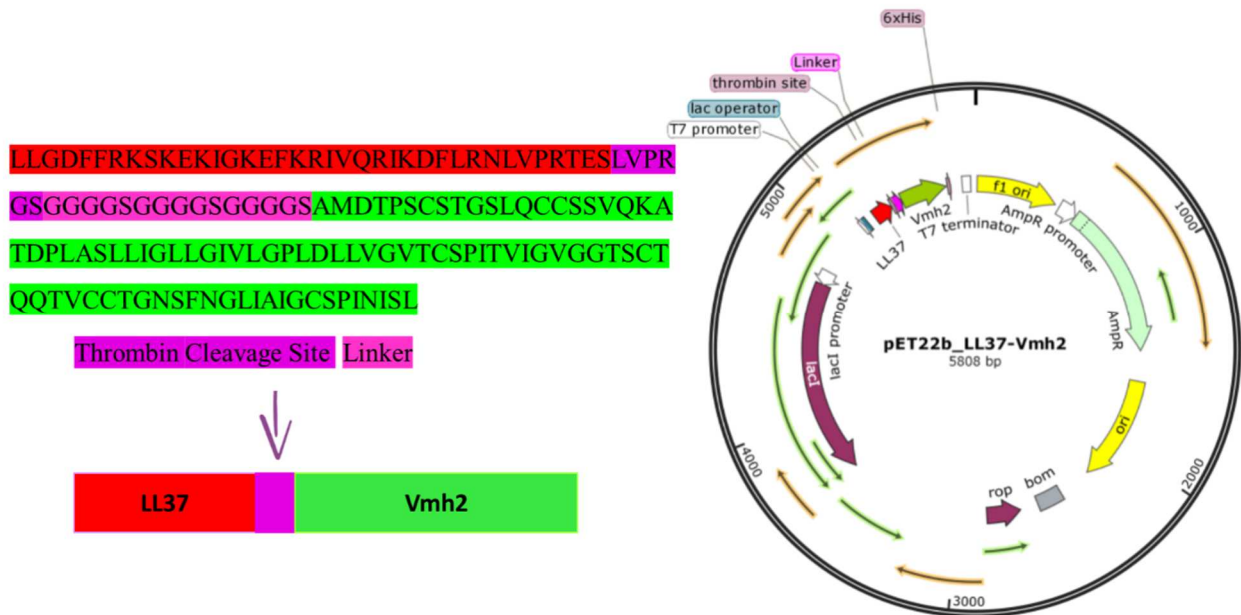

Fig. 27 – LL37-Vmh2 amminoacidic sequences and vector map

Production of LL37-Vmh2

Recombinant cells from solid culture were inoculated in 10 mL of LB medium in a 100 mL flask. This preculture was grown over-night at 37°C on a rotary shaker (180 rpm), then a volume of suspension sufficient to reach a final OD$_{600}$ value of 0.08 was used to inoculate 250 ml flasks containing 50 mL of selective medium. Cells were grown at 37°C on a rotary shaker (180 rpm).
Cultures of recombinant E. coli were carried out to improve protein production varying the growth conditions (medium composition and growth phase of induction):

Table 7 – Different broth formulation

Different broth formulation
LB (1% tryptone, 0.5% yeast extract, 1% NaCl)
LB 2% Glu
LB 2% Glu 3% EtOH
TB (1.2% tryptone, 2.4% yeast extract, 0.94% K$_2$HPO4, 0.28% KH$_2$PO$_4$, 0.4% glycerol)
TB 3% EtOH

After protein expression induction (1mM Isopropyl β-D-1-thiogalactopyranoside IPTG), the bacteria were harvested by centrifugation, resuspended in opportune volume of lysis buffer (100mM Tris-HCl, 10mM EDTA, 2M UREA, 2% Triton X-100, pH=8) with final concentration of 20 OD / mL , and disrupted by sonication (40% amplitude) using a medium power tip (MD 72) for 30 minutes (30" ON and 30" OFF), cooling the system in an ice bath.

Purification of LL37-Vmh2

E. coli cellular lysate was centrifuged using Amicon Centricon Centrifugal Units (Regenerated Cellulose Membrane) with a 30 KDa cut-off in order to separate the targeted fusion protein from the other lysate proteins taking advantage from its low molecular weight (14 KDa). After that the protein was recovered, a dilution in denaturing buffer (Tris-HCl 100mM, EDTA 10mM, UREA 8M and DTT 10mM, pH=8) was made to reach an efficient denaturation of the protein. A dialysis towards 60% ethanol, using Amicon 3 KDa Centricons was performed in order to allow the protein to reach the correct folding. Protein concentration after dialysis was determined with µPierce660 assay.

LL37-Vmh2 immobilization

To immobilize the chimera protein on the polystyrene support, the following method was set up. 100 or 300 µl of LL37-Vmh2 (0.1 and 0.05 µg/ µl) in 60% ethanol were loaded into a 96 well flat plate (as polystyrene support) and incubated over night at 28 °C and at room temperature, then washed three times with the same solvent in order to remove the proteins that did not adhere to the surface. After three washes, the immobilization yield was calculated as the difference between the quantity used for immobilization and that measured in the washes.

Bio-film assay

An overnight culture of *S. epidermidis* strain O-47, grown in Brain Heart Infusion (BHI) broth (37g/L), was diluted to a cell concentration of ~ 0.001 OD$_{600 \text{ nm}}$. A volume of 200 µl of this culture was added to each well of a 96-well flat-bottomed polystyrene plate, previously functionalized with LL37-Vmh2 and Vmh2 used as control. As a negative control, the same culture was added to wells treated with only 60% ethanol. The plates were incubated aerobically for 24 h at 37°C. Planktonic cells were gently removed after the incubation; each well was washed three times with PBS (Phosphate Buffered Saline) and dried by gently tapping in an inverted position on a piece of paper towel. The biofilm formation was measured using crystal violet staining. In detail, each well was stained with 0.1% crystal violet and incubated for 15 min at room temperature, rinsed twice with double-distilled water, and thoroughly dried. The dye bound to the adherent cells was solubilized with 20% (v/v) glacial acetic acid and 80% (v/v) ethanol. After incubation for 30 min at room temperature, the optical density was measured at 590 nm to quantify the total biomass of the biofilm formed in each well.

For the confocal microscopy analysis, biofilms were formed on Nunc™ Lab-Tek® 8-well Chamber Slides (n° 177445; Thermo Scientific, Ottawa, ON, Canada). In brief, overnight cultures of *S. epidermidis* O-47 grown in BHI were diluted to a cell concentration of about 0.001 $OD_{600\ nm}$. and inoculated into each well of a chamber slide, previously functionalized. As a negative control, the same culture was added to wells treated with only 60% ethanol solution. The bacterial culture was incubated at 37°C for 20 h in well coated with LL37-Vmh2 and Vmh2 used as control in order to assess anti-biofilm activity and influence on cell viability of coating proteins. The biofilm cell viability was determined with the FilmTracer™ LIVE/DEAD® Biofilm Viability Kit (Molecular Probes, Invitrogen, Carlsbad, California) following the manufacturer's instructions. After rinsing with filter-sterilized PBS, each well of the chamber slide was filled with 300µL of a working solution of fluorescent stains, containing the SYTO® 9 green fluorescent nucleic acid stain (10 µM) and Propidium iodide, and the red-fluorescent nucleic acid stain (60 µM), and incubated for 20-30 minutes at room temperature, protected from light. All the excess stain was removed by rinsing gently with filter-sterilized PBS. All the microscopic observations and image acquisitions were performed with a confocal laser scanning microscope (CLSM) (LSM700-Zeiss, Germany) equipped with an Ar laser (488 nm), and a He-Ne laser (555 nm). Images were obtained using a 20X/0.8 objective. The excitation/emission maxima for these dyes were approximately 480/500nm for the SYTO® 9 stain and 490/635 nm for propidium iodide. Z-stacks were obtained by driving the microscope to a point just out of focus on both the top and bottom of the biofilms. Images were recorded as a series of .tif files with a file-depth of 16 bits. For each condition two independent biofilm samples were used.

Results and Discussion

Production and characterization of chimeric hydrophobins

The synthetic gene LL37-Vmh2 was inserted into the plasmid pET22b and transformed into *E. coli* BL21(DE3). Recombinant clones were grown in LB at 37°C and induced as already reported[26]. After protein production, the cells were fractioned separating soluble cytoplasmatic fraction from inclusion bodies and proteins analyzed by SDS- PAGE (Fig.28)
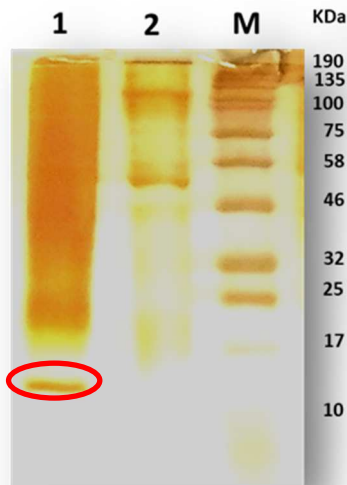
Fig. 28 – Silver stained SDS-PAGE. M: marker; lane 1: soluble part of *E. coli* lysate; lane 2: *E. coli* inclusion bodies

A band at the expected molecular weight was detected in the soluble part of cellular lysate. In order to separate the chimeric protein from the high molecular weight proteins, ultrafiltration was performed. LL37-Vmh2 was recovered in the ultrafiltrate (lane 2 of Fig.29), while the rest of the sample in the centricon unit was discarded (lane 1 of Fig.29).
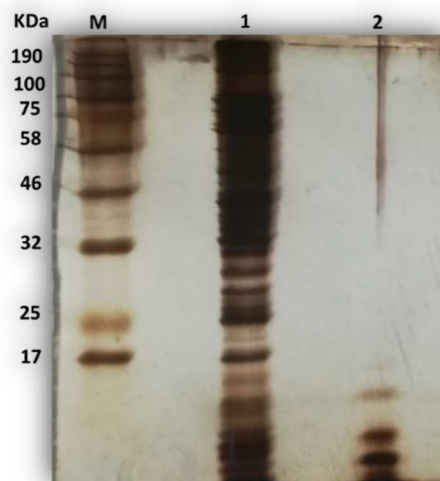
Fig. 29 – Silver stained SDS-PAGE. M: marker; lane 1: *E. coli* soluble lysate ; lane 2: low molecular weight fraction (LL37-Vmh2)

Then, several experiments, varying broth composition and cell growth phase induction, were carried out in order to optimize the LL37-Vmh2 expression. The evaluation of the LL37-Vmh2 production was carried out calculating the amount of low molecular weight proteins obtained in each test. In the standard conditions a production level of about 1mg per L of culture broth was calculated, while a three times increase was obtained (3.5mg/L) when cells were grown in TB and protein induction was performed with IPTG induction at the stationary phase.

## Immobilization of LL37-Vmh2 on polystyrene surface

The low molecular weight proteins recovered after ultrafiltration were immobilized without further purification procedures, taking into account that the ability to stably adhere on surfaces is a peculiar property of the chimera proteins. However, the fusion protein adhered only partially on the polystyrene surface and no satisfying immobilization yield was obtained (Table 8 LL37-Vmh2 a). Considering that the chimeric protein was produced in soluble form in the reducing environment of the *E. coli* cytoplasm, its inefficient adhesive capability could probably be due to an incorrect folding. For this reason, the protein LL37-Vmh2 was completely denatured by dilution in a denaturing buffer and then slowly refolded and dialysed against 60% ethanol (LL37-Vmh2 b). After this treatment, adhesion capability of LL37-Vmh2 chimera protein was increased tenfold, reaching an immobilization yield of about 50%.

Table 8 – LL37-Vmh2 immobilization yield

Samples	Amount of deposited protein (µg)	Amount of unbound protein (µg)	% Yield
LL37-Vmh2 a	5	5.0 ±0.5	-
LL37-Vmh2 a	10	9.5±0.8	5±2
LL37-Vmh2 b	5	4.1±0.5	19 ±4
LL37-Vmh2 b	10	4.9±0.4	51±2

Biofilm assay

The binding of bacteria to abiotic materials is a pivotal step toward the establishment of a device-associated infection. As reported by Artini and coworkes[24], Vmh2 is able to interfer with the adhesive ability of *S. epidermidis*, even if the hydrophobin had no bactericidal activity. Then, the influence of the deposition of both LL37-Vmh2 and Vmh2 on polystyrene surfaces in *S. epidermidis* biofilm formation was evaluated. In particular, the clinical isolate O-47 strain, a strong biofilm producer[27], has been selected for preliminary studies. The functionalization of polystyrene multi-wells was performed by covering the bottom and the walls of the wells using LL37-Vmh2 and Vmh2 as control. To have the same amount of immobilized protein different initial concentrations are deposited, taking into account the lower immobilization yield of the chimera protein. The coating effect on biofilm formation was then assessed. The data are reported as the percentage of *S. epidermidi*s residual biofilm formed on coated wells with respect to the uncoated ones. As previously reported, the biofilm formation on Vmh2 coated surfaces was inhibited (Fig.30).
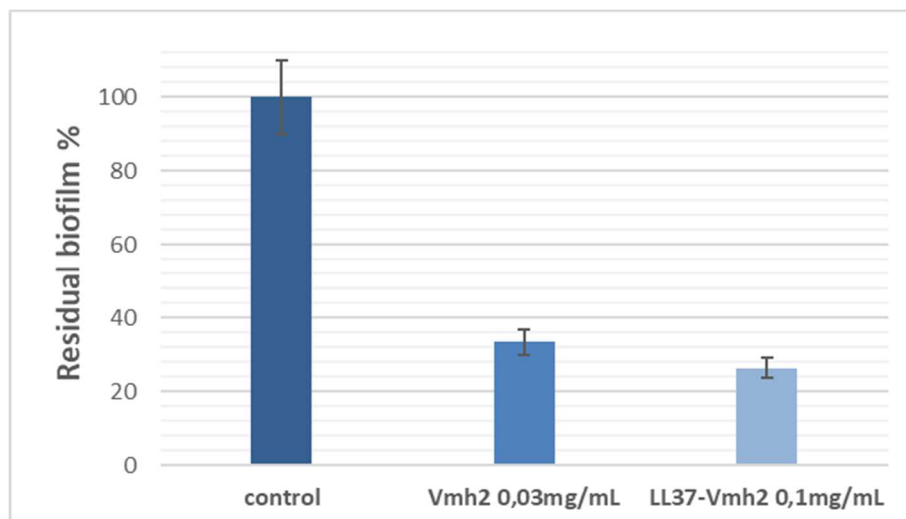
Fig. 30 – The effect of Vmh2 from *P. ostreatus* and the chimera protein LL37-Vmh2 coating on the residual O-47 *S. epidermidis* biofilm formation in BHI medium. The biofilm formation was evaluated after 24 h incubation in polystyrene plates previously coated with the protein solutions. The data are reported as the percentage of residual biofilm.

The inhibition was higher than 50% in the tested conditions for all the samples. According to the results obtained, LL37-Vmh2 chimera protein seems to prevent the biofilm formation process of O-47 *S. epidermidis* to the same extent of Vmh2.

CLSM analysis of biofilm

The inhibition of *S. epidermidis* O-47 biofilm formation was further investigated by confocal laser scanning microscopy (CLSM) to analyze the biofilm structure and the biomass distribution by means of three-dimensional biofilm images. LIVE/DEAD staining was used to visualize the viability of cells embedded in the biofilm (green indicates viable cells and red indicates damaged cells). As shown in Fig.31A, the three images were clearly different, showing a remarkably inhomogeneous biofilm only in the case of LL37-Vmh2. However, the absence of red points, showed that LL37-Vmh2, as well as Vmh2, influenced the adhesive properties of *S. epidermidis* and did not compromise cell viability. To obtain detailed and accurate descriptions of the differences between biofilms, all the CLSM image stack data were further analyzed using the COMSTAT image analysis software package[28]. As expected, the values of the biomass and the average thickness of the biofilm obtained in LL37-Vmh2 coated wells were significantly lower if compared to the Vmh2-coated and uncoated ones (Fig.31B). Moreover, the analysis revealed that the roughness coefficient resulted higher in the case of LL37-Vmh2 than Vmh2 and uncoated wells (Fig.31B). This dimensionless factor provides a measure of how much the thickness of a biofilm varies, and it is thus used as a direct indicator of biofilm heterogeneity, confirming that the presence of LL37-Vmh2 coating inhibited biofilm formation in several areas.
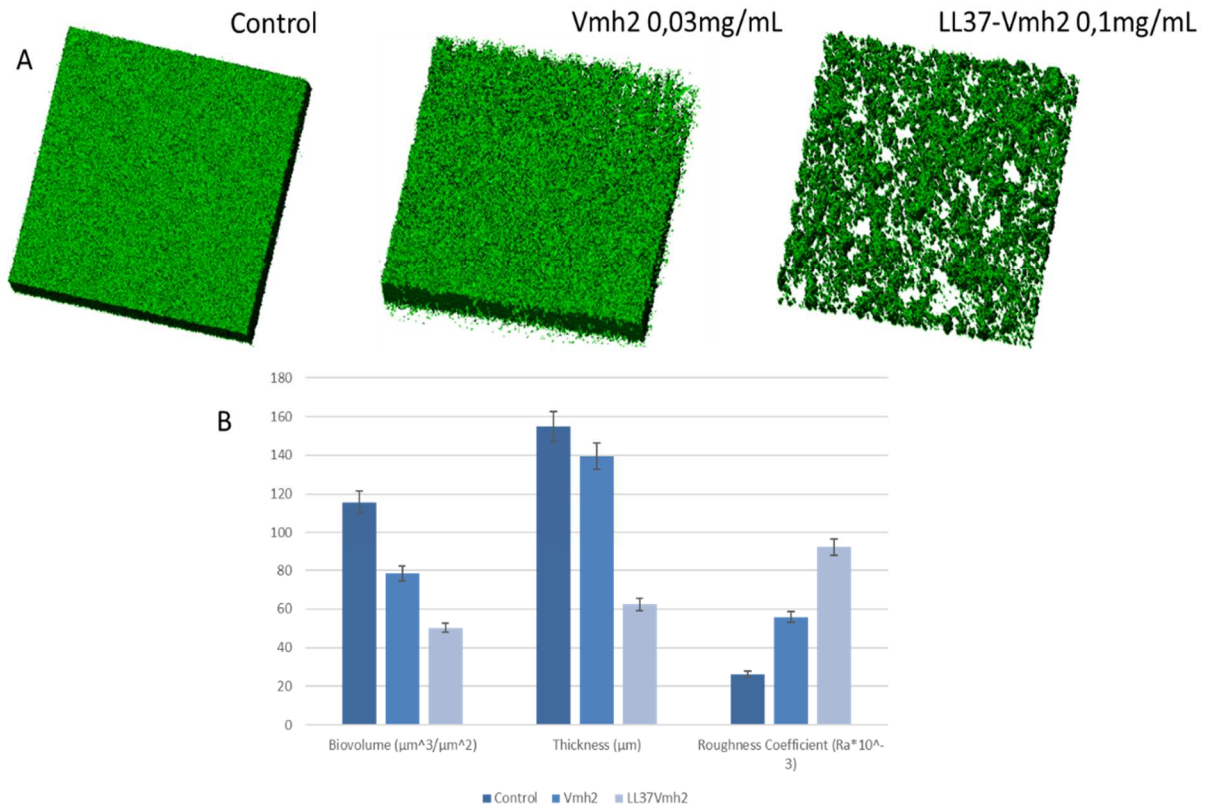
Fig. 31 – A: CLSM analysis of *S.epidermidis* biofilms structure. Analysis of the effect of different coating was reported: S. epidermidis O-47 biofilm on an uncoated polystyrene well (Control); on Vmh2-coated polystyrene wells; and on LL37-Vmh2-coated polystyrene wells. The three-dimensional biofilm structures were obtained using the LIVE/DEAD® Biofilm Viability Kit. The green fluorescence (SYTO9) indicates viable cells and the red fluorescence (PI) indicates dead cells. The Z-stack analysis of the *S. epidermidis* O-47 biofilm in all tested conditions is reported; **B**: COMSTAT quantitative analysis of the biomass, average thickness and roughness coefficient of the biofilms at all the tested conditions.

Further investigation should clarify if the heterogeneity of the formed biofilm is due to a heterogenous coating layer. If this was the case, a homogeneous LL37-Vmh2 layer should determine a complete *S. epidermidis* biofilm inhibition.

3.2 Chimera protein: Antibody-Hydrophobin

Antibodies are a modular defense and represent a powerful weapon system in defending our body against foreign objects like bacteria and viruses. They perform their function through a specific chemical interaction between antigen-antibody.

ScFv Antibodies

During the past decade, advances in recombinant antibody technology have greatly facilitated the genetic manipulation of antibody fragments[29,30]. The genetic manipulation of recombinant antibodies thus improved our understanding about the structure and function of immunoglobulins. Furthermore, these advances have led to the development of a large variety of engineered antibody molecules for research, diagnosis, and therapy with an improved specificity in comparison to conventional antibody technology. Once cloned, it is then possible to increase the affinity and specificity of antigen binding by mimicking somatic hypermutation during an immune response[31]. Since 1975, Kohler and Milstein have introduced the hybridoma technology which enabled a defined specificity of monoclonal antibodies to be

produced in consistent quality as well as in large quantities in the laboratory. However, monoclonal antibody producing technology is very laborious and time consuming. Furthermore, small mammals like mice do not always provide the high-affinity antibody response to particular antigen needed for sensitive assay development[32]. These limitations of traditional techniques have led several research groups to investigate the use of phage display in producing Single-chain antibody fragment (scFv) antibodies[33] (Fig.32).
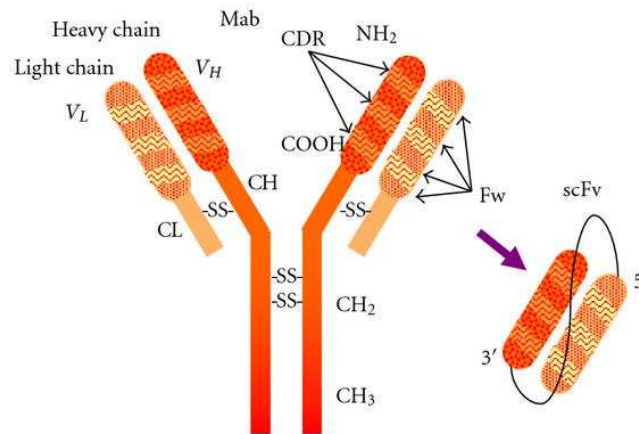
Fig. 32 – Antibody model showing subunit composition and domain distribution along the polypeptide chains. Single-chain fragment variable (scFv) antibody generated by recombinant antibody technology appears in the shaded area (Zuhaida Asra Ahmad, 2012).

scFv is a small engineered antibody, in which the variable heavy chain (VH) and light chain (VL) of the antibody molecule are connected by a short, flexible polypeptide linker. Using scFv for detection of antigen has several advantages, i) the retention of the specific affinity to the antigen, though usually lower than its original antibody; ii), scFv can be produced in large quantity in bacterial expression system at low cost[34]; iii) it is easy to be manipulated to be adapted to different applications, for example, fusion with protein drug to target and kill pathogens or with marker molecules for detection purposes[35,36]. The most commonly used linker contains a 15-combination of glycine and serine residues (GGGGS)$_3$ that provides flexibility and enhances the hydrophilicity of the peptide backbone[37]. ScFvs are predominantly monomeric when the linker is at least 12 residues[38]. When VH and VL domains are joined with a linker of 3-12 residues, it cannot assemble into a functional Fv domain, and instead, the VH and VL domains of one scFv associate with those of a second scFv molecule to form dimers (diabodies). Reducing the linker length below three residues promotes the assembly of scFvs into trimers (triabodies)[38,39]. Recently, the technology has been improved through recombinant DNA technology and antibody engineering whereby antibody genes can now be cloned and expressed successfully as a fragment in bacteria[33], on mammalian cell and yeast[40], plant, and also insect cells. In comparison to the parental antibody, these minimized antibodies have several advantages in clinical practices including better tumor penetration or more rapid blood clearance[41–43].

Anti-mesothelin humans antibody

Antibody immobilization onto solid surface has been studied extensively for a number of applications including immunoassays, biosensors, and affinity chromatography. For most of these applications, a critical aspect is the orientation of antigen-binding

site with respect to the surface. With the aim to overcome this problem, in this section, the anti-mesothelin antibody has been used as first example of an antibody fused to an hydrophobin. Mesothelin is a 40-kDa cell surface glycoprotein that is physiologically expressed at the cell surface of mesothelial cells lining the pleura, pericardium and peritoneum and overexpressed in several human tumors such as pancreatic cancers, ovarian cancers, mesotheliomas, and some other cancers. The biological function of mesothelin is not known but soluble forms of mesothelin can be found in fluids from patients affected by these cancers. Measurement of mesothelin in the blood may be useful for the diagnosis and to follow the course of some of these patients. Furthermore, mesothelin is an attractive candidate for targeted therapy, given its limited expression in normal tissues and high expression in several cancers[44,45].

The fusion protein immobilization on solid surface will be an interesting approach in applications such as Immunoassays (Elisa Kit) and drug delivery.

System design

The gene fusion between hydrophobin Vmh2 from *P. ostreatus* and scFv HN1 (VH-(Gly3Ser)3-VL) was cloned (NdeI and XhoI) into the plasmid pET22b (+) in frame with the TEV (Tobacco Etch Virus) cleavage site under the control of the T7 promoter. The amminoacidic sequences of HN1-Vmh2 (900 bp) is showed below:

MQVQLVQSGAEVKRPGASVQVSCRASGYSINTYYMQWVRQAPGAGLEWMG
VINPSGVTSYAQKFQGRVTLTNDTSTNTVYMQLNSLTSADTAVYYCARWAL
WGDFGMDVWGKGTLVTVSSGGGGSGGGGSGGGGSDIQMTQSPSTLSASIGD
RVTITCRASEGIYHWLAWYQQKPGKAPKLLIYKASSLASGAPSRFSGSGSGTD
FTLTISSLQPDDFATYYCQQYSNYPLTFGGGTKLEIKENLYFQGAMDTPSCSTG
SLQCCSSVQKATDPLASLLIGLLGIVLGPLDLLVGVTCSPITVIGVGGTSCTQQT
VCCTGNSFNGLIAIGCSPINISL

V_H Linker V_L TEV site Vmh2

The recombinant plasmid pET22b (+)-HN1-Vmh2 was transformed in *E. coli* BL21 (DE3) to be expressed in functional form.

Production and characterization of chimeric hydrophobins

The HN1-Vmh2 protein was produced starting from an expression vector containing the sequence coding for the fusion protein. The protein was produced using transformed BL21 *E. coli* cells. Recombinant clones cultures were incubated in LB medium at 37 °C. When the cell growths reached a 0.6 OD_{600nm} value, 1mM IPTG was added in one of the flasks in order to induce the protein expression. The growth trend of *E. coli* is shown in the Fig.33A. It appears that the cell growth is influenced by the expression of LL-37. Cellular pellets were collected after centrifugation of the cell cultures, and an SDS-PAGE (15% acrylamide) analysis of the cell extracts, obtained by cell disruption with Cracking Buffer (10% w/v SDS, Tris-HCl 0.25M pH6.8, 20% v/v glycerol, EDTA 4mM pH8, 6M urea), was carried out, and showed in Fig.33B.
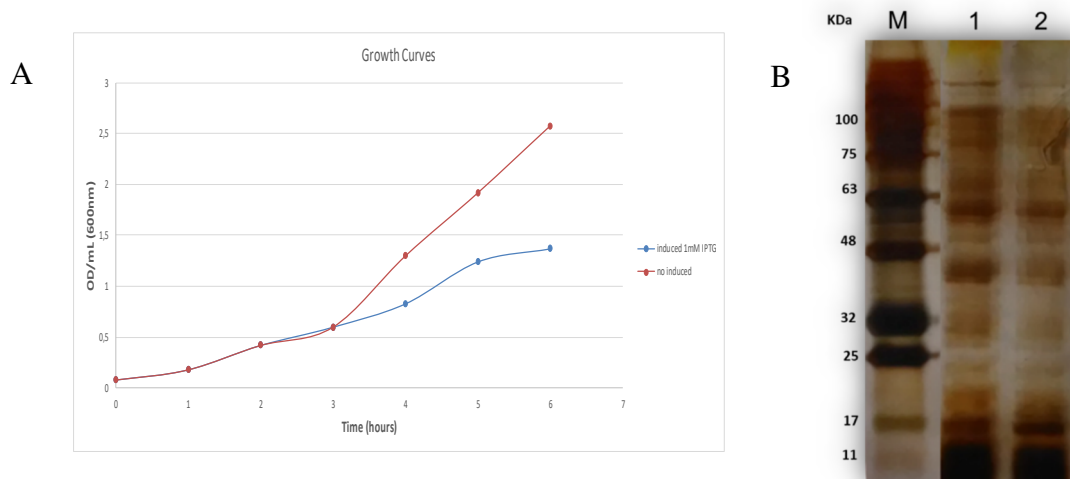
Fig. 33 – A: HN1-Vmh2 growth curves at 37°C in LB; **B:** SDS–PAGE (0.1 OD): M: marker; lane 1: BL21 *E. coli* cellular extract after induction; lane 2: BL21 *E. coli* cellular extract

No appreciable differences were observed between an IPTG-induced BL21 recombinant cell extracts and a normal recombinant BL21 cell extract. Moreover, the band corresponding to the HN1-Vmh2 protein (at a molecular weight of about 45 kDa), could of other bands of *E. coli* cytoplasmic proteins with similar molecular weight. Therefore, to localize HN1-Vmh2, the collected cellular pellets were processed using the French press to lyse cells and separating soluble fraction from inclusion bodies, as Piscitelli and coworkers reported[26] . Samples of the soluble and insoluble parts of cell extract, and also the first washing of the insoluble part (done with lysis buffer), were collected and observed by SDS-PAGE. the results are shown below.
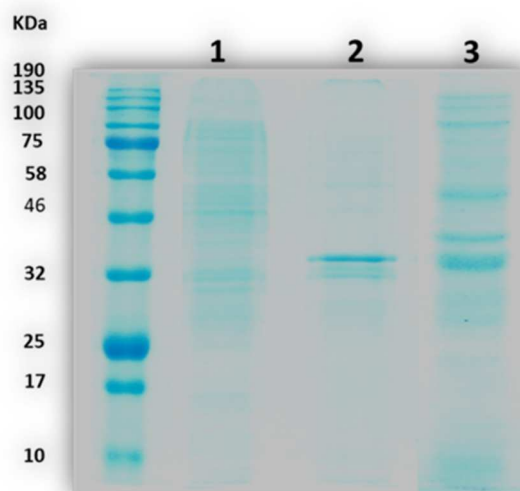
Fig. 34 – SDS-PAGE; M: marker; lane 1: BL21 *E. coli* inclusion bodies; lane 2: inclusion bodies first wash; lane 3: BL21 *E. coli* lysate soluble fraction.

Bands at the expected molecular weight (about 45KDa) were detected in the soluble part of cellular lysate and in the first washing of the insoluble fraction. To identify the chimera protein, the band in lane 2 were cut and subjected to *in situ* hydrolysis protocol with trypsin. the obtained peptide mixture was analyzed by mass spectrometry analysis by MALDI-TOF; the interpretation of the obtained spectrum

provided a 20% sequence coverage of HN1 (Table 9). This could be an initial indication about the presence of HN1-Vmh2 chimera protein in the analyzed peptide mixture, Further analysis will be carried out in order to better understand the distribution of this protein in the soluble or insoluble part of the *E. coli* extract.

Table 9 – Identification by MALDI-TOF

Peptides	Sequence	Experimental m / z	Expected m / z
186-196	(K)ASSLASGAPSR(F)	1003,5372	1003,5167
14-24	(K)RPGASVQVSCR(A)	1216,5883	1216,6215
25-39	(R)ASGYSINTYYMQWVR(Q)	1838,8732	1838,8530

3.3 Conclusions

The adhesive properties of hydrophobin Vmh2, isolated by *P. ostreatus*, make this protein a very useful tool in the design of new molecules that possess adhesive moieties that adhere to hydrophilic or hydrophobic surfaces. The production of these new chimera proteins through BL21 *E. coli* recombinant expression is very advantageous in terms of protein yield and production cost. However, designing these chimera proteins are not trivial: a number of factors that may influence the production and purification of these proteins have to be carefully considered, and each fusion protein has its own physical-chemical characteristics that doesn't allow the definition of a general method for their production. The LL37-Vmh2 fusion protein was identified within the soluble fraction of BL21 *E. coli* cell extract obtained after a mechanical cell disruption, despite the fact that other Vmh2 fusion proteins were identified in the inclusion bodies. However, the reducing environment of *E. coli* cytoplasm doesn't allow the fusion protein to reach the correct folding, thus affecting the adhesive capabilities of the fusion protein. A refolding protocol was developed and the yield of adhesion of the fusion protein increased. This gave the possibility to carry out preliminary experiments for investigate the anti-biofilm and anti-microbial capabilities of LL37-Vmh2. These experiments, according to Vmh2, confirm S. epidermidis antibiofilm activity but show new properties of the layers of LL37-Vmh2 affecting the biofilm structure.

HN1-Vmh2 fusion protein was identified, although its localization was not clear. It may be useful to define new strategies for the production of these two fusion proteins, for example carrying out their production into an *E. coli* strain that possesses a more suitable intracellular environment for the correct folding of both LL37-Vmh2 and HN1-Vmh2 and / or design opportune tags to improve their recovery.

3.4 References

1. Moon, J.-Y., Henzler-Wildman, K. A. & Ramamoorthy, A. Expression and purification of a recombinant LL-37 from Escherichia coli. *Biochim. Biophys. Acta - Biomembr.* **1758,** 1351–1358 (2006).

2. Ho, M., Feng, M., Fisher, R. J., Rader, C. & Pastan, I. A novel high-affinity human monoclonal antibody to mesothelin. *Int. J. Cancer* **128,** 2020–2030 (2011).

3. Longobardi, S. *et al.* Environmental Conditions Modulate the Switch among Different States of the Hydrophobin Vmh2 from Pleurotus ostreatus. *Biomacromolecules* **13,** 743–750 (2012).

4. HIRSCH, J. G. Phagocytin: a bactericidal substance from polymorphonuclear leucocytes. *J. Exp. Med.* **103,** 589–611 (1956).

5. Zhao, X., Wu, H., Lu, H., Li, G. & Huang, Q. LAMP: A Database Linking Antimicrobial Peptides. *PLoS One* **8,** e66557 (2013).

6. Conlon, J. M. & Sonnevend, A. in *Methods in molecular biology (Clifton, N.J.)* **618,** 3–14 (2010).

7. Radek, K. & Gallo, R. Antimicrobial peptides: natural effectors of the innate immune system. *Semin. Immunopathol.* **29,** 27–43 (2007).

8. Peters, B. M., Shirtliff, M. E. & Jabra-Rizk, M. A. Antimicrobial Peptides: Primeval Molecules or Future Drugs? *PLoS Pathog.* **6,** e1001067 (2010).

9. Zasloff, M. Antimicrobial peptides of multicellular organisms. *Nature* **415,** 389–395 (2002).

10. Schauber, J. & Gallo, R. L. Antimicrobial peptides and the skin immune defense system. *J. Allergy Clin. Immunol.* **122,** 261–266 (2008).

11. Ganz, T. The Role of Antimicrobial Peptides in Innate Immunity. *Integr. Comp. Biol.* **43,** 300–304 (2003).

12. Niyonsaba, F., Iwabuchi, K., Matsuda, H., Ogawa, H. & Nagaoka, I. Epithelial cell-derived human β-defensin-2 acts as a chemotaxin for mast cells through a pertussis toxin-sensitive and phospholipase C-dependent pathway. *Int. Immunol.* **14,** 421–426 (2002).

13. Hancock, R. E. & Scott, M. G. The role of antimicrobial peptides in animal defenses. *Proc. Natl. Acad. Sci. U. S. A.* **97,** 8856–61 (2000).

14. Nijnik, A., Pistolic, J., Filewod, N. C. J. & Hancock, R. E. W. Signaling pathways mediating chemokine induction in keratinocytes by cathelicidin LL-37 and flagellin. *J. Innate Immun.* **4,** 377–86 (2012).

15. Kindrachuk, J. *et al.* Manipulation of innate immunity by a bacterial secreted peptide: Lantibiotic nisin Z is selectively immunomodulatory. *Innate Immun.* **19,** 315–327 (2013).

16. Tossi, A., Sandri, L. & Giangaspero, A. Amphipathic, α-helical antimicrobial peptides. *Biopolymers* **55,** 4–30 (2000).

17. Zhang, L. & Gallo, R. L. *Antimicrobial peptides. CURBIO* **26,** (2016).

18. Powers, J.-P. S. & Hancock, R. E. . The relationship between peptide structure and antibacterial activity. *Peptides* **24,** 1681–1691 (2003).

19. Scott, M. G. & Hancock, R. E. W. Cationic Antimicrobial Peptides and Their Multifunctional Role in the Immune System. *Crit. Rev. Immunol.* **20,** 24 (2000).

20. Boman, H. G. Innate immunity and the normal microflora. *Immunol. Rev.* **173,** 5–16 (2000).

21. Zanetti, M. Cathelicidins, multifunctional peptides of the innate immunity. *J. Leukoc. Biol.* **75,** 39–48 (2004).

22. Vandamme, D., Landuyt, B., Luyten, W. & Schoofs, L. A comprehensive summary of LL-37, the factotum human cathelicidin peptide. *Cell. Immunol.* **280,** 22–35 (2012).

23. Bucki, R., Leszczyńska, K., Namiot, A. & Sokołowski, W. Cathelicidin LL-37: A Multitask Antimicrobial Peptide. *Arch. Immunol. Ther. Exp. (Warsz).* **58,** 15–25 (2010).

24. Artini, M. *et al.* Hydrophobin coating prevents *Staphylococcus epidermidis* biofilm formation on different surfaces. *Biofouling* **33,** 601–611 (2017).

25. Li, Y. Recombinant production of antimicrobial peptides in Escherichia coli: A review. *Protein Expr. Purif.* **80,** 260–267 (2011).

26. Piscitelli, A., Pennacchio, A., Longobardi, S., Velotta, R. & Giardina, P. Vmh2 hydrophobin as a tool for the development of "self-immobilizing" enzymes for biosensing. *Biotechnol. Bioeng.* **114,** 46–52 (2017).

27. Vuong, C., Gerke, C., Somerville, G. A., Fischer, E. R. & Otto, M. Quorum-Sensing Control of Biofilm Factors in *Staphylococcus epidermidis. J. Infect. Dis.* **188,** 706–718 (2003).

28. Givskov, M. *et al.* Quantification of biofilm structures by the novel computer program comstat. *Microbiology* **146,** 2395–2407 (2000).

29. Boss, M. A., Kenten, J. H., Wood, C. R. & Emtage, J. S. Assembly of functional antibodies from immunoglobulin heavy and light chains synthesised in *E. coli. Nucleic Acids Res.* **12,** 3791–3806 (1984).

30. Kontermann, R. E. & Müller, R. Intracellular and cell surface displayed single-chain diabodies. *J. Immunol. Methods* **226,** 179–188 (1999).

31. Gram, H. *et al.* In vitro selection and affinity maturation of antibodies from a naive combinatorial immunoglobulin library. *Proc. Natl. Acad. Sci. U. S. A.* **89,** 3576–80 (1992).

32. O'Connor, S. J. M. *et al.* The rapid diagnosis of acute promyelocytic leukaemia

using PML (5E10) monoclonal antibody. *Br. J. Haematol.* **99,** 597–604 (1997).

33.	Skerra, A. & Plückthun, A. Assembly of a functional immunoglobulin Fv fragment in Escherichia coli. *Science* **240,** 1038–41 (1988).

34.	Schier, R. *et al.* Isolation of High-affinity Monomeric Human Anti-c-erbB-2 Single chain Fv Using Affinity-driven Selection. *J. Mol. Biol.* **255,** 28–43 (1996).

35.	Winter, G., Griffiths, A. D., Hawkins, R. E. & Hoogenboom, H. R. Making Antibodies by Phage Display Technology. *Annu. Rev. Immunol.* **12,** 433–455 (1994).

36.	Vaughan, T. J. *et al.* Human Antibodies with Sub-nanomolar Affinities Isolated from a Large Non-immunized Phage Display Library. *Nat. Biotechnol.* **14,** 309–314 (1996).

37.	Dolezal, O. *et al.* Single-chain Fv multimers of the anti-neuraminidase antibody NC10: the residue at position 15 in the VL domain of the scFv-0 (VL–VH) molecule is primarily responsible for formation of a tetramer–trimer equilibrium. *Protein Eng. Des. Sel.* **16,** 47–56 (2003).

38.	Hudson, P. J. & Kortt, A. A. High avidity scFv multimers; diabodies and triabodies. *J. Immunol. Methods* **231,** 177–189 (1999).

39.	Atwell, J. L. *et al.* scFv multimers of the anti-neuraminidase antibody NC10: length of the linker between VH and VL domains dictates precisely the transition between diabodies and triabodies. *Protein Eng. Des. Sel.* **12,** 597–604 (1999).

40.	Ho, M., Nagata, S. & Pastan, I. Isolation of anti-CD22 Fv with high affinity by Fv display on human cells. *Proc. Natl. Acad. Sci. U. S. A.* **103,** 9637–42 (2006).

41.	Huston, J. S. *et al.* Single-chain Fv radioimmunotargeting. *Q. J. Nucl. Med.* **40,** 320–33 (1996).

42.	Dana Jones, S. & Marasco, W. A. Antibodies for targeted gene therapy: extracellular gene targeting and intracellular expression. *Adv. Drug Deliv. Rev.* **31,** 153–170 (1998).

43.	Colcher, D. *et al.* Pharmacokinetics and biodistribution of genetically-engineered antibodies. *Q. J. Nucl. Med.* **42,** 225–41 (1998).

44.	Chang, K., Pastan, I. & Willingham, M. C. Isolation and characterization of a monoclonal antibody, K1, reactive with ovarian cancers and normal mesothelium. *Int. J. cancer* **50,** 373–81 (1992).

45.	Chang, K. & Pastan, I. Molecular cloning of mesothelin, a differentiation antigen present on mesothelium, mesotheliomas, and ovarian cancers. *Proc. Natl. Acad. Sci. U. S. A.* **93,** 136–40 (1996).

CHAPTER 4

4. CONCLUSIONS

The present PhD project has successfully reached the goal to develop versatile and straightforward systems of surface functionalization by immobilization of hydrophobin-protein chimera. The genetic fusion of the target proteins to the self-assembling moiety of Vmh2 is an alternative and effective strategy of protein immobilization. Indeed, Vmh2 hydrophobin allowed not only a stable binding to the surfaces, but also enabled exposure of target protein to the surroundings. Furthermore, no additional treatment was required, since Vmh2 spontaneously self-assembles at the interfaces. The advantages of this strategy are the ease and effectiveness of the immobilization procedure.

The achieved results are listed below:

• A chimera formed by the hydrophobin Vmh2 and the laccase POXA1b (PoxA1b-Vmh2) was produced and secreted by *P. pastoris*. This fused enzyme was immobilized and used to develop an easy-to-use optical biosensing platform to detect phenolic compounds in real matrices of food and biomedical interest.

• A one-step bio-functionalization procedure of graphene with PoxA1b-Vmh2 was set up. Herein, this biofunctionalized graphene was easily deposited on GCE and exploited for the development of a biosensor to monitor catechol. This device could represent a valid and sensitive alternative for the detection of catechol in real samples with electrochemical methods.

• A chimera formed by Vmh2 and the anti-microbial peptide LL37 (LL37-Vmh2) was produced in *E. coli*. The layers formed by deposition of LL37-Vmh2 were used to inhibit the bio-films formation of the pathogen *S. epidermidis* to produce functionalized medical devices.

• A chimera formed by Vmh2 and the anti-mesothelin antibody HN1 (HN1-Vmh2) was produced in *E. coli*. Production of this fused protein lays the foundation for smart immobilization procedures of antibodies on different surfaces for immunoassays, such as Elisa Kit, and for drug delivery.

• Furthermore, during the six months stay at the CNRS of Grenoble, the direct electron transfer of the native laccase POXC from *P. ostreatus* was investigated using different modified electrodes. Results suggest that this native laccase is of great interest as a biocathode for new bioelectrocatalytic applications.

COMMUNICATIONS and PUBLICATIONS

Communications
Poster

- Alfredo Maria Gravagnuolo, Paola Cicatiello, Anna Pennacchio, **Ilaria Sorrentino**, Jane Politi, Luca De Stefano, Alessandra Piscitelli, Paola Giardina: "Fungal hydrophobins, proteins with potential in drug delivery" CRS Italy Chapter WORKSHOP 2017 Fisciano Campus (SA)- Italy, October 26-28, 2017
- **Ilaria Sorrentino**, Solène Gentil, Yannig Nedellec, Alessandra Piscitelli, Paola Giardina, Giovanni Sannia, Alan Le Goff: "POXC: a high-performance multicopper enzyme for O_2 reduction in enzymatic biofuel cells". Oxizymes conference 2018, Queen's University Belfast, Northen Ireland from 8-10 July2018

Oral presentation

- Alessandra Piscitelli, **Ilaria Sorrentino**, Ilaria Stanzione, Paola Giardina: "Self-immobilizing laccase through genetic fusion with hydrophobin". Oxizymes conference 2018, Queen's University Belfast, Northen Ireland from 8-10 July2018.

Publications
P1-. A. Piscitelli, P. Cicatiello, A. M. Gravagnuolo, **I. Sorrentino**, C. Pezzella and P. Giardina. " Applications of Functional Amyloids from Fungi: Surface Modification by ClassI Hydrophobins". *Biomolecules* **2017**, 7, 45; doi:10.3390/biom7030045
P2- Ilaria Sorrentino, Solène Gentil, Yannig Nedellec, Serge Cosnier, Alessandra Piscitelli, Paola Giardina and Alan Le Goff. "POXC laccase from *Pleurotus ostreatus* : a high-performance multicopper enzyme for direct Oxygen Reduction Reaction operating in a proton-exchange membrane fuel cell". *ChemElectroChem* **2018** doi.org/10.1002/celc.201801264
P3- Ilaria Sorrentino, Paola Giardina and Alessandra Piscitelli. "Straightforward laccase immobilization by means of a laccase-hydrophobin chimera" **Submitted to "Applied Microbiology and Biotechnology"**
P4- Paola Cicatiello, **Ilaria Sorrentino**, Alessandra Piscitelli, Paola Giardina. "Spotlight on class I Hydrophobins: their intriguing biochemical properties and industrial prospectives" **Book chapter submitted to "Grand challenges in fungal biotechnology" Springer**

Experience in foreign laboratories
September 2017- March 2018: Visiting PhD student in the laboratory of Dr. Alan Le Goff, at Department of Molecular Chemistry, Groupe Biosystèmes Electrochimiques et Analytiques, Université Grenoble Alpes, France. The stage was focused on the Direct wiring of laccases on nanomaterials.

APPENDIX